Lecture Notes

PARALLEL COORDINATES

Alfred Inselberg[1]
School of Mathematical Sciences
Tel Aviv University
Tel Aviv, Israel
aiisreal@math.tau.ac.il
&
Visiting Professor
Computer Science Department
Korea University
Seoul, Korea

[1] Senior Fellow San Diego SuperComputing Center

Chapter 1

Preview

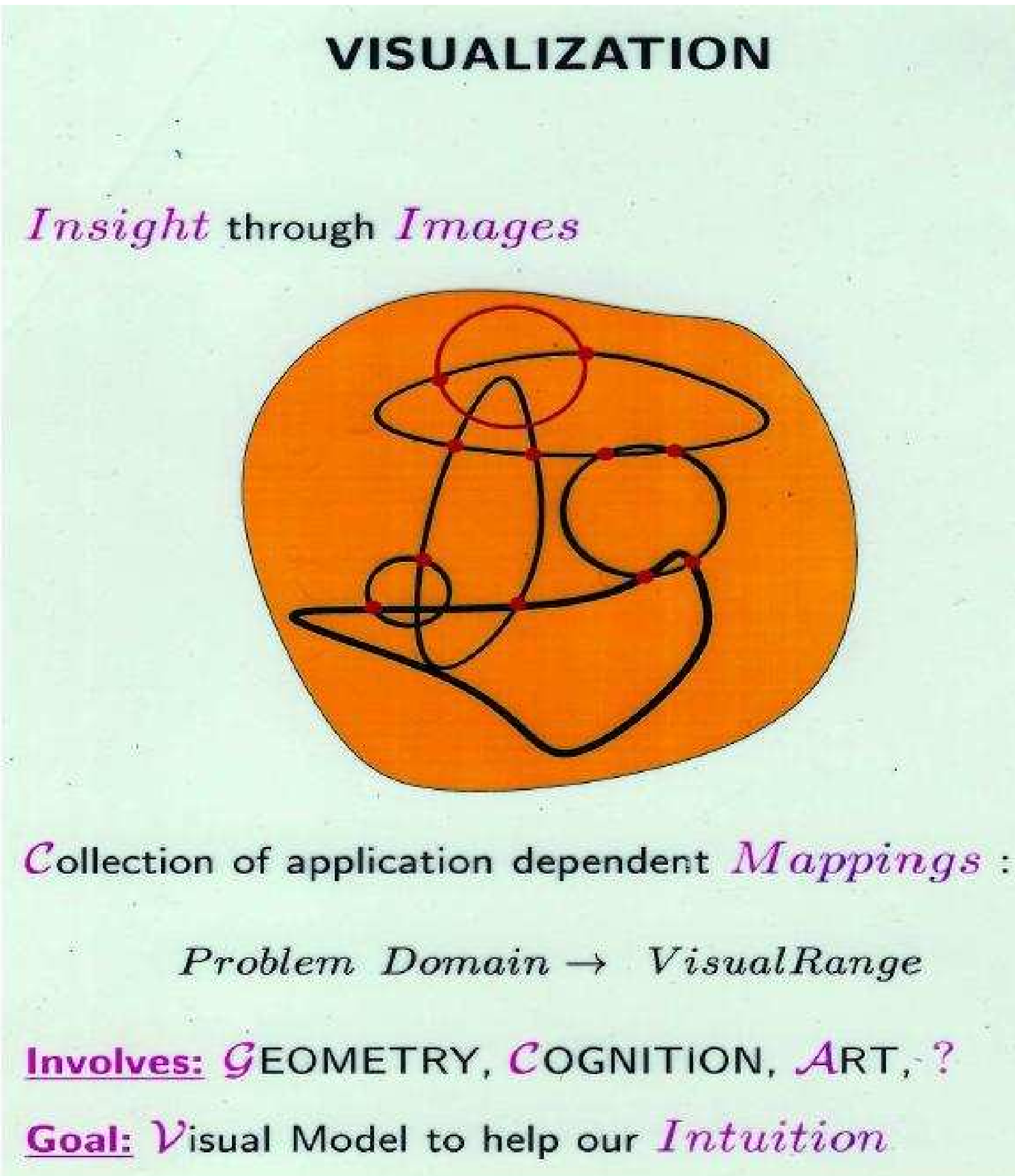

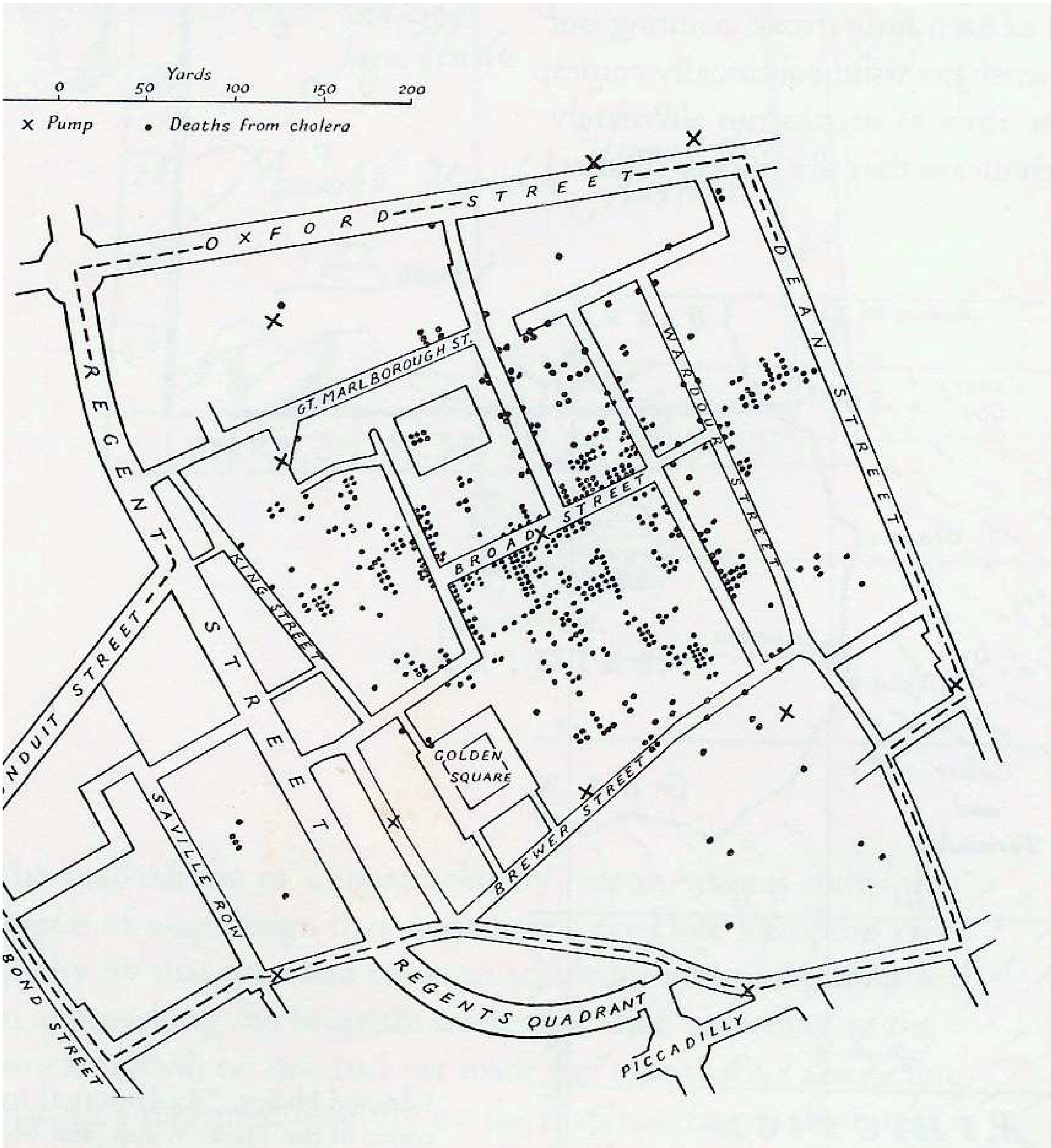

Figure 1.1: Cholera epidemic in London 1854. Dr. Snow placed dots at the addresses of the deceased and saw the concentration of deaths around the Broad street water pump. From E.W.Gilbert, Geog. J. 124] (1958) – By permission from E.R.Tufte " The Visual Display of Quantitative Information", Graphic Press 1983 p. 24

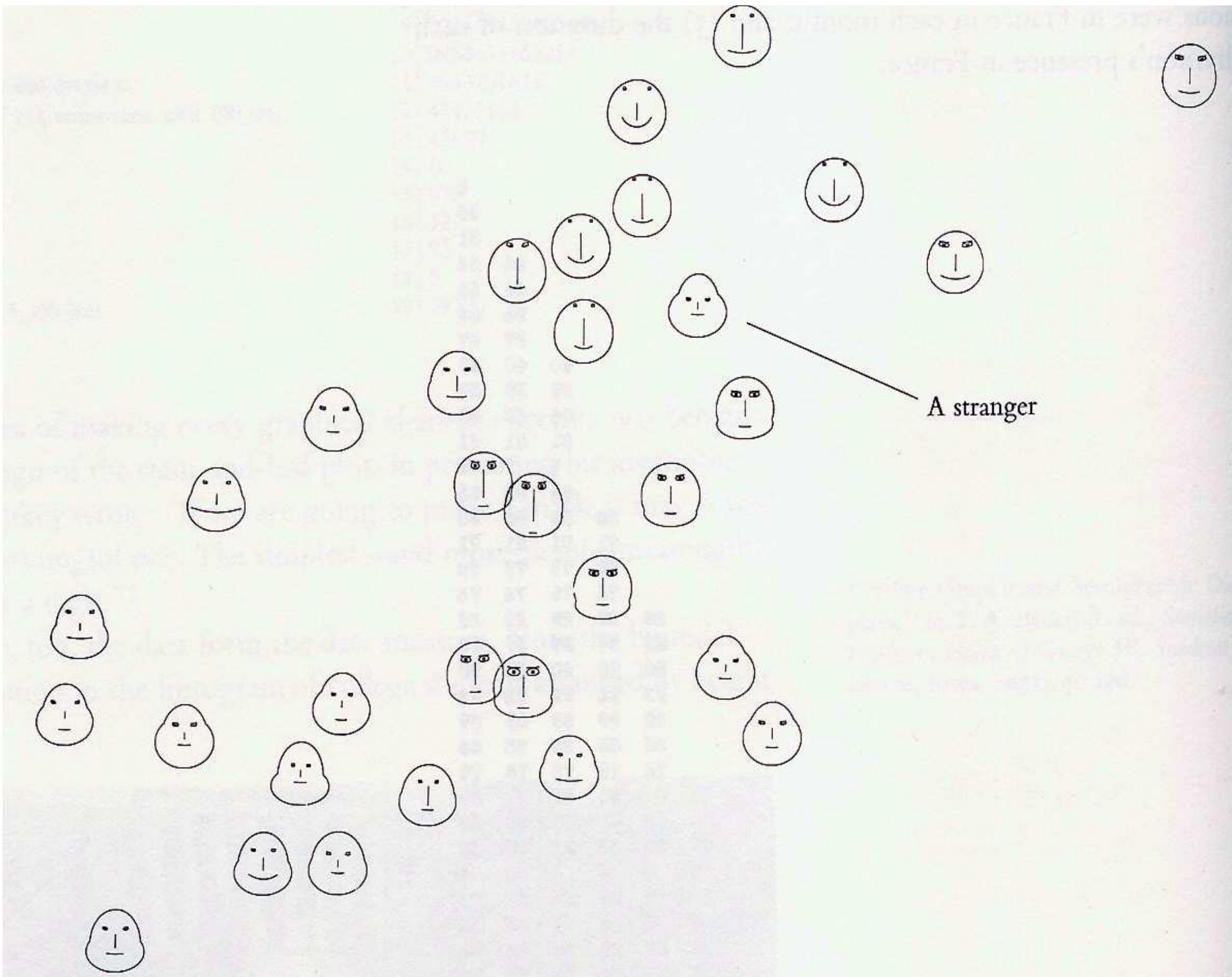

Figure 1.2: Multivariate data mapped into faces; each parameter corresponds to and is measured on a facial feature. H. Chernoff, JASA 68 (1973)

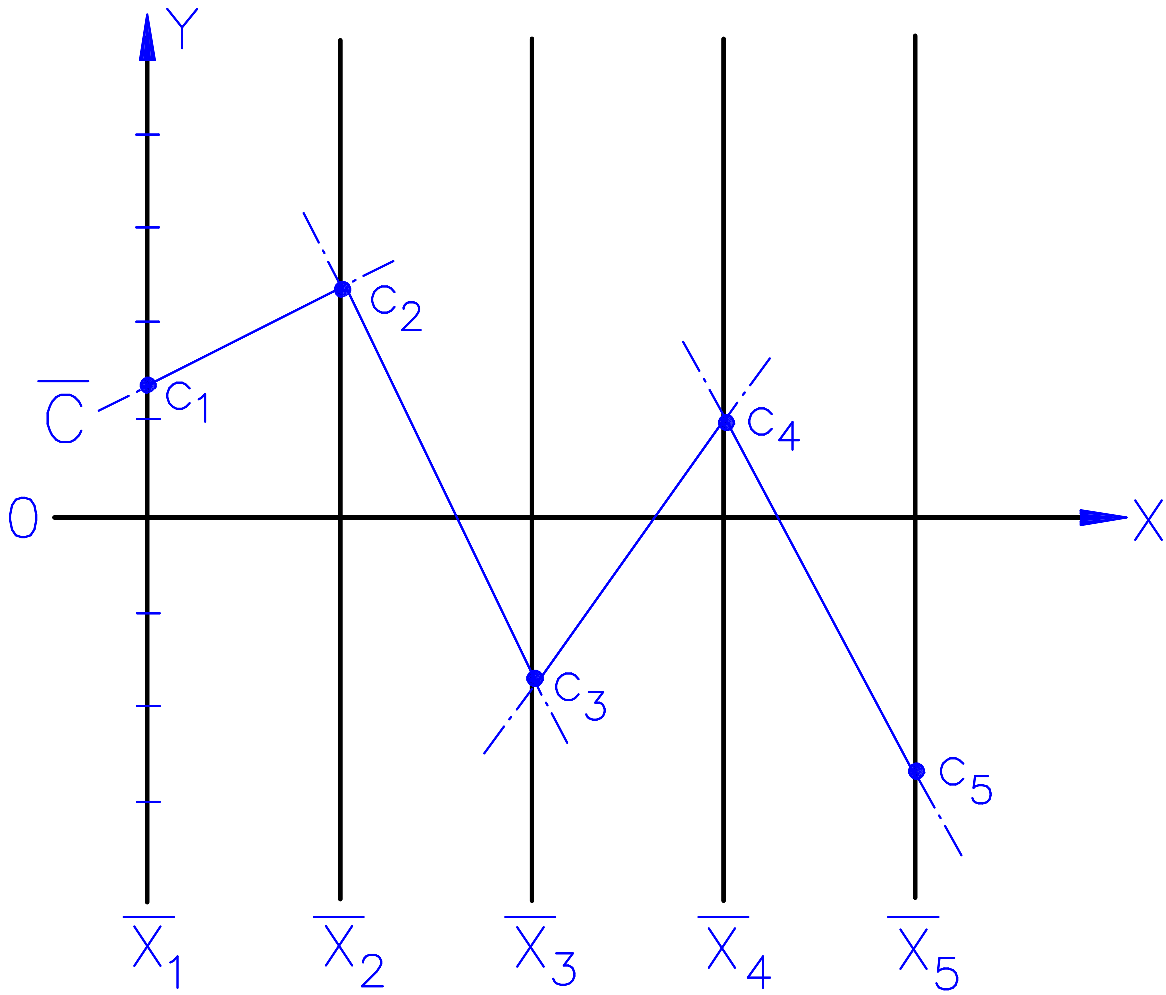

Figure 1.3: Parallel Coordinates – Point in 5-D , $C = (c_1, c_2, c_3, c_4, c_5)$

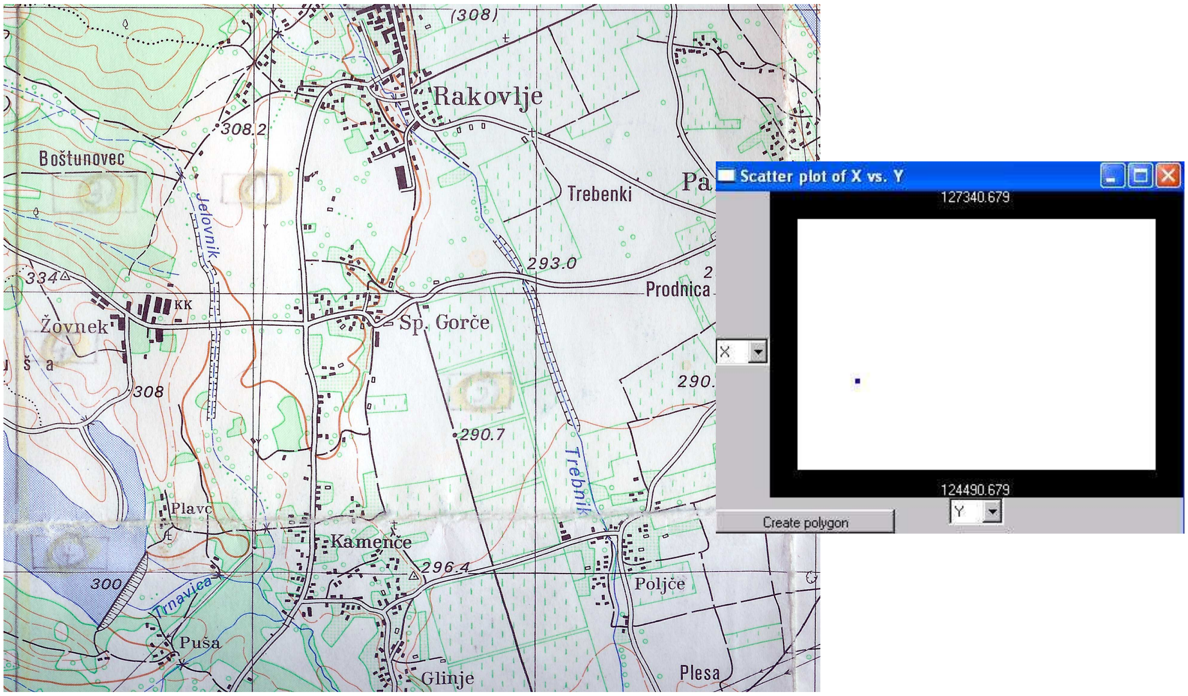

Figure 1.4: (Left)Region of Slovenia where 7 types of ground emissions were measured by the LandSat Thematic Mapper and shown in subsequent figures – Thanks to Dr. Ana Tretjak and Dr. Niko Schlamberger, Statistics Office of Slovenia. (Right) The display corresponds to the map's rectangular region, the dot marks the position where the 7-tuple shown in the figure below was measured.

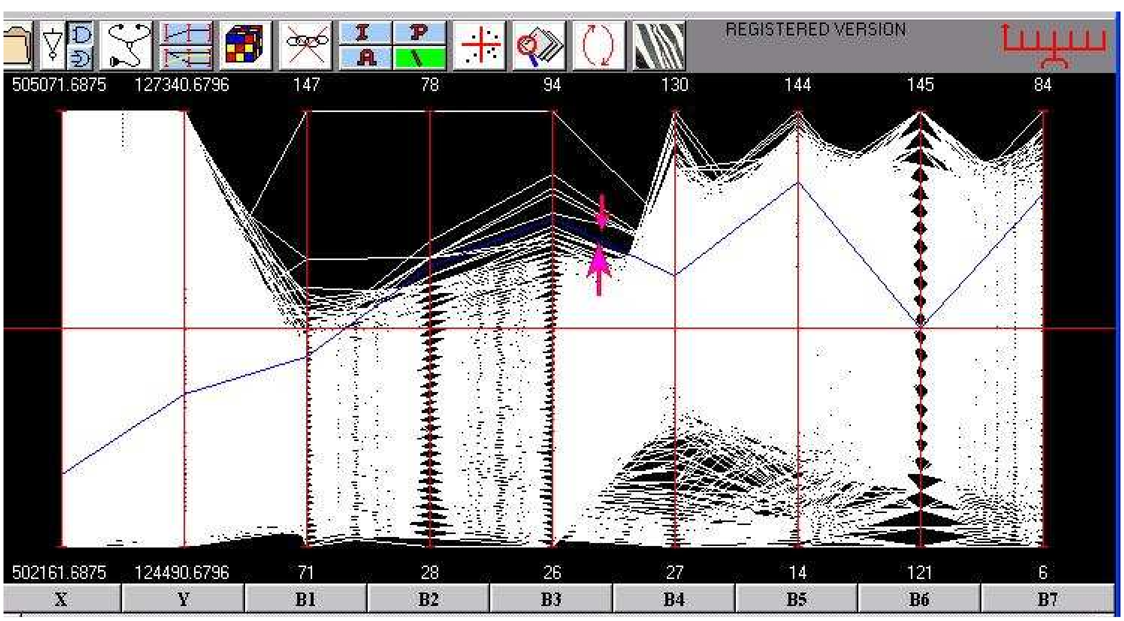

Figure 1.5: Query showing a single data item: the X, Y (position also shown on the right of above Fig. and values of the 7-tuple $(B1, B2, B3, B4, B5, B6, B7)$ at that point.

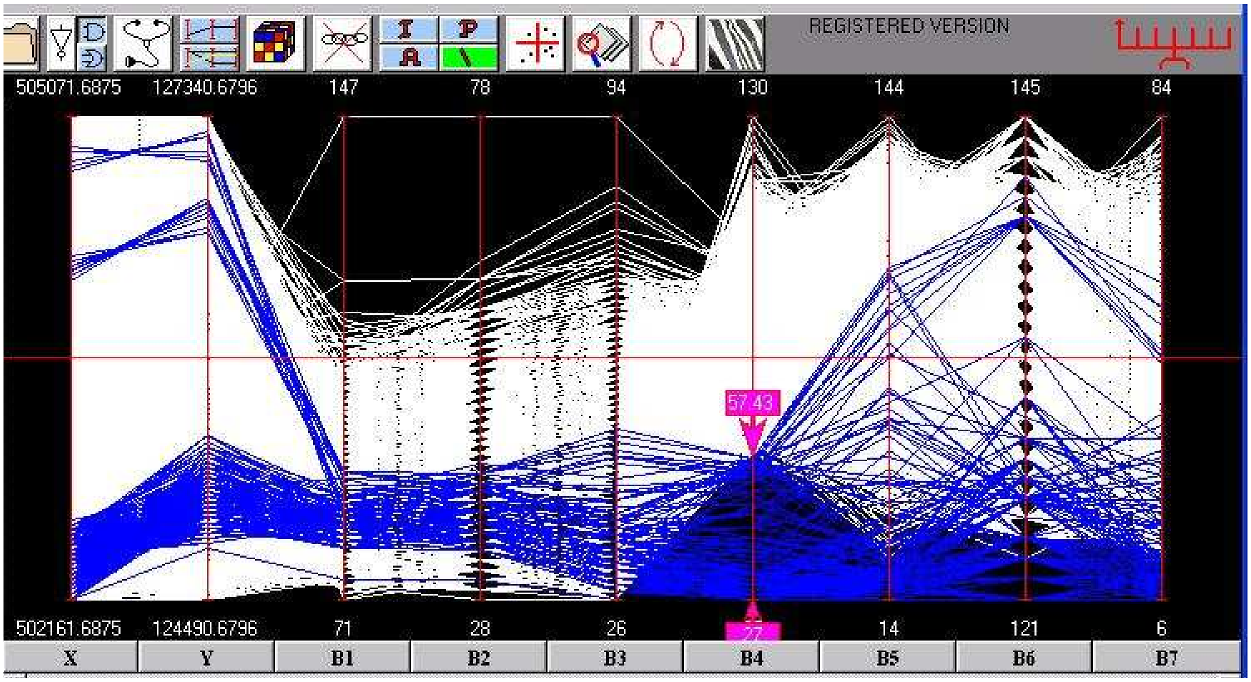

Figure 1.6: Finding water regions. The contrast due to density differences around the lower values of $B4$ is the *visual cue* prompting this query.

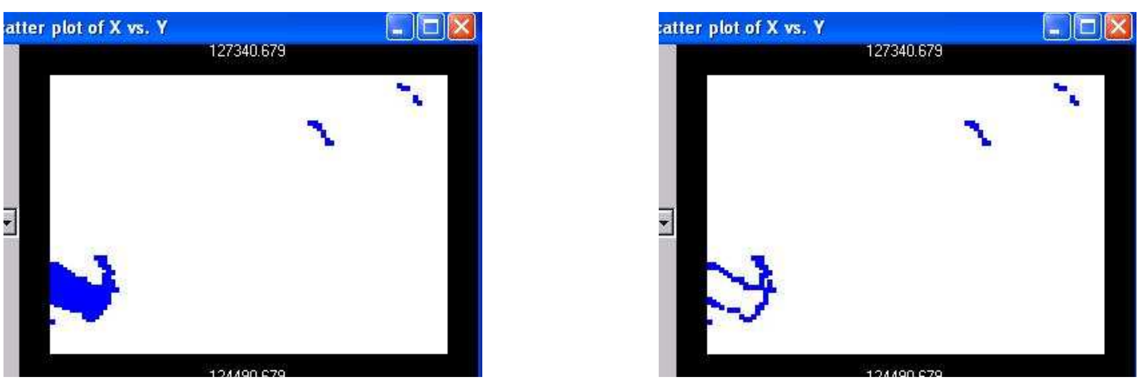

Figure 1.7: (Left)The lake and – result of query shown in Fig. **??** and (Right) just its boundary – result of query shown in the next Fig. **??**.

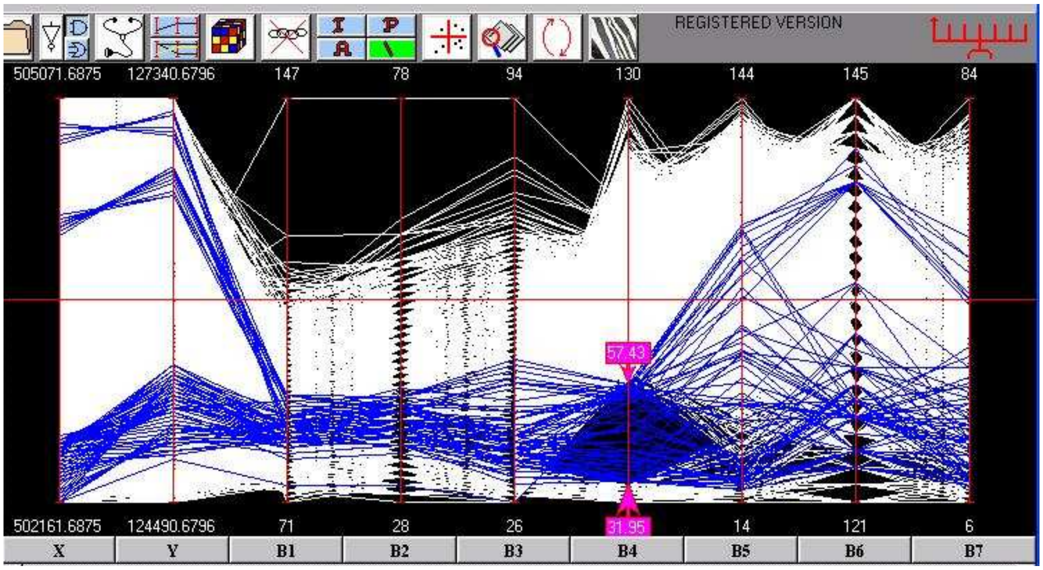

Figure 1.8: Query finding the water's edge.

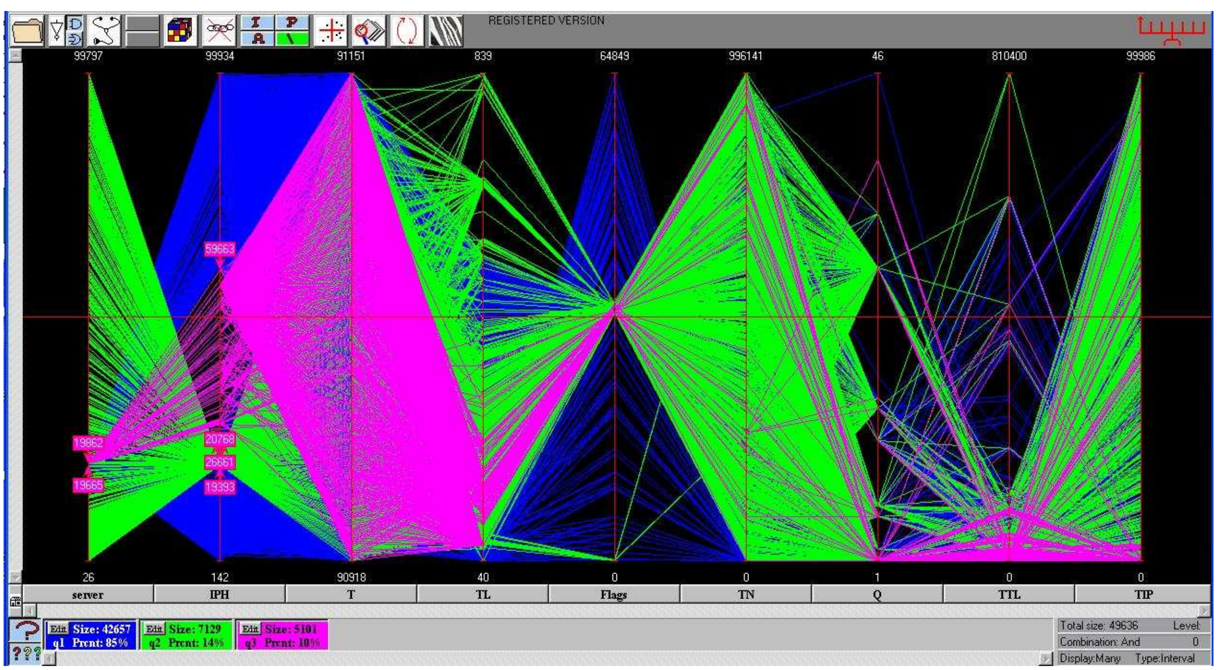

Figure 1.9: Detecting Network Intrusion from Internet Traffic Flow Data. Note the many-to-one relations.

Chapter 2

The Plane $\mathbb{R}^2$ with $\|$-coords

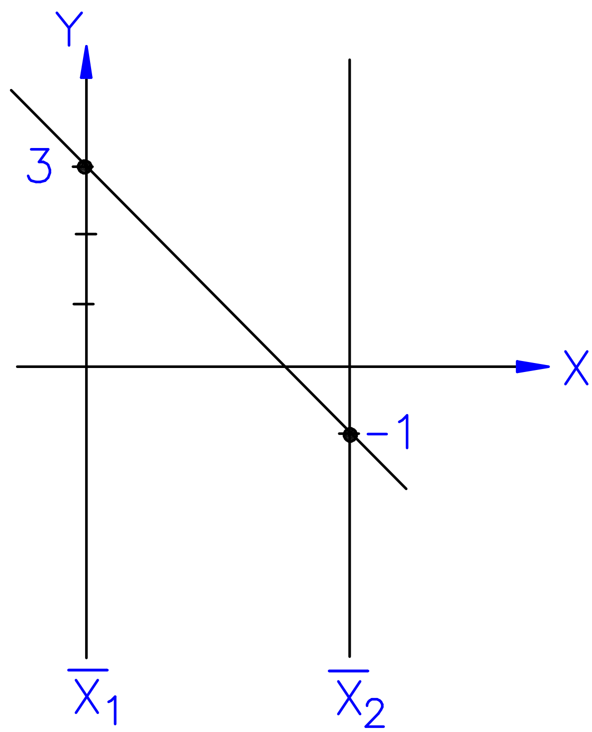

Figure 2.1: Points on the plane are represented by lines – example $(3, -1)$.

With d the distance between the axes the correspondence is :

$$\textit{line} \quad \ell : x_2 = mx_1 + b \quad \longleftrightarrow \quad \textit{point} \quad \bar{\ell} : (\frac{d}{1-m}, \frac{b}{1-m}) \qquad m \neq 1 \, . \tag{2.1}$$

Lines with negative slope $m < 0$ (negative correlation) are mapped into points between the axes, $m > 1$ to the left of the $\bar{X}_1$ and $0 < m < 1$ to the right of the $\bar{X}_2$ axes. To include lines with $m = 1$ the Euclidean plane $\mathbb{R}^2$ is embedded in the Projective plane $\mathbb{P}^2$. Then a line with slope $m = 1$ is mapped in the *direction* also called *ideal point* with slope b/d.

Homogeneous coordinates are very convenient and the conversion to/from Cartesian is easy i.e. $Cartesian \quad (a, b) \to (a, b, 1) \to k(a, b, 1) \quad for\ k \neq 0$.

Sometimes it is preferable to describe the line ℓ by :

$$\ell : a_1x_1 + a_2x_2 + a_3 = 0 \tag{2.2}$$

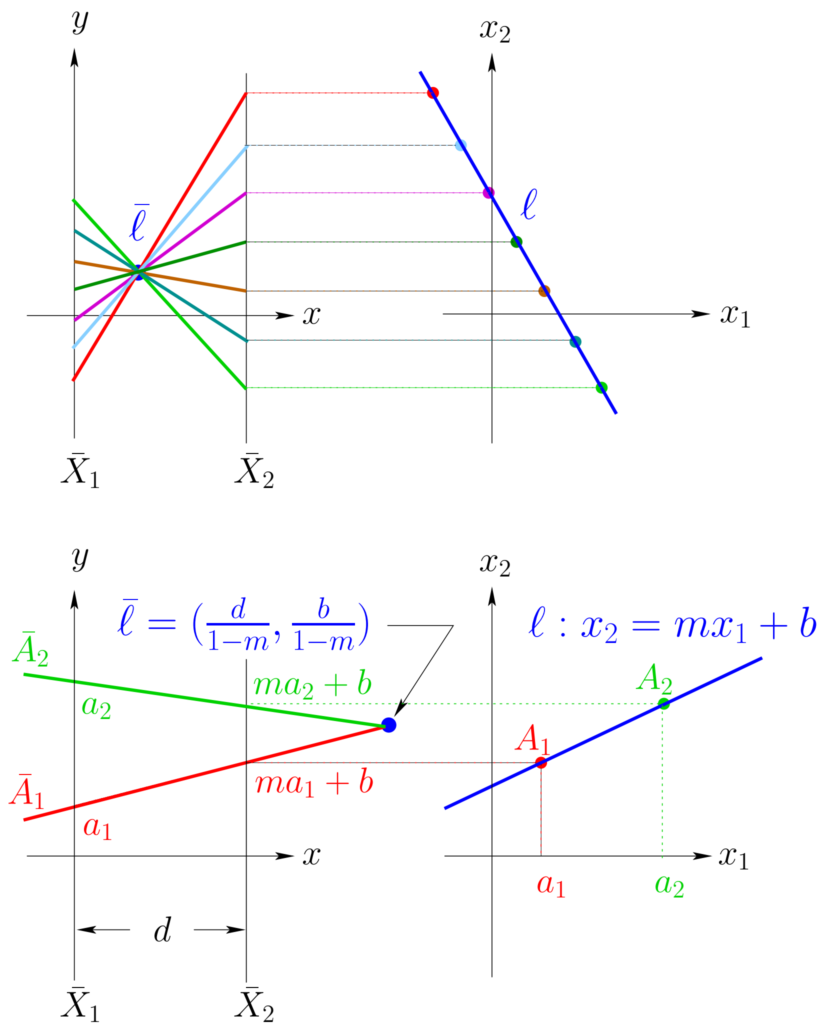

Figure 2.2: Conversely, lines are represented by points inducing a point $\longleftrightarrow$ line duality.

and for $a_2 \neq 0$, $m = -\frac{a_1}{a_2}$ and $b = -\frac{a_3}{a_2}$, providing the correspondence :

$$\ell : [a_1, a_2, a_3] \longrightarrow \bar{\ell} : (da_2, -a_3, a_1 + a_2). \tag{2.3}$$

In turn this specifies a linear transformation between the triples ℓ and $\bar{\ell}$:

$$\bar{\ell} = Al \quad , l = A^{-1}\bar{\ell},$$

where ℓ and $\bar{\ell}$ are considered as column vectors. The 3×3 matrix is :

$$A \;=\; \begin{bmatrix} 0 & d & 0 \\ 0 & 0 & -1 \\ 1 & 1 & 0 \end{bmatrix} \;,\; A^{-1} \;=\; \begin{bmatrix} -1/d & 0 & 1 \\ 1/d & 0 & 0 \\ 0 & -1 & 0 \end{bmatrix}. \tag{2.4}$$

which can be easily computed by taking 3 simple triples, like for example, [1,0,0], [0,1,0] and [0,0,1] for ℓ. For the other half of the duality, we look into the point $P \rightarrow \bar{P}$ line correspondence which is given by:

$$P : (p_1, p_2, p_3) \longrightarrow \bar{P} : [(p_1 - p_2), dp_3, -dp_1]. \tag{2.5}$$

Again taking P and $\bar{P}$ as column vectors we have:

$$\bar{P} = B^{-1}P \quad , P = B\bar{P}$$

with

$$B^{-1} \;=\; \begin{bmatrix} -1 & 1 & 0 \\ 0 & 0 & -d \\ d & 0 & 0 \end{bmatrix} \;,\; B \;=\; \begin{bmatrix} 0 & 0 & 1/d \\ 1 & 0 & 1/d \\ 0 & -1/d & 0 \end{bmatrix}. \tag{2.6}$$

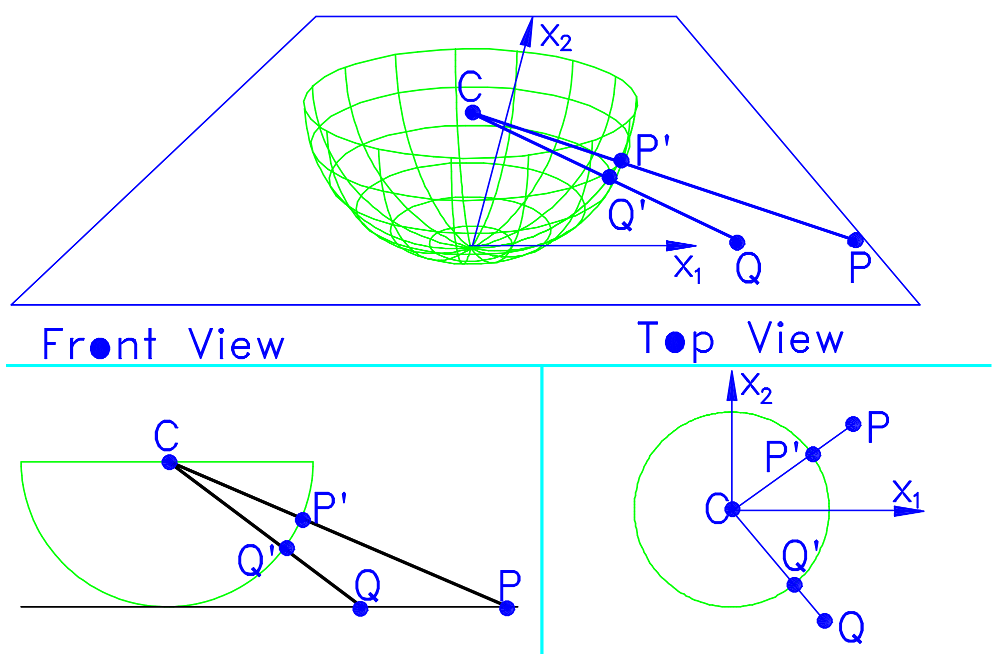

Figure 2.3: Model of the Projective Plane

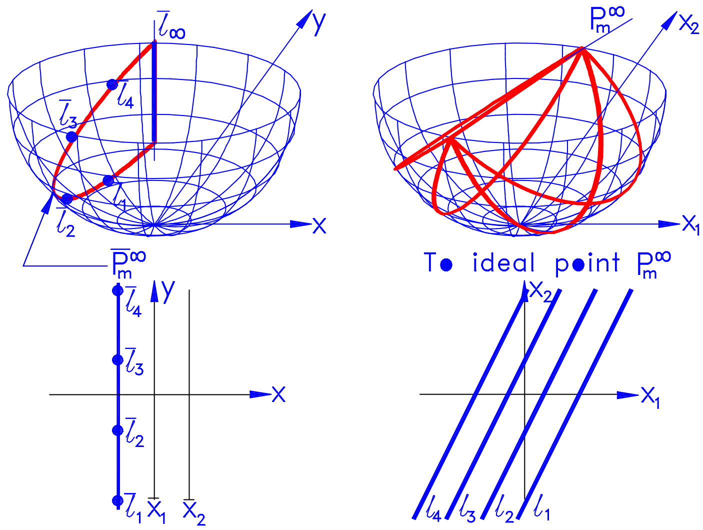

Figure 2.4: Under the duality parallel lines map into points on the same vertical line. On the projective plane model, the great semi-circles representing the lines share the same diameter since the lines have the same ideal point (direction). An ideal point in the direction with slope m is mapped into the vertical line $\bar{P}_m^\infty$.

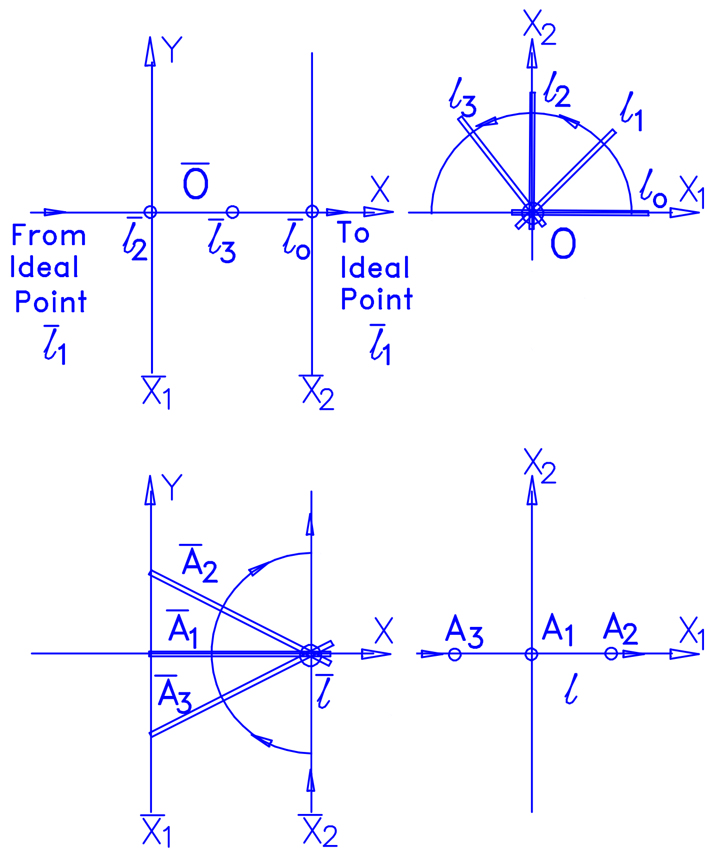

Figure 2.5: Duality: Rotation of a line about a point $\leftrightarrow$ Translation of a point on a line.

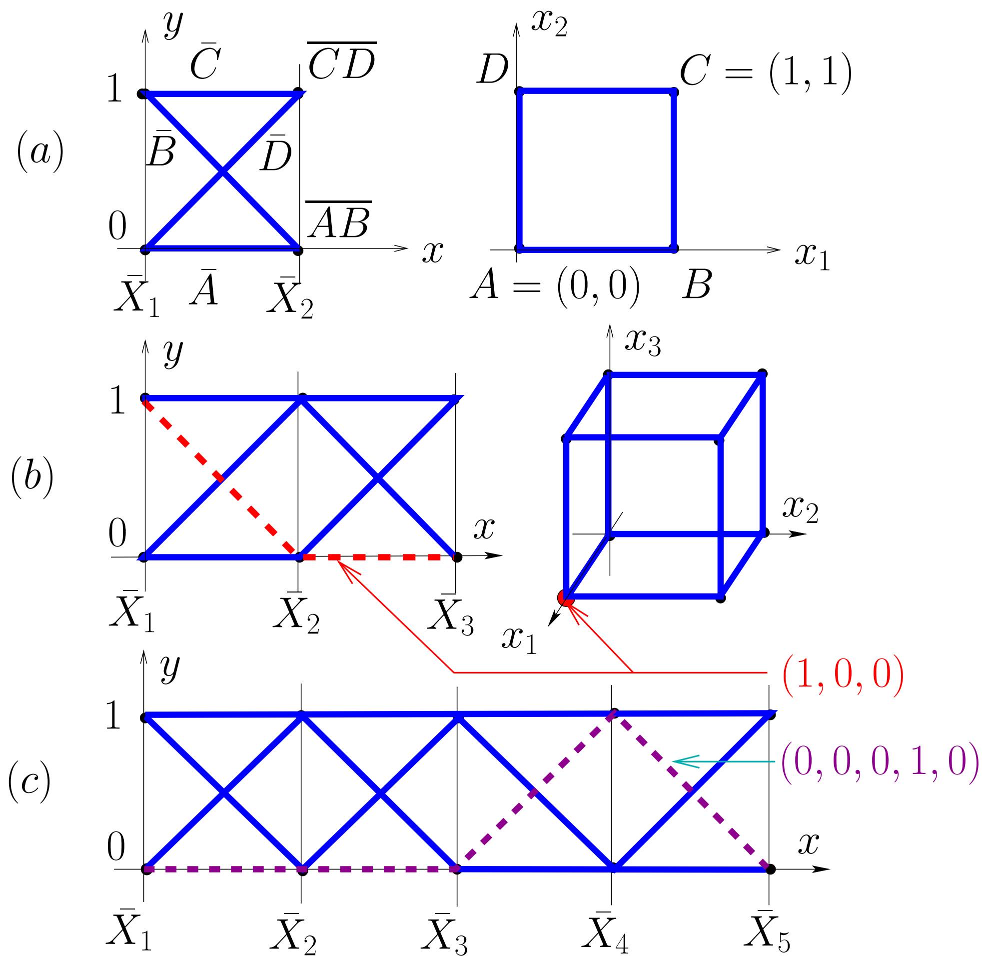

Figure 2.6: (a) Square (b) 3-D cube (c) 5-D hypercube all with edges of unit length. Vertices, edges & faces of all order are visible.

Chapter 3

Multidimensional Lines

Adjacent Variables Form

What is "a line in $\mathbb{R}^N$" ?
In $\mathbb{R}^3$ a line is the intersection of two planes. So a line ℓ in $\mathbb{R}^N$ is the intersection of $N-1$ non-parallel hyperplanes. Equivalently, it is the set of points (specified by N-tuples) which satisfy a set of $N-1$ linearly independent linear equations.

$$\ell \quad : \quad \begin{cases} \ell_{1,2} & : \; x_2 \; = \; m_2 x_1 \; + \; b_2 \\ \ell_{2,3} & : \; x_3 \; = \; m_3 x_2 \; + \; b_3 \\ \quad \cdots & \\ \ell_{i-1,i} & : \; x_i \; = \; m_i x_{i-1} \; + \; b_i \\ \quad \cdots & \\ \ell_{N-1,N} & : \; x_N \; = \; m_N x_{N-1} \; + \; b_N \quad , \end{cases} \tag{3.1}$$

Each equation contains a pair of *adjacently* labeled variables. In the $x_{i-1}x_i$-plane the relation labeled $\ell_{i-1,i}$ is a line, and by our *point* $\leftrightarrow$ *line* duality which we have already found (eq. (3) in Chapter 1) it can be represented by a point $\bar{\ell}_{i-1,i}$.

$$\bar{\ell}_{i-1,i} = (\frac{1}{(1-m_i)} + (i-2) \; , \; \frac{b_i}{(1-m_i)})$$

or in homogeneous coordinates :

$$\bar{\ell}_{i-1,i} = ((i-2)(1-m_i) + 1 \; , \; b_i \; , \; 1-m_i). \tag{3.2}$$

There are $N-1$ such points for $i = 2, \ldots, N$ which represent the line ℓ.

Base Variable Form

Another common way of describing a line $\ell \subset \mathbb{R}^N$ is in terms of one, sometimes called the *base*, variable which after appropriate relabeling may be taken as x_1. Then

$$\ell \quad : \quad \begin{cases} \ell_{1,2} & : \ x_2 \ = \ m_2^1 x_1 \ + \ b_2^1 \\ \ell_{1,3} & : \ x_3 \ = \ m_3^1 x_1 \ + \ b_3^1 \\ \quad \cdots & \\ \ell_{1,i} & : \ x_i \ = \ m_i^1 x_1 \ + \ b_i^1 \\ \quad \cdots & \\ \ell_{1,N} & : \ x_N \ = \ m_N^1 x_1 \ + \ b_N^1 \end{cases} , \tag{3.3}$$

and the $N-1$ points representing it are :

$$\bar{\ell}_{1,i} \ = \ (i-1, \ b_i^1, \ 1-m_i^1) \ , \tag{3.4}$$

Intersection and non-intersections of lines

It is convenient to illustrate the situation in 4-D using the base-variable representation of a line:

$$x_i = v_i T + p_{o,i} \ \ = \ 1, 2, 3 \ . \tag{3.5}$$

and shown in Fig. **??**. There the intersection of two lines described by eq. (**??**), each represented by 3 indexed points $\bar{\ell}_{Ti}$, is constructed. For T denoting time and $x_1 \ x_2 \ x_3$ the space coordinates of a particle moving with constant velocity $\vec{V} = (v_1 \ v_2 \ v_3)$ and initial position $P_o = (p_{o,1} \ , p_{o,2} \ , p_{o,3})$ eq. (**??**), and equivalently it's 3 point representation, provide the complete trajectory information of the particle. The two sets of triple points $\bar{\ell}_{Ti}$ and $\bar{\ell}'_{Ti}$ describe the trajectories of two moving particles. The construction in Fig. **??** shows that two such particles collide since they go through the same point in space **at the same time** (i.e. there is a time-space intersection). Perhaps some of the power of the $\|$-coordinate representation can be appreciated from this simple example.

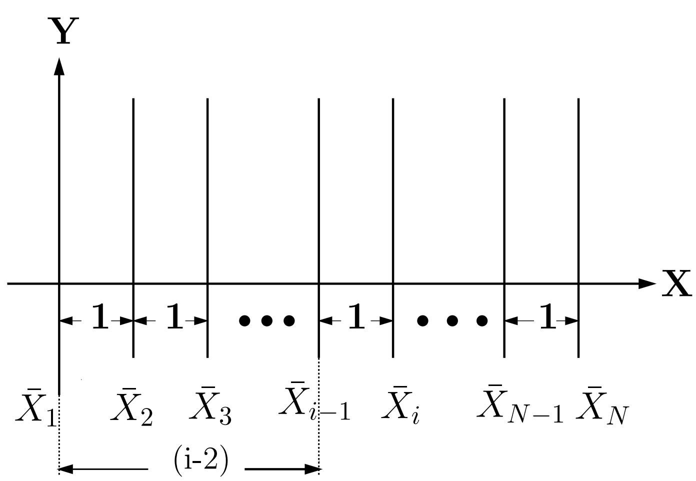

Figure 3.1: Spacing between adjacent axes is 1 unit.

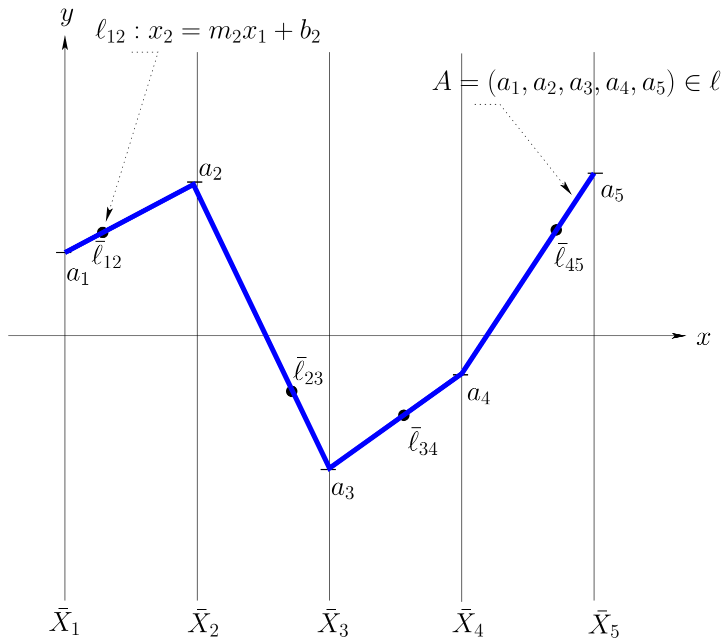

Figure 3.2: Point on line in 5-D.

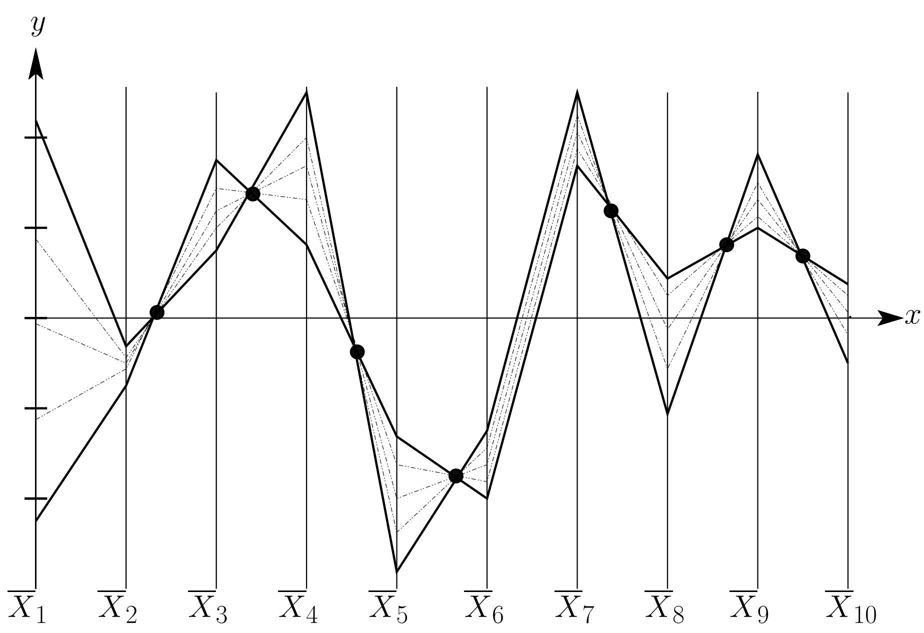

Figure 3.3: Line interval in 10-D – the thicker polygonal lines represent it's end-points. The adjacent variables representation, consisting of nine properly indexed points, is obtained by the sequential intersections of the polygonal lines' linear portions. Note that $\bar{\ell}_{1,2}$ is to the right of the X_2-axis and $\bar{\ell}_{6,7}$ is an ideal point. The remaining points are in between the corresponding pairs of axes.

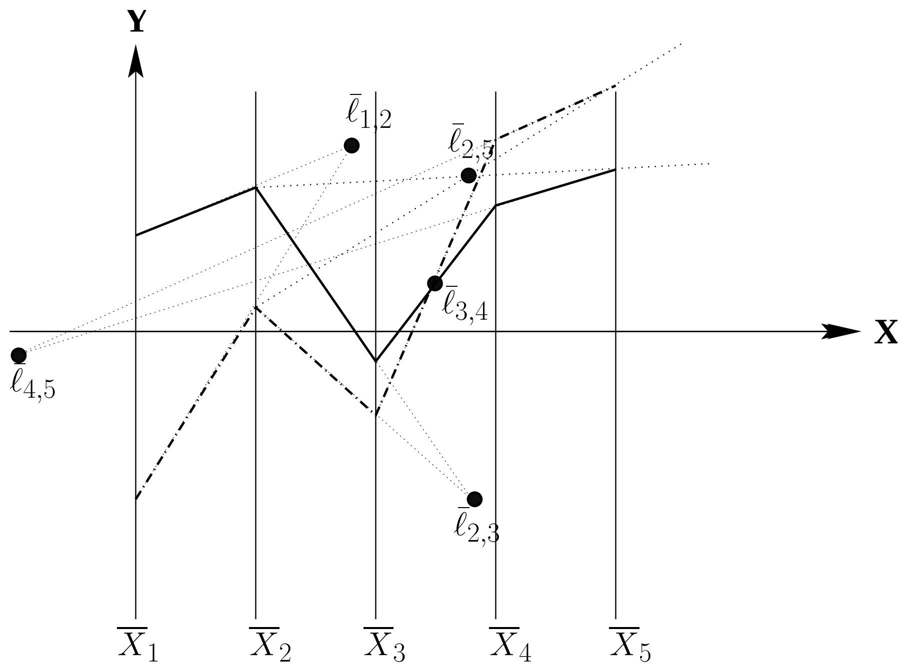

Figure 3.4: Algorithm for constructing a pairwise linear relation, in this case $\bar{\ell}_{25}$, given the $N-1$ points, $\bar{\ell}_{i-1,i}$, representing the line.

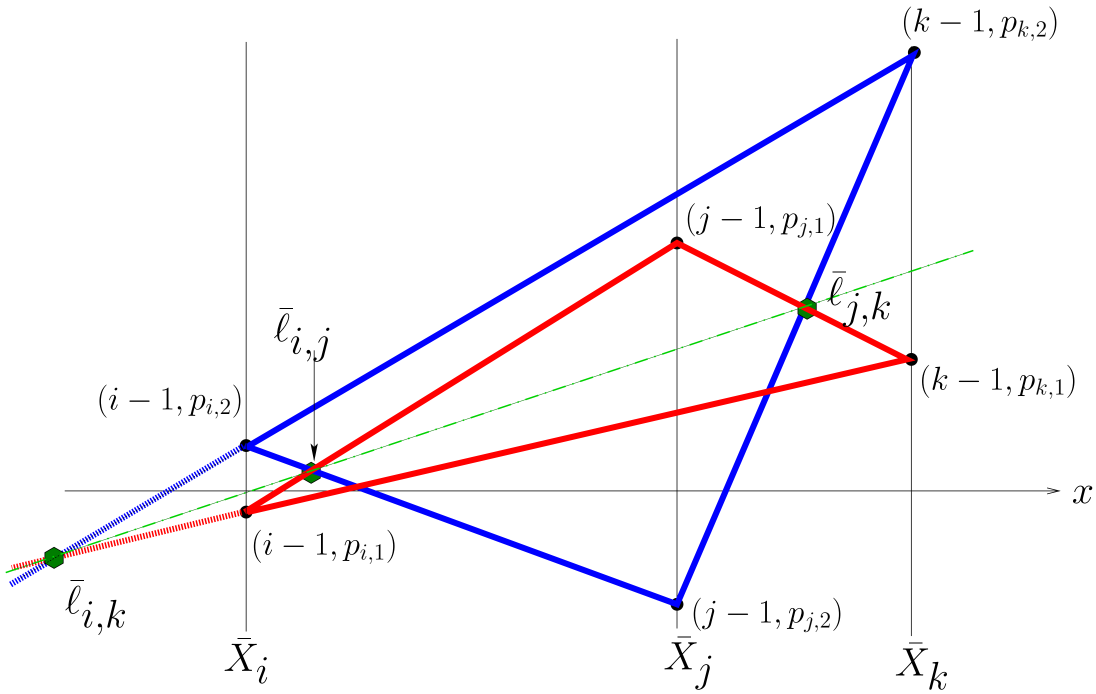

Figure 3.5: The Collinearity for the 3 points $\bar{\ell}_{i,j}, \bar{\ell}_{j,k}, \bar{\ell}_{i,k}$. The two triangles are in perspective with respect to the ideal point in vertical direction. The y-axis is offscale.

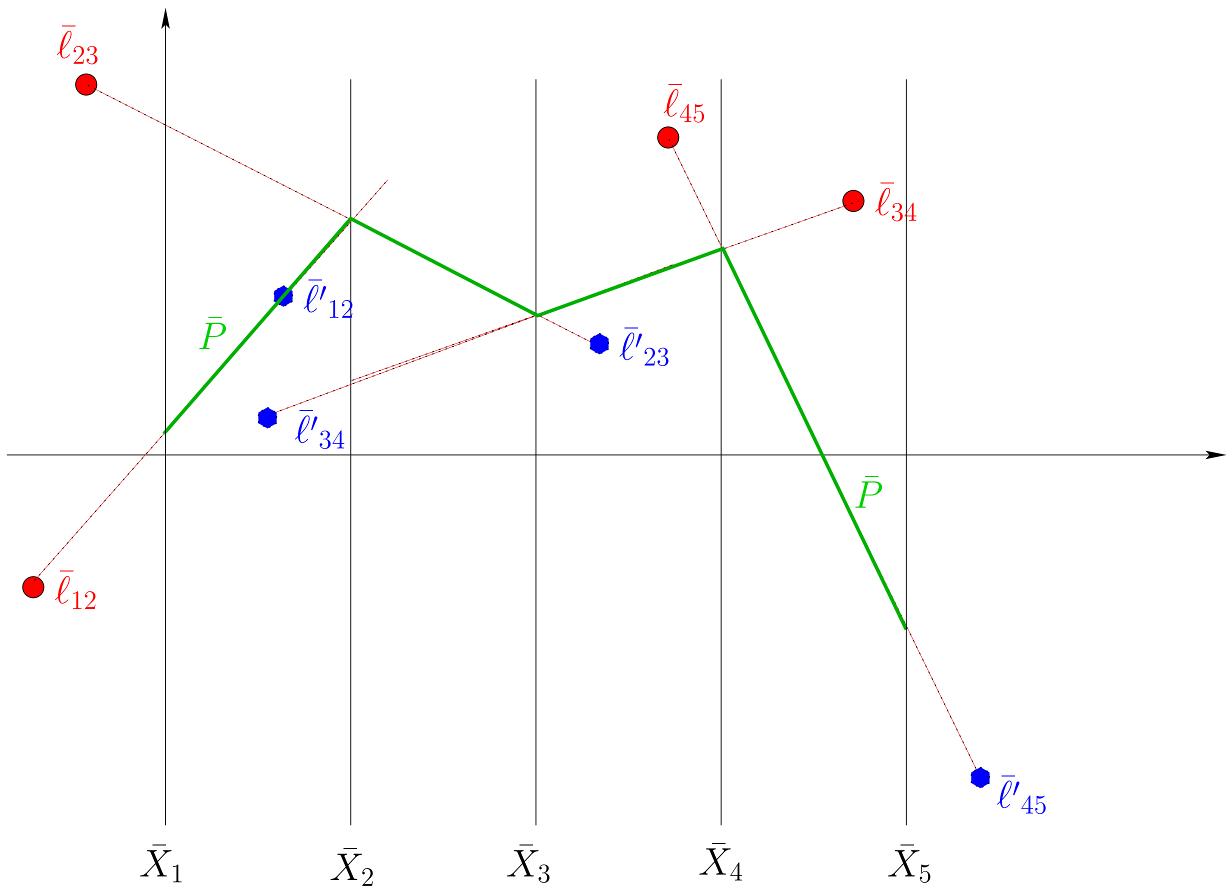

Figure 3.6: Two intersecting lines in 5-D.

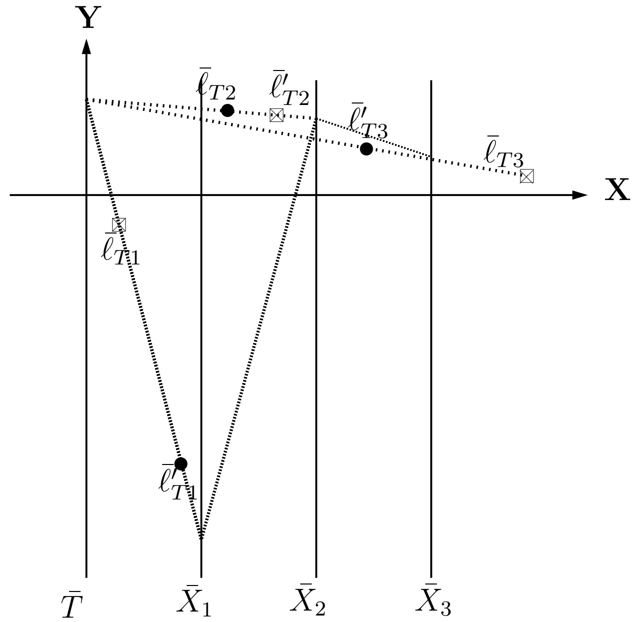

Figure 3.7: Intersection, for the base-variable line description, of two lines in 4-D. This provides the space **and time** coordinates of the place where two particles moving with constant velocity collide.

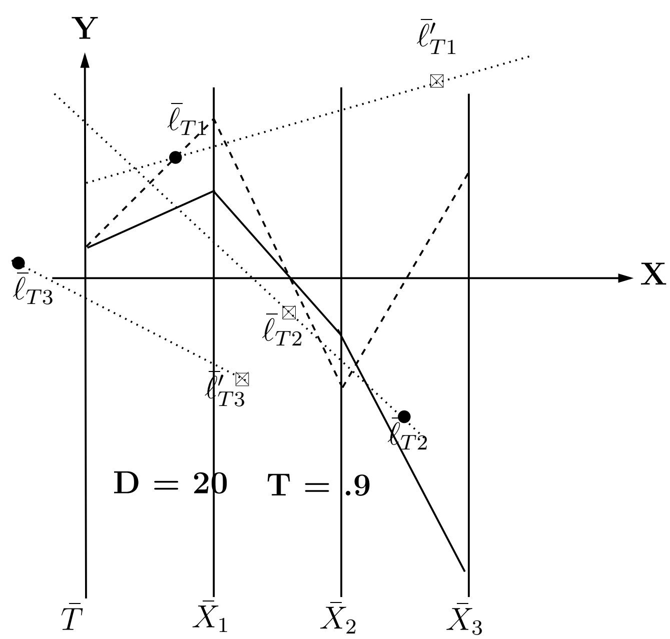

Figure 3.8: Non-intersection between two lines in 4-D. Here the minimum distance is 20 and occurs at time = .9. Note the maximum gap on the $\bar{T}$-axis formed by the lines joining the $\bar{\ell}$'s with the same subscript. The polygonal lines representing the points where the minimum distance occurs are shown and they have the *same* value of T.

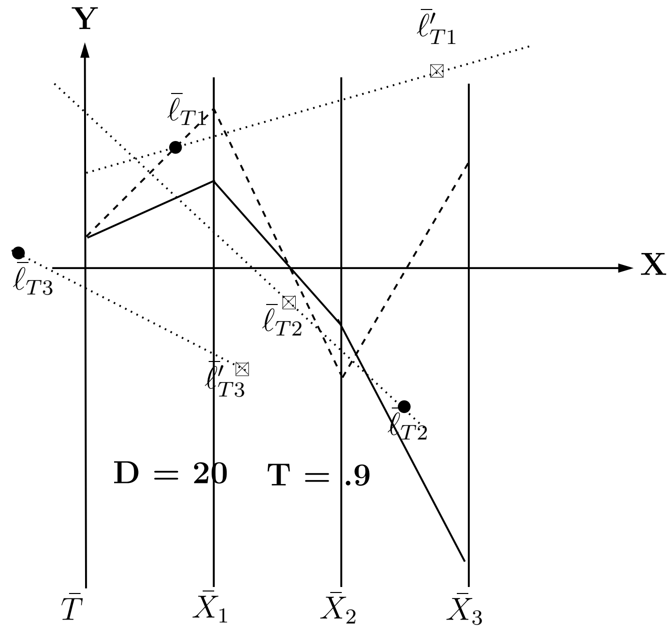

Figure 3.9: Non-intersection between two lines in 4-D. Here the minimum distance is 20 and occurs at time = .9. Note the maximum gap on the $\bar{T}$-axis formed by the lines joining the $\bar{\ell}$'s with the same subscript. The polygonal lines representing the points where the minimum distance occurs are shown and they have the *same* value of T.

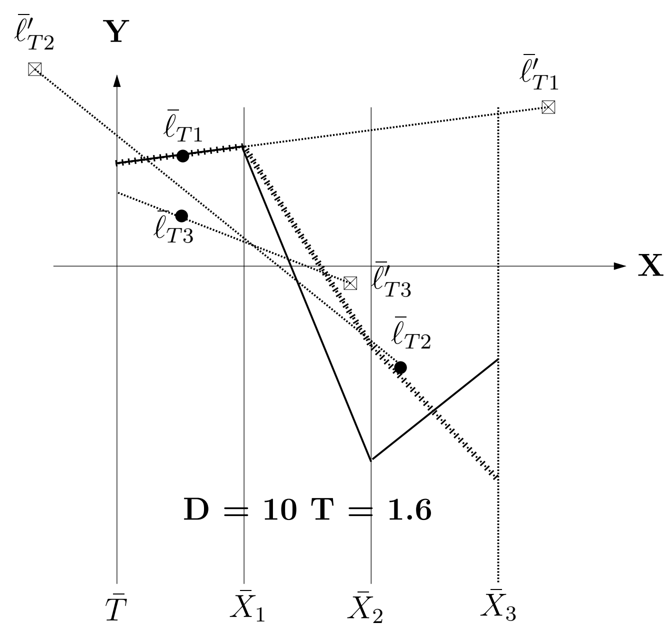

Figure 3.10: Non-intersection between two lines in 4-D. Here the minimum distance is 10 and occurs at time = 1.6. Note the the diminishing maximum gap on the $\bar{T}$-axis formed by the lines joining the $\bar{\ell}$'s with the same subscript and compare with Fig. **??**. The polygonal lines representing the points where the minimum distance occurs are shown.

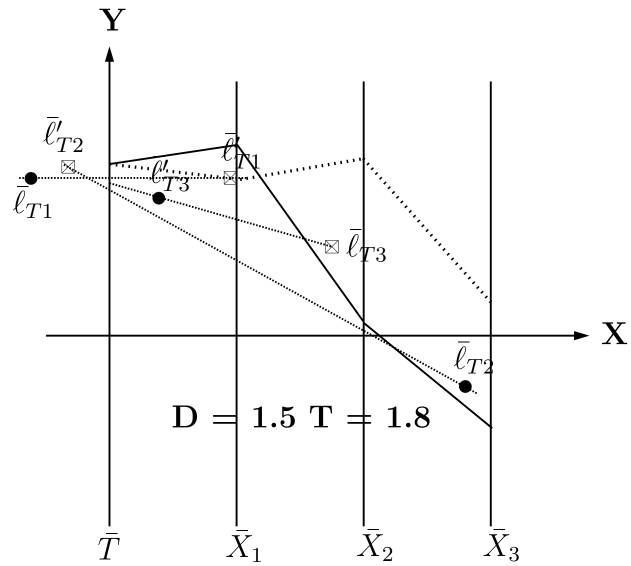

Figure 3.11: Near intersection between two lines in 4-D. Here the minimum distance is 1.5 and occurs at time = 1.8. Note the the diminished maximum gap on the $\bar{T}$-axis formed by the lines joining the $\bar{\ell}$'s with the same subscript. The polygonal lines representing the points where the minimum distance occurs are shown.

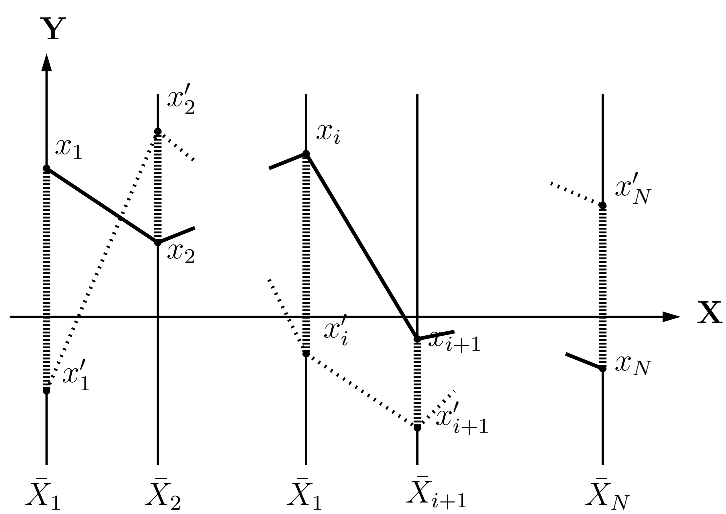

Figure 3.12: L_1 distance between the points $P = (x_1, ..., x_i, ..., x_N)$ and $P' = (x'_1, ..., x'_i, ..., x'_N)$.

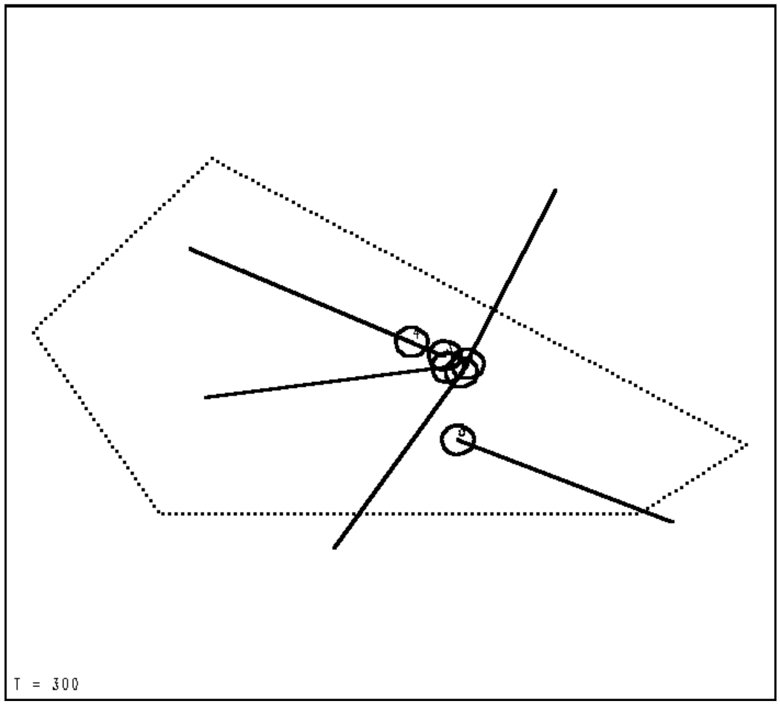

Figure 3.13: Conflicts, indicated by overlaping circles, within the next 5 minutes.

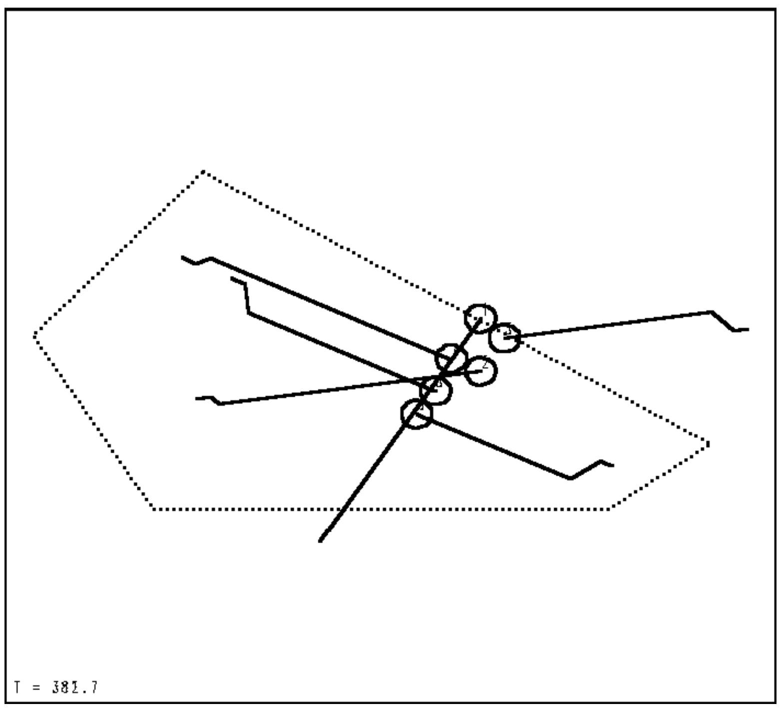

Figure 3.14: Conflict resolution with parallel-offset maneuvers. Three pairs of tangent circles.

Chapter 4

Planes, p-flats & Hyperplanes

Vertical Line Representation

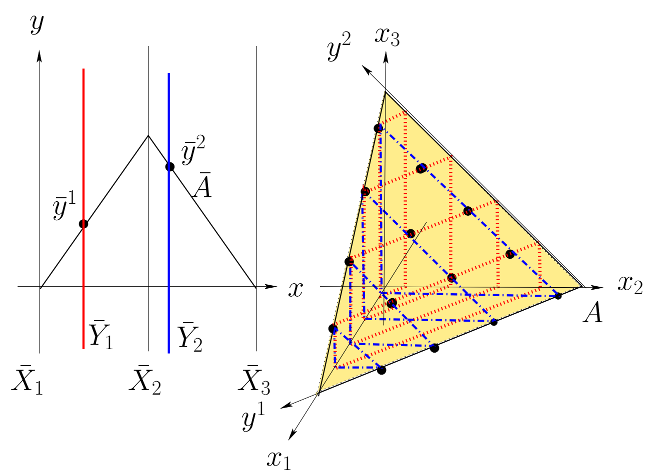

Figure 4.1: A plane π in $\mathbb{R}^3$ represented by two vertical lines and a polygonal line.

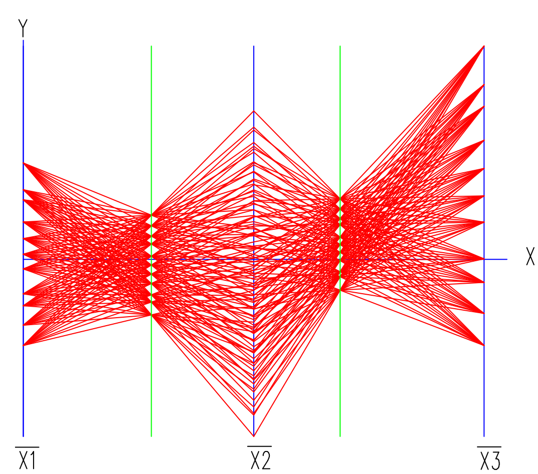

Figure 4.2: A set of coplanar points on a regular grid in $\mathbb{R}^3$ with the two vertical lines pattern.

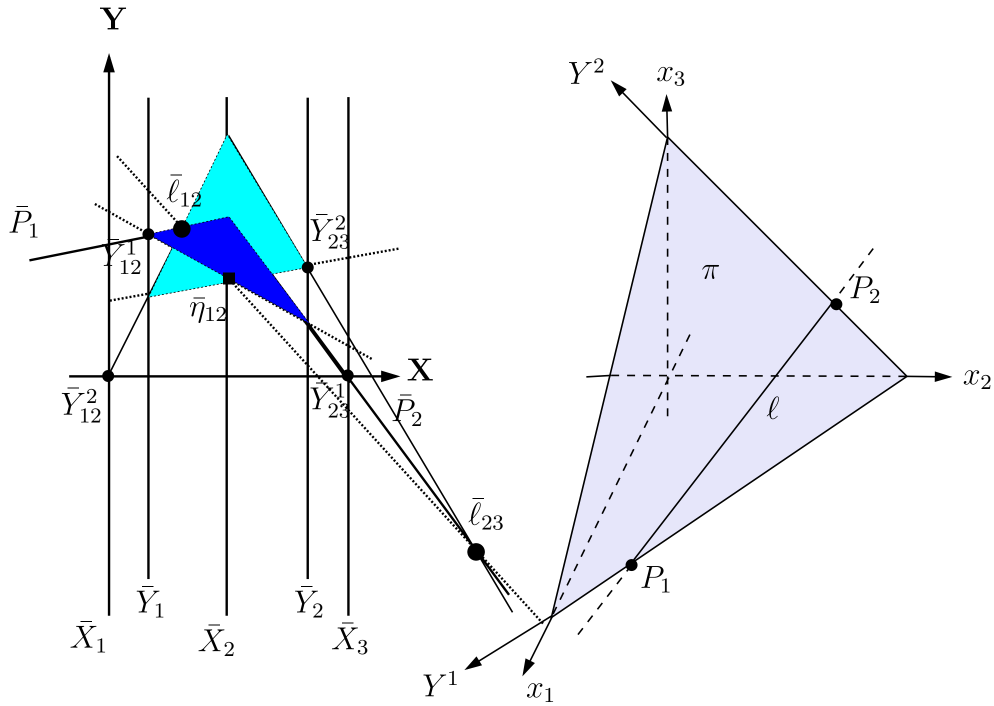

Figure 4.3: A line ℓ on a plane π is represented by one point $\bar{\eta}_{12}$ with respect the coordinates axes $\bar{Y}_1$ and $\bar{Y}_2$. This point is collinear with the two points $\bar{\ell}_{12}$ and $\bar{\ell}_{23}$ – a consequence of Desargues Projective Geometry theorem.

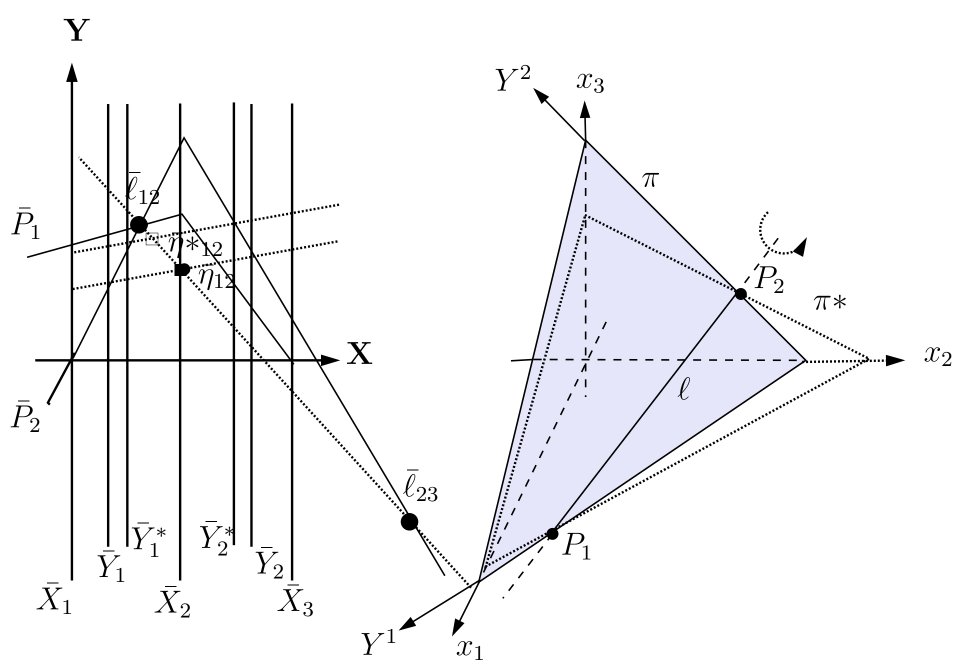

Figure 4.4: Rotation of a plane about a line $\leftrightarrow$ Translation of a point along a line.

$$\ell : \begin{cases} \ell_{12} & : \quad x_2 = m_2 x_1 + b_2 \\ \ell_{23} & : \quad x_3 = m_3 x_2 + b_3 \quad . \end{cases} \tag{4.1}$$

each value of k determines a position of the rotated plane and, in turn, the translated position $\bar{\eta}_{12}$:

$$\bar{\eta}_{12} = \left(\frac{m_3^2 - 2m_3 - k^2}{m_3^2 - m_3 + k^2(m_2 - 1)} \quad , \quad - \frac{b_2 k^2 + m_3 b_3}{m_3^2 - m_3 + k^2(m_2 - 1)} \right) \tag{4.2}$$

In $\mathbb{R}^N$ a hyperplane is represented by a coordinate system with $N-1$ vertical axes and a polygonal line representing the origin.

Representation by Indexed Points

The family of "Super-Planes" $\mathcal{E}$

Define the axes positions by $(d_1, d_2, ..., d_N)$ as shown in Fig. **??** and consider the set of points $P \in \mathbb{R}^N$ whose representation in $\|$-coords collapses to a straight line. That is, $\bar{P} \, : \, y = mx + b \Rightarrow$

$$P = (md_1 + b, \, md_2 + b, \ldots, md_N + b) = m(d_1, \, d_2, \ldots, d_N) + b(1, \ldots, 1) \; . \tag{4.3}$$

Allowing $m, b \in \mathbb{R}$ to vary, it is clear that for each axes spacing $(d_1, d_2, ..., d_N)$ the P form a 2-dimensional subspace in $\mathbb{R}^N$ called *super-plane* (abbr. *sp*).

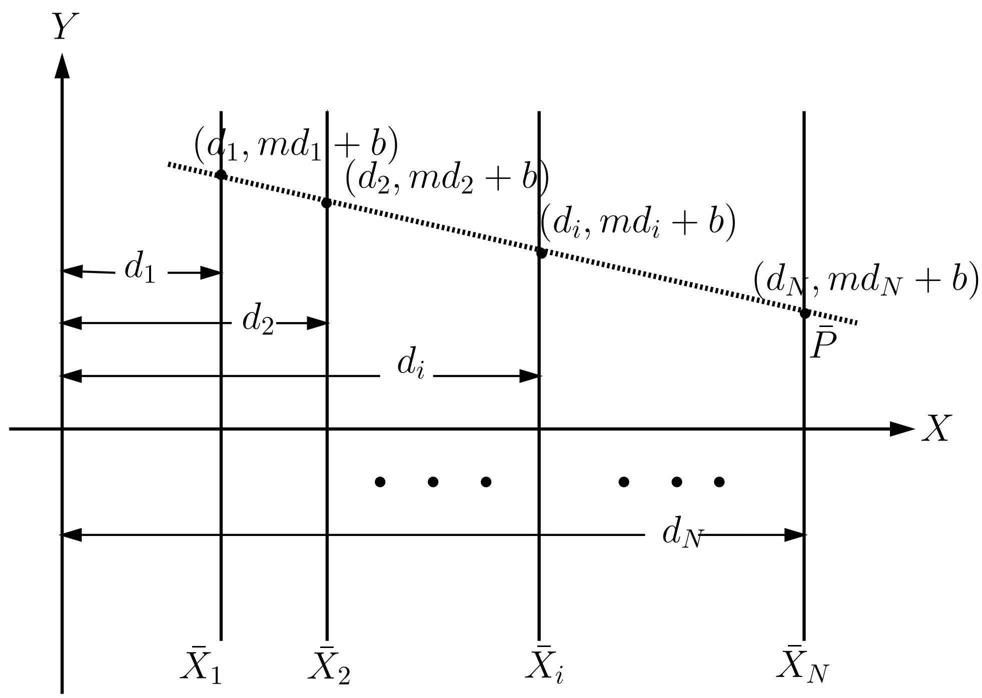

Figure 4.5: Points in $\mathbb{R}^N$ represented by lines.

Setting $m = b = 0$ and $m = 0, b = 1$ it is seen that each *sp* contains the points $(0, 0, ..., 0), (1, 1, ..., 1)$ and hence contains the line u on these two points. The collection of *sp* for all axes spacings is the family of 2-dimensional subspaces on the line u and plays a very important role in the development. Note that for a line on an *sp* all its representing points coincide.

For $\mathbb{R}^3$ the *sp* are given by:

$$\pi^s : (d_3 - d_2)x_1 + (d_1 - d_3)x_2 + (d_2 - d_1)x_3 = 0\,. \tag{4.4}$$

For the standard axes spacing used so far i.e. $d_1 = 0, d_2 = 2, d_3 = 2$ the corresponding *sp*, called the first *sp* is :

$$\pi^s_1 : x_1 - 2x_2 + x_3 = 0 \tag{4.5}$$

For a plane

$$\pi \ : \ c_1x_1 + c_2x_2 + c_3x_3 = c_o\ , \tag{4.6}$$

Next the axis $\bar{X}_1$ is translated to the position $\bar{X}'_1$ one unit to the right of the $\bar{X}_3$ providing the new axes spacing $d_1 = 4, d_2 = 1, d_3 = 2$. The corresponding *sp* is

$$\pi^s_{1'} : x_1 + x_2 - 2x_3 = 0\ . \tag{4.7}$$

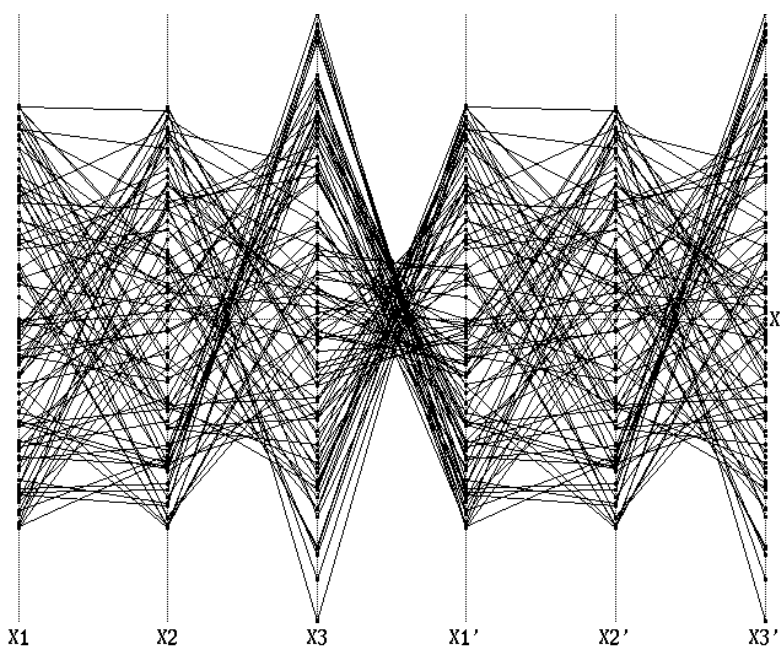

Figure 4.6: On the first 3 axes is a set of polygonal lines representing a randomly sampled set of points on a plane $\pi \subset \mathbb{R}^3$.

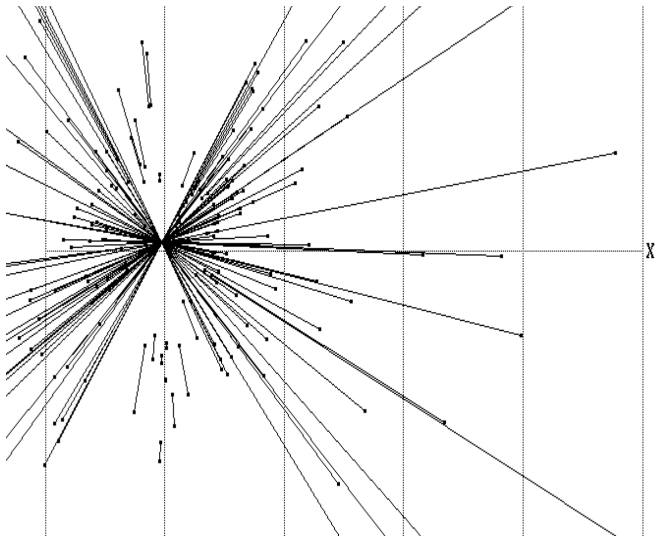

Figure 4.7: Coplanarity! In ∥-coords joining the pairs of points representing lines on a plane forms a pencil of lines on a point. The point shown is $\bar{\pi}_{123}$ in eq. (??). Recall also the 3-point-collinearity for multidimensional lines (previous chapter).

$$\ell_\pi = \pi \cap \pi_1^s \ : \begin{cases} \ell_{\pi_{12}} : \ \ x_2 = -\frac{c_1 - c_3}{c_2 + 2c_3} x_1 + \frac{c_o}{c_2 + 2c_3} \\ \\ \ell_{\pi_{23}} : \ \ x_3 = -\frac{2c_1 + c_2}{c_3 - c_1} x_2 + \frac{c_o}{c_3 - c_1}. \end{cases} , \tag{4.8}$$

The two points representing ℓ_π coincide since $\ell \subset \pi_1^s$ and in homogeneous coordinates

$$\bar{\pi}_{123} = \bar{\ell}_{\pi_{12}} = \bar{\ell}_{\pi_{23}} = (c_2 + 2c_3,\, c_o,\, c_1 + c_2 + c_3) \ . \tag{4.9}$$

This is the first indexed point for the representation of π. To understand its significance follow the next two figures. Next, the x_1 values of the coplanar points shown in Fig. **??**

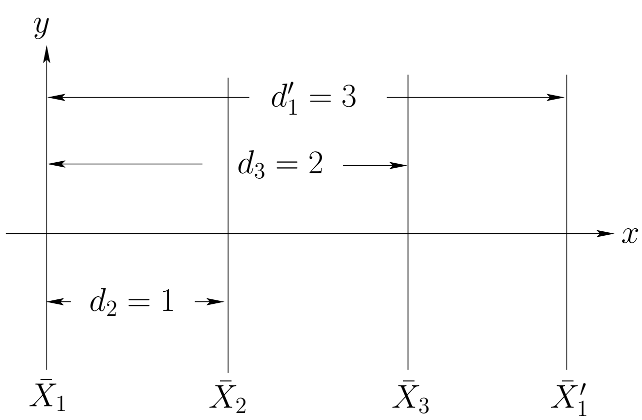

Figure 4.8: The axes spacing for the second super-plane $\pi^s_{1'}$.

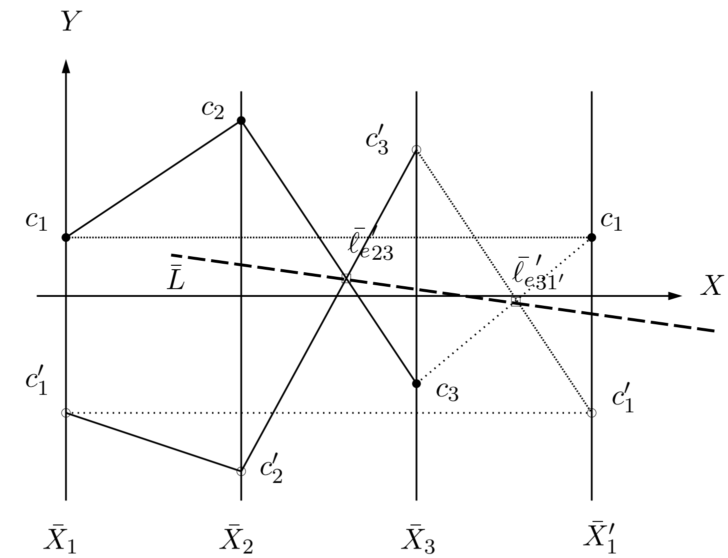

Figure 4.9: Transferring the values from the $\bar{X}_1$ to the $\bar{X}_{1'}$-axis.

are transfered to the $\bar{X}_{1'}$ axis – see Fig. **??** – and the construction in Fig. **??** is repeated providing the second point

$$\bar{\pi}_{231'} = \bar{\ell}'_{\pi_{1'2}} = \bar{\ell}'_{\pi_{23}} = (3c_1 + c_2 + 2c_3,\ c_o,\ c_1 + c_2 + c_3). \tag{4.10}$$

seen in Fig. **??**. These two points represent the plane π since their coordinates are uniquely determined by the coefficients of the plane in eq. (**??**).Geometrically, we have

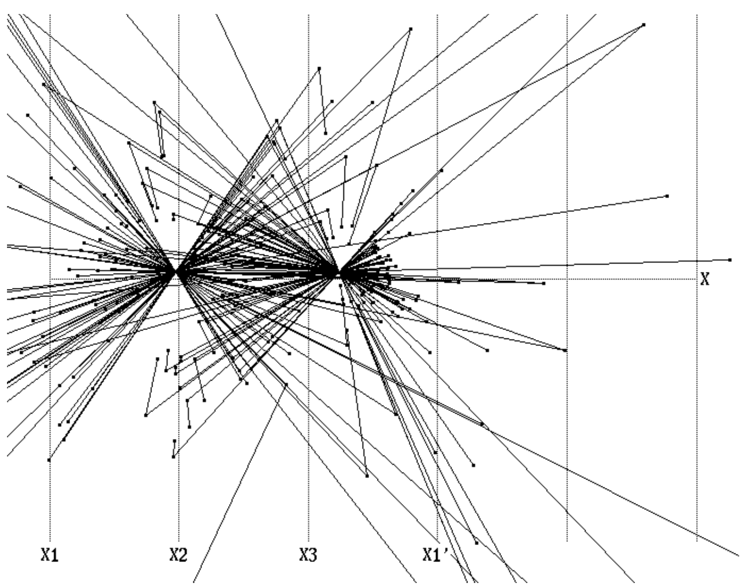

Figure 4.10: The plane π represented by two points

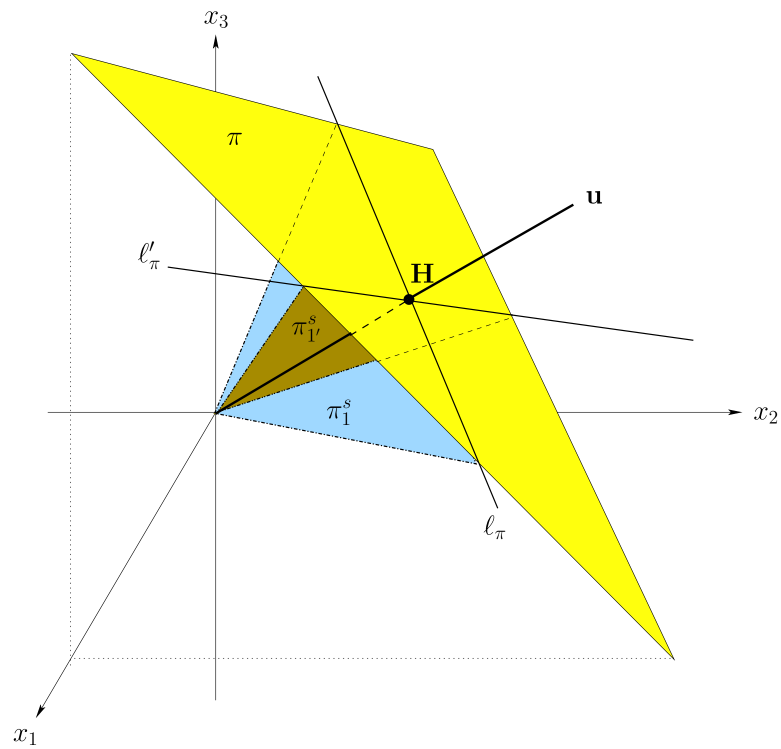

Figure 4.11: The intersections of a plane π with the two super-planes ${\pi^s}_1$ and $\pi^s_{1'}$ are two lines ℓ_π , ℓ'_π which specify the plane and provide its representation. This is the equivalent of the previous figure in Cartesian coordinates.

specified the plane π by the two lines $\ell_\pi,\ \ell'_\pi \subset \pi$ shown in Fig. **??**. A plane in $\mathbb{R}^3$ can be specified in terms of any two intersecting lines it contains. The reason for choosing the lines in the *sp* is that in $\|$-coords such lines are represented by **one** rather than two points and there are further advantages. Note that

$$\bar{\pi}_{231'} - \bar{\pi}_{123} = (3c_1, 0, 0)\ . \tag{4.11}$$

The four Indexed Points

Continuing, the $\bar{X}_2$ and $\bar{X}_3$ axes are each translated to positions $\bar{X}'_2$ and $\bar{X}'_3$ 3 units to the right providing the third

$$\pi^s_{1'2'} : -2x_1 + x_2 + x_3 = 0\ , \tag{4.12}$$

and similarly the fourth *sp* $\pi^s_{1'2'3'}$ enabling the construction of two more points shown in Fig. **??** As for the previous 2 points

$$\left\{ \begin{array}{l} \bar{\pi}_{31'2'} - \bar{\pi}_{231'} = (3c_2, 0, 0) \\ \bar{\pi}_{31'2'} - \bar{\pi}_{1'2'3'} = (3c_3, 0, 0)\ . \end{array} \right. \tag{4.13}$$

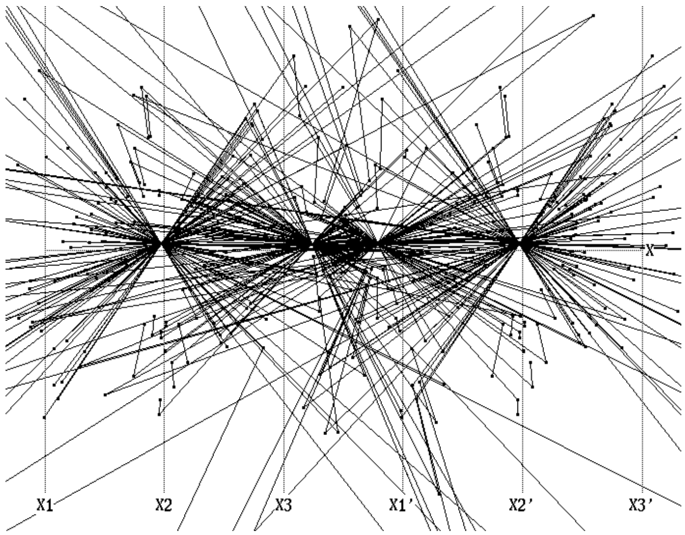

Figure 4.12: The plane π intersected with four super-planes. Each point represents one of the intersection lines.

It is easiy checked that the axes translations correspond to 120^o rotations of the *sp* π_1^s about the line u on the points $(0,0,0),(1,1,1)$ with $\pi_{1'2'3'}$ coinciding with π_1^s. To simplify notation the index permutation is unimportant so that $\pi_{231'} = \pi_{1'23}$. The representation of a hyperplane in $\mathbb{R}^N$ is given in terms of $N-1$ indexed points and an example is shown in Fig. **??** to **??**.

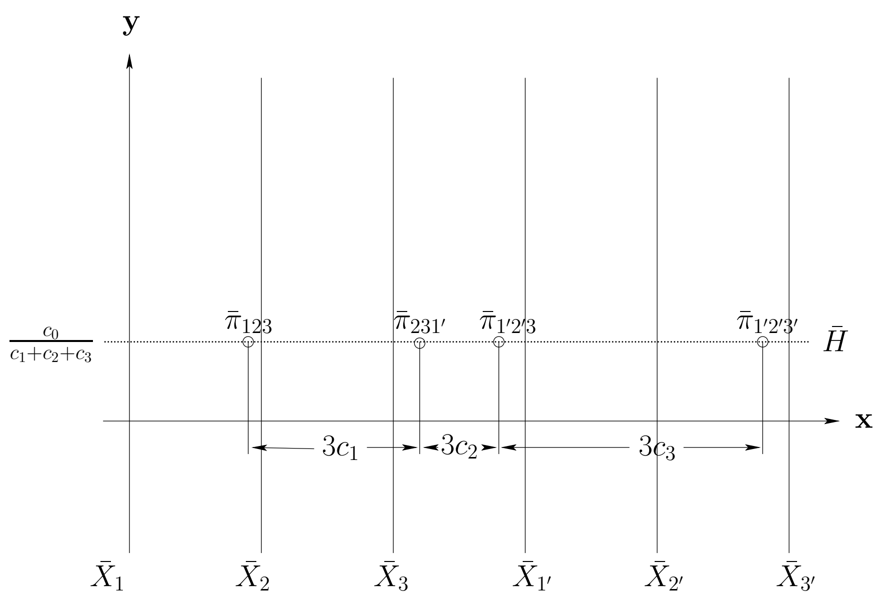

Figure 4.13: The distances between adjacent points are proportional to the *normalized* coefficients (divided by $S = c_1+c_2+c_3$) of $\pi : c_1x_1+c_2x_2+c_3x_3 = c_0$. The proportionality constant is the dimensionality of the space. The plane's equation can be read from the picture!

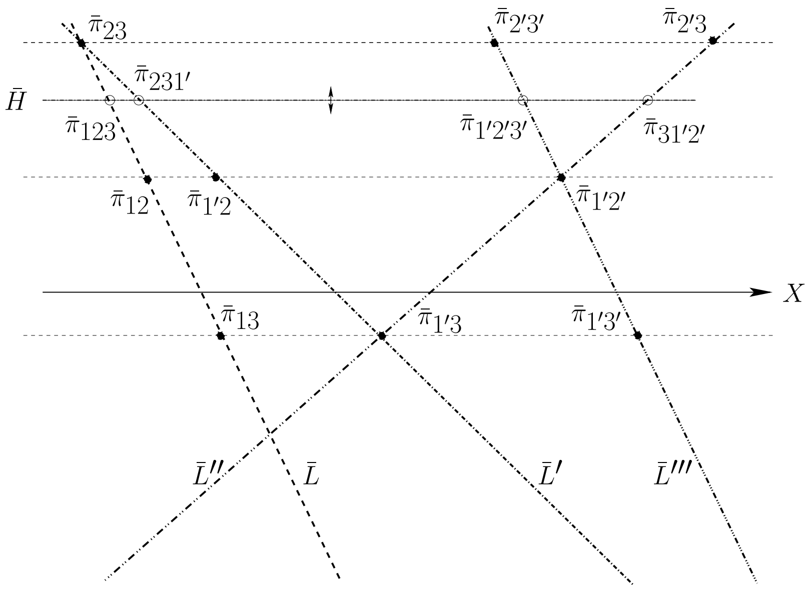

Figure 4.14: Rotation of a 2-flat (plane) about a 1-flat(line) in $\mathbb{R}^3$ corresponds to a translation of the points with 3 indices on the horizontal line $\bar{H}$ along the lines $\bar{L}$, $\bar{L}'$, $\bar{L}''$, $\bar{L}'''$ joining the points with 2 indices.

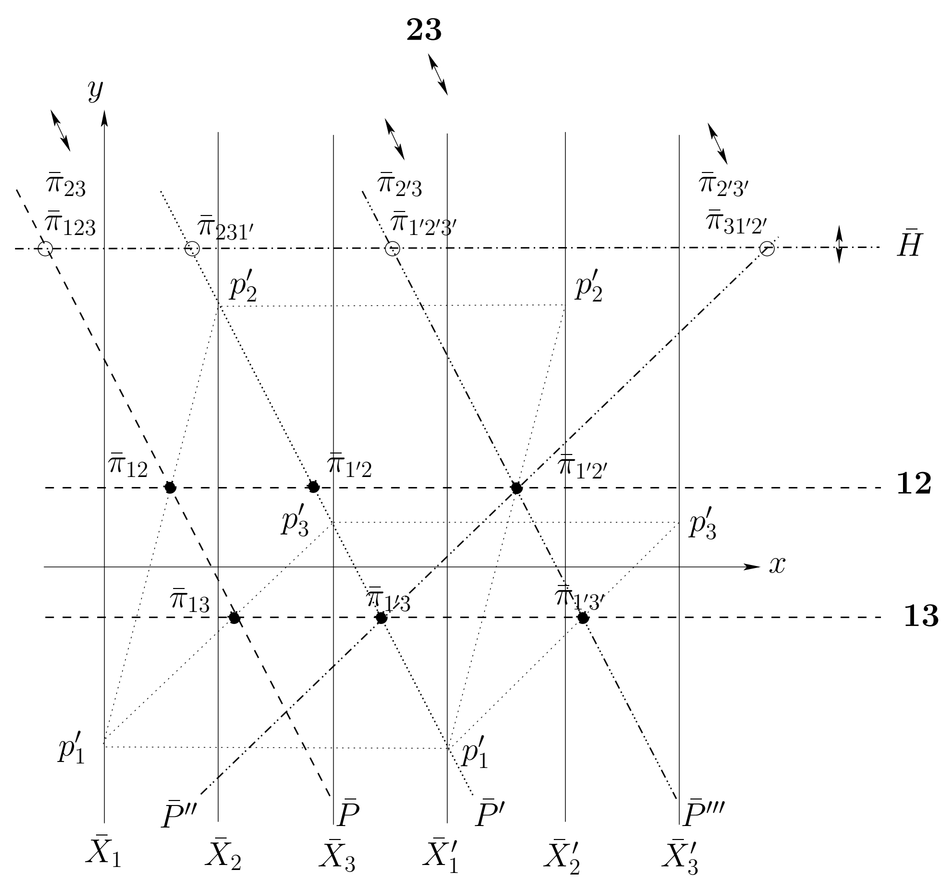

Figure 4.15: Rotation of a plane π^2 about a line π^1 such that c_1 remains constant.

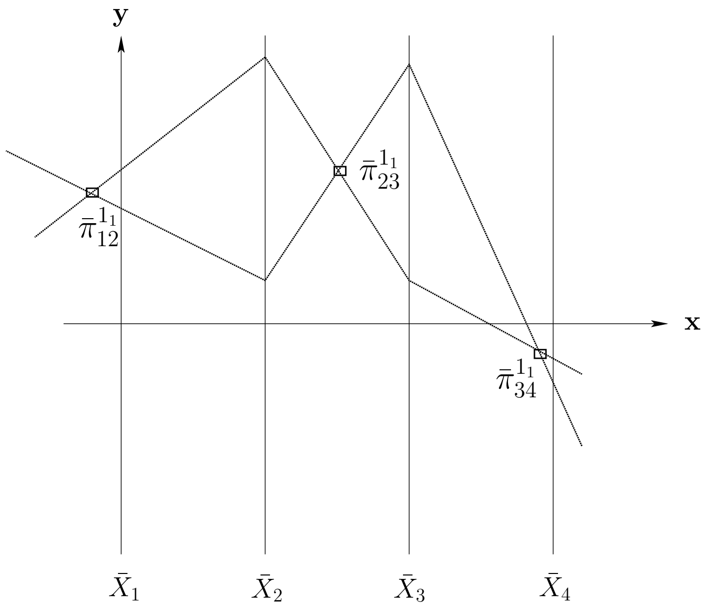

Figure 4.16: Recursive Construction in $\mathbb{R}^4$ – 1st step. A pair of points (polygonal lines) determines a line (1-flat) π^{1_1} represented by the 3 constructed points $\bar{\pi}^{1_1}_{i,i-1}$, $i = 1, 2, 3, 4$.

.

$\mathcal{R}$emarkably, the collinearity construction property can be extended to higher dimensions enabling the recursive (on the dimensionality) construction of the representation of p-flats for $2 \leq p \leq N - 1$. To achieve this some intermediate steps are needed. In the ensuing, we denote by $\pi^s_{1'...i'}$ the "super-plane" constructed by translating the axes $\bar{X}_1, \ldots, \bar{X}_i$ to the new positions $\bar{X}_{1'}, \ldots, \bar{X}_{i'}$. Here $d_i = N + i - 1$ and for easy reference the partially translated standard axes spacing is denoted by $S_{1'...i'}$.

The underpining of the construction algorithm for the point representation of a 2-flat $\pi^2 \subset \mathbb{R}^3$, as we saw, is the collinearity property. Namely for *any* $\pi^1 \subset \pi^2$ the points $\bar{\pi}^1_{12},\ \bar{\pi}^1_{13},\ \bar{\pi}^1_{23}$ are collinear with $\bar{\pi}_{123}$. The generalization for p-flats is also true. Without entering into the technical details yet for $\pi^{(p-2)_1},\ \pi^{(p-2)_2} \subset \pi^{(p-1)} \subset R^N$, let $\bar{L}_1$ and $\bar{L}_2$ be the lines determined by the corresponding two points

$$\bar{L}_1 \ : \ \bar{\pi}^{(p-2)_1}_{123...(p-1)}, \bar{\pi}^{(p-2)_1}_{23...(p-1)p}, \bar{L}_2 \ : \ \bar{\pi}^{(p-2)_2}_{123...(p-1)}, \bar{\pi}^{(p-2)_2}_{23...(p-1)p} .$$

Then

$$\bar{\pi}^{(p-1)}_{123...p} = \bar{L}_1 \cap \bar{L}_2 .$$

This is the basic recursive construction implied in the *Representation Mapping* stated formally below. Though the notation looks cumbersome the idea is not and to clarify it we illustrate it for $N = 4, p = 3$ in Figs. **??** through **??**. Starting with the polygonal lines on a 3-flat π^{3_1}, first the points $\bar{\pi}^{1_i}_{12}$, , $\bar{\pi}^{1_i}_{23}$, $\bar{\pi}^{1_i}_{34}$, representing 1-flats (lines) on π^3, are constructed and joined to form polygonal lines having 3 vertices (the points) joined by **two** lines. From the intersection of these new polygonal lines the points $\bar{\pi}^{2_j}_{123}$, , $\bar{\pi}^{2_j}_{234}$, representing 2-flats on π^{3_1}, are constructed. At any stage a point representing $\bar{\pi}^r$, where the superscript is the flat's dimension, is obtained by *any pair* of lines joining points representing a flat $\bar{\pi}^{r-1}$ where $\pi^{r-1} \subset \pi^r$

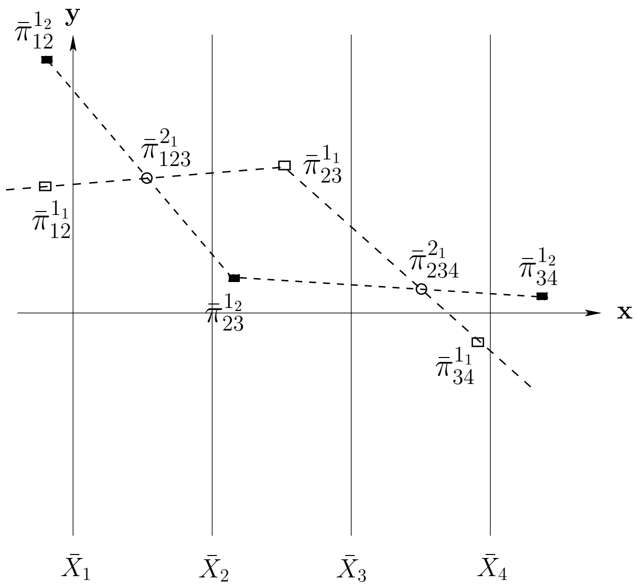

Figure 4.17: Recursive Construction in $\mathbb{R}^4$– 2nd step. The 1-flat π^{1_1} and another π^{1_2}, represented by the 3 black points, determine a 2-flat (plane) π^{2_1} represented by the two points $\bar{\pi}^{2_1}_{123}$, $\bar{\pi}^{2_1}_{234}$. These points are the intersections of the two polygonal lines joining the points obtained from the previous step representing 1-flats.

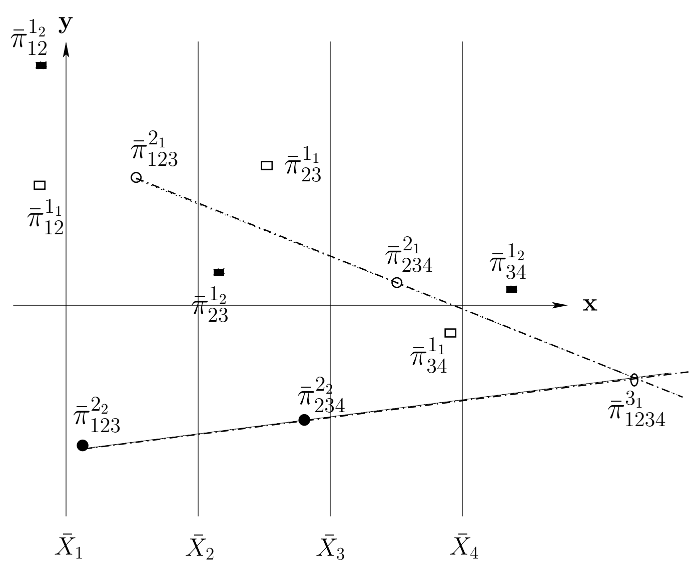

Figure 4.18: Recursive Construction in $\mathbb{R}^4$ – 3rd step. Two 2-flats, π^{2_1} constructed above and another π^{2_2} represented by the 2 black points, determine a 3-flat π^{3_1}. Pairs of points representing the same 2-flat are joined and their intersection is the point $\bar{\pi}^{3_1}_{1234}$. This is one of the 3 points representing the 3-flat. The "debris" from the previous constructions, points with fewer than 4 indices, can be discarded.

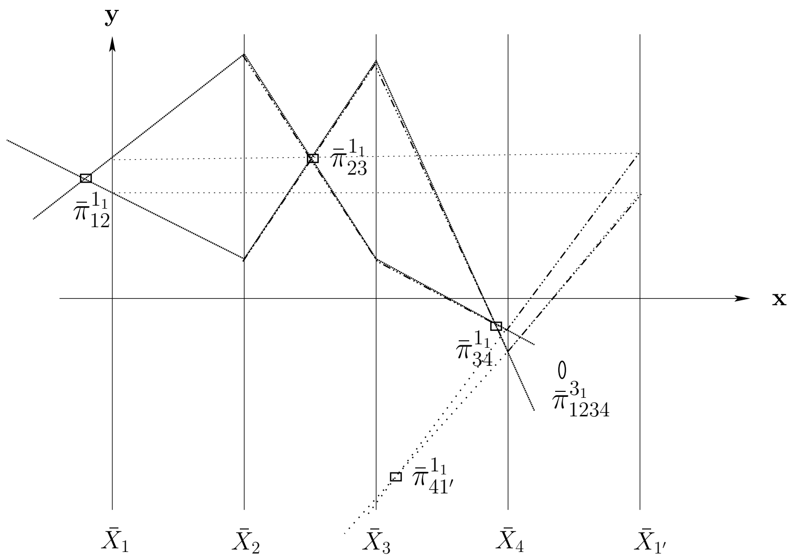

Figure 4.19: Recursive Construction in 4-D – 4th step. A new axis $\bar{X}_{1'}$ is placed one unit to the right of $\bar{X}_3$ and the x_1 values are transfered to it from the $\bar{X}_1$ axis. Points are now represented by new polygonal lines between the $\bar{X}_2$ and $\bar{X}_{1'}$ axes and one of the points $\bar{\pi}^{1_1}_{41'}$, representing the 1-flat π^{1_1} on the new triple of $\|$-coords axes, is constructed as in 1st step.

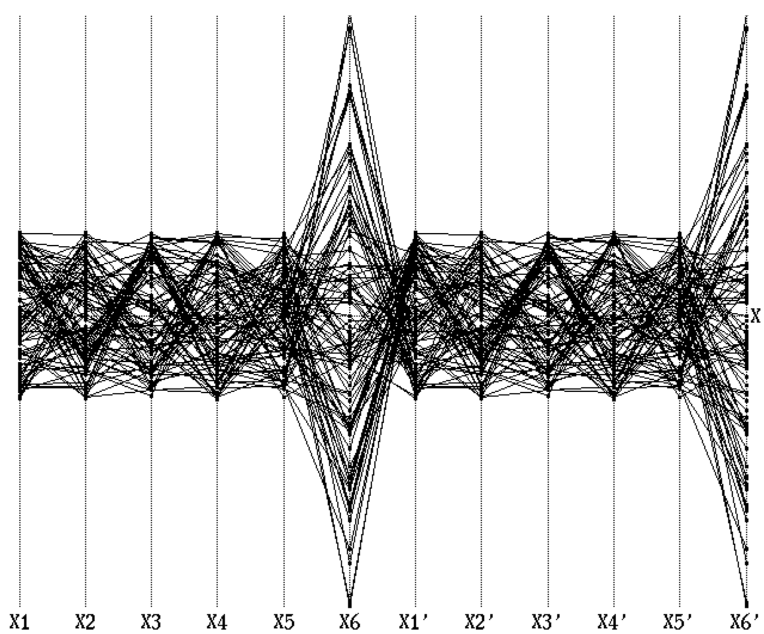

Figure 4.20: Polygonal lines on the $\bar{X}_1 \ldots \bar{X}_6$ axes representing randomly selected points on a 5-flat $\pi^5 \subset \mathbb{R}^6$.

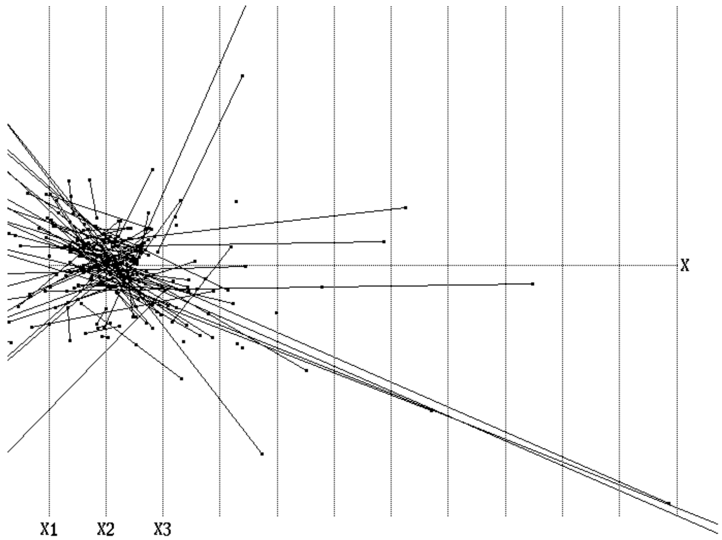

Figure 4.21: The $\bar{\pi}^{1_i}_{12}$, $\bar{\pi}^{1_i}_{23}$ portions of the 1-flats $\subset \pi^5$ constructed from the polygonal lines shown in Fig. **??**, no evident pattern.

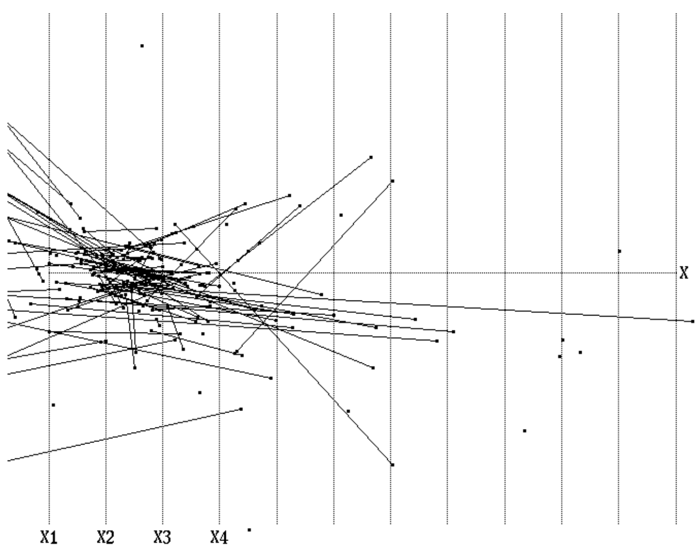

Figure 4.22: The $\bar{\pi}^{2_i}_{123}$, $\bar{\pi}^{2_i}_{234}$ portions of the 2-flats $\subset \pi^5$ constructed from the polygonal lines joining $\bar{\pi}^{1_i}_{12}$, $\bar{\pi}^{1_i}_{23}$, $\bar{\pi}^{1_i}_{34}$.

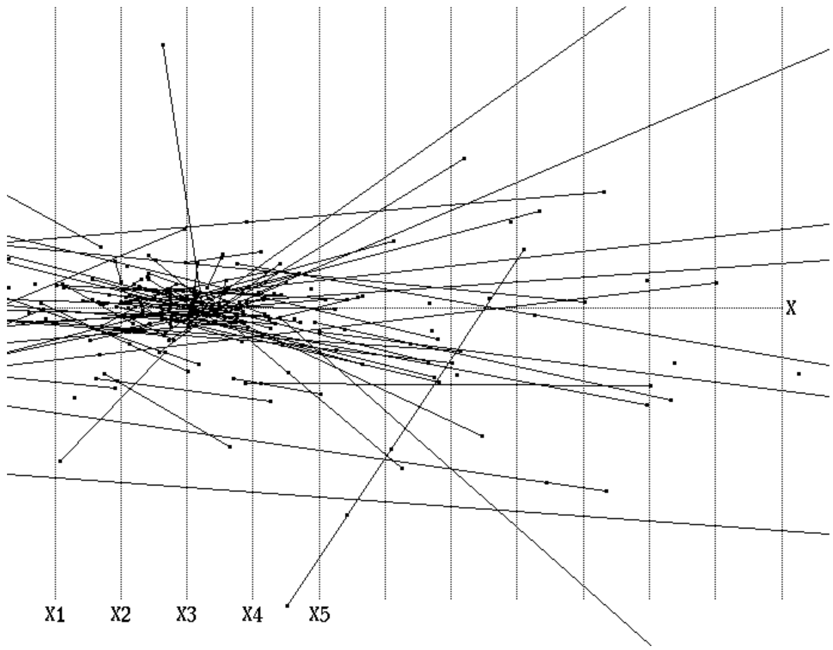

Figure 4.23: The $\bar{\pi}^{3_i}_{1234}$, $\bar{\pi}^{3_i}_{2345}$, of the 3-flats $\subset \pi^5$ constructed from the polygonal lines joining $\bar{\pi}^{2_i}_{123}$, $\bar{\pi}^{2_i}_{234}$, $\bar{\pi}^{2_i}_{345}$. Nothing yet ... but wait!

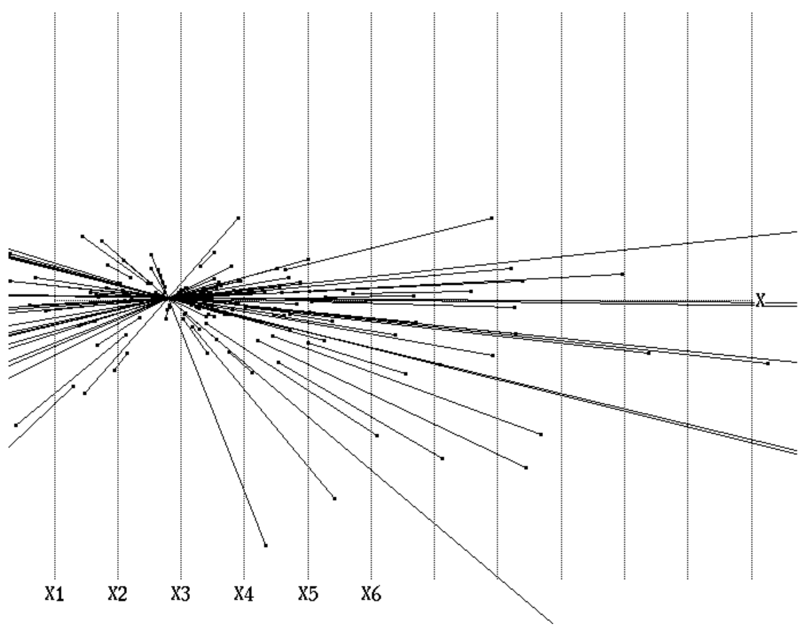

Figure 4.24: This is it! The $\bar{\pi}^{4_i}_{12345}$, $\bar{\pi}^{4_i}_{23456}$ of the 4-flats $\subset \pi^5$ constructed from the polygonal lines joining $\bar{\pi}^{3_i}_{1234}$, $\bar{\pi}^{3_i}_{2345}$, $\bar{\pi}^{3_i}_{3456}$. This shows that the original points whose representation is in Fig. **??** are on a 5-flat in $\mathbb{R}^6$. The remaining points of the representation are obtained in the same way.

Figure 4.25: The full representation of π^5. The coefficients of its equation are still the distances between sequentially indexed points as in Fig. ?? for $\mathbb{R}^3$.

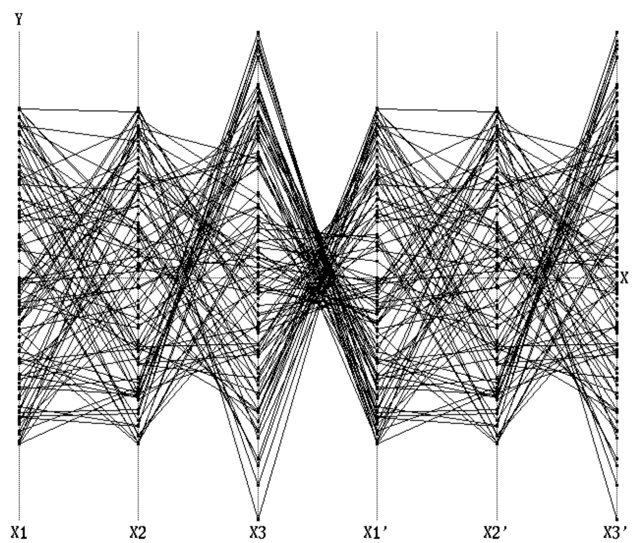

Figure 4.26: Polygonal lines representing a randomly selected set of "nearly" coplanar points (i.e. on a "slab")

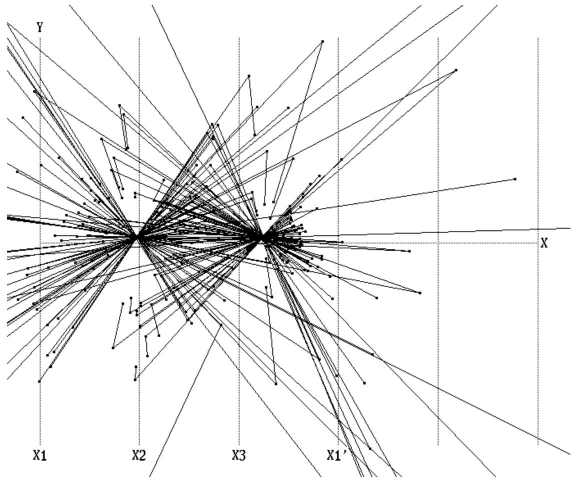

Figure 4.27: Representation of lines formed from the points shown in Fig. ??. The pattern for “near-coplanarity” is very similar to that obtaind from coplanarity

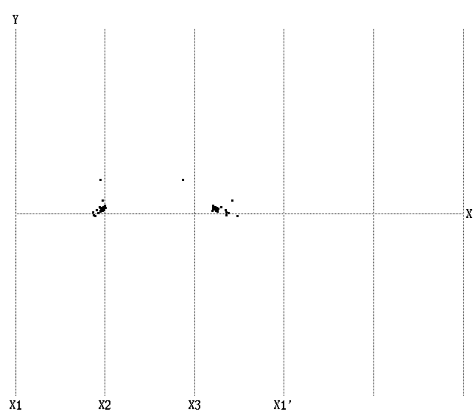

Figure 4.28: Close clusters from the intersection of the lines shown in Fig. ??

Chapter 5

Curves

Point-Curves and Line-Curves

$\mathcal{R}$ecall the point-to-line correspondence in the plane

$$P : (p_1, p_2, p_3) \longrightarrow \bar{P} : [(p_1 - p_2), dp_3, -dp_1] \ , \tag{5.1}$$

where the distance between the x_1 and x_2 axes is d, and the triples within [...] and within (...) denote line and point homogeneous coordinates respectively. For regular (i.e. in the Euclidean plane) points

$$P : (p_1, p_2, 1) \longrightarrow \bar{P} : [(p_1 - p_2), d, -dp_1].$$

The second half of the duality is the line-to-point correspondence :

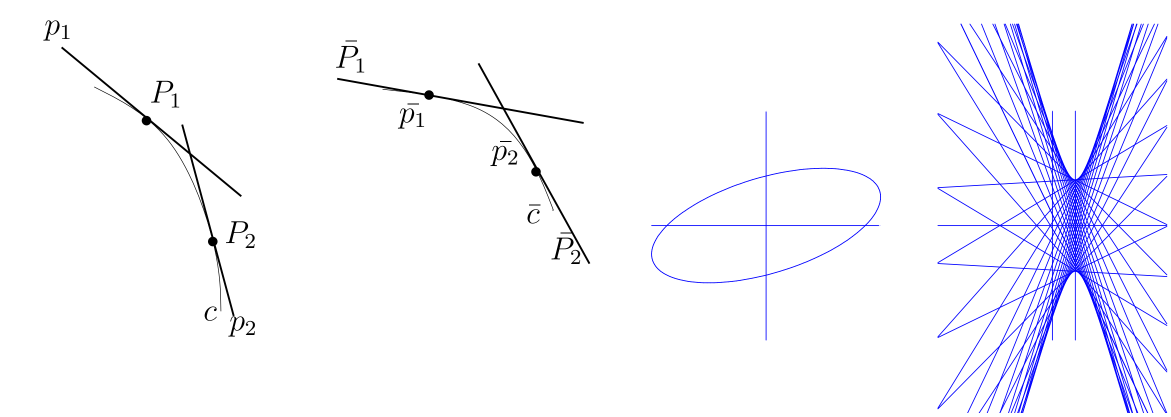

Figure 5.1: **Point-curve** and their **line-curve** images.

$$\ell : [a_1, a_2, a_3] \longrightarrow \bar{\ell} : (da_2, -a_3, a_1 + a_2), \tag{5.2}$$

for the line $\ell : a_1x_1 + a_2x_2 + a_3 = 0$. When $a_2 \neq 0$, the slope of ℓ is $m = -\frac{a_1}{a_2}$ and the intercept $b = -\frac{a_3}{a_2}$ so :

$$\ell : [m, -1, b] \longrightarrow \bar{\ell} : (d, b, 1 - m). \tag{5.3}$$

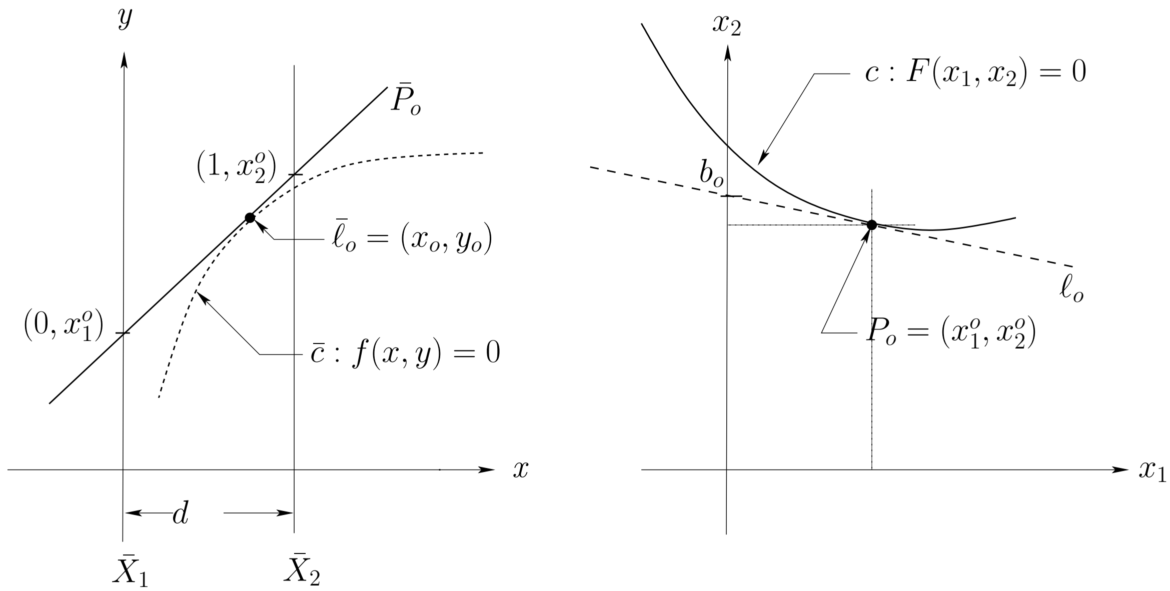

Figure 5.2: Obtaining the *point-curve* $\bar{c}$ directly from the *point-curve* c.

A way to obtain (**??**) from (**??**) is to find the *envelope* of all the lines $\bar{P}$ which are the images of the points $P \in \ell$. Applied to each point of a smooth point-curve c results in the image $\bar{c}$ a line-curve as shown in Fig. **??** and the correspondence.

$$point - curve \leftrightarrow line - curve\,.$$

Point-Curves from Point-Curves

$\mathcal{E}$arly in the development (1980) of $\|$-coords the direct construction of the a curve's image as a **point curve** was accomplished as outlined below. Among benefits this when applied judiciously avoids **over-plotting** by the plethora of the lines which are the tangents at the *non-convex* portions of the image curve. Consider a general planar curve c given by :

$$c \;:\; F(x_1, x_2) = 0, \tag{5.4}$$

Substituting in eq. (**??**) yields the point-coordinates

$$x = \frac{\partial F/\partial x_2}{(\partial F/\partial x_1 + \partial F/\partial x_2)}\;,\; y = \frac{(x_1 \partial F/\partial x_1 + x_2 \partial F/\partial x_2)}{(\partial F/\partial x_1 + \partial F/\partial x_2)}. \tag{5.5}$$

There is an important special case when the original point-curve is given explicitly by $x_2 = g(x_1)$. Then eq. (**??**) reduces to :

$$x = \frac{1}{1 - g'(x_1)}\;,\; y = \frac{x_2 + x_1 g'(x_1)}{1 - g'(x_1)} \tag{5.6}$$

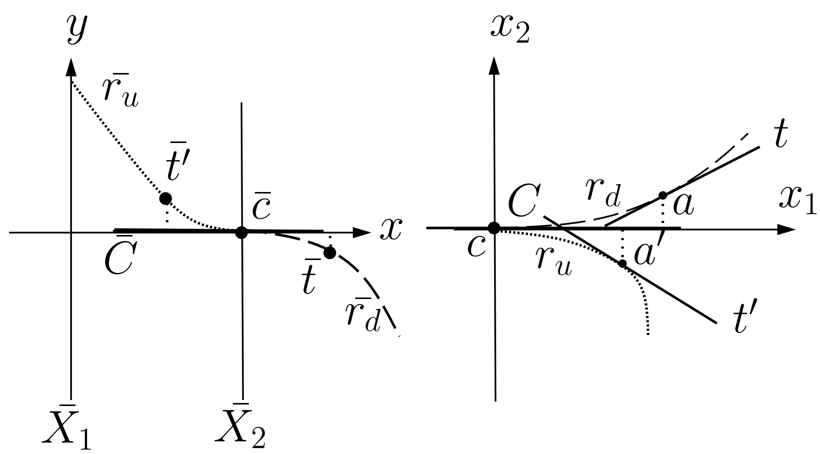

Figure 5.3: Cusp $\leftrightarrow$ Inflection point duality is independent of the curves' orientation.

Conic Transforms

The treatment is particularly pleasing for the conic sections which are described by the quadratic function

$$\begin{aligned} F(x_1, x_2) &= A_1 {x_1}^2 + 2A_4 x_1 x_2 + A_2 {x_2}^2 + 2A_5 x_1 + 2A_6 x_2 + A_3 = \\ &= (x_1, x_2, 1) \begin{pmatrix} A_1 & A_4 & A_5 \\ A_4 & A_2 & A_6 \\ A_5 & A_6 & A_3 \end{pmatrix} \begin{pmatrix} x_1 \\ x_2 \\ 1 \end{pmatrix}, \end{aligned} \tag{5.7}$$

where the type of conic is determined by the sign of the *discriminant* $\Delta = ({A_4}^2 - A_1 A_2)$. The coefficient matrix is denoted by A and its determinant, which plays an important role in the development, is

$$detA = A_3(A_1 A_2 - {A_4}^2) - A_1 {A_6}^2 - A_2 {A_5}^2 + 2A_4 A_5 A_6 \ . \tag{5.8}$$

For conics, using the identity that for a polynomial F of degree n $F(\mathbf{x}) = 0 \Rightarrow \nabla F \cdot \mathbf{x} = \nabla F \cdot \mathbf{x} - nF$ with the second expression being linear, eq. (**??**) and becomes

$$\begin{aligned} x &= \frac{A_4 x_1 + A_2 x_2 + A_6}{[(A_1 + A_4)x_1 + (A_2 + A_4)x_2 + (A_5 + A_6)]} \\ y &= -\frac{A_5 x_1 + A_6 x_2 + A_3}{[(A_1 + A_4)x_1 + (A_2 + A_4)x_2 + (A_5 + A_6)]} \ . \end{aligned} \tag{5.9}$$

These are *Mobius*[1] transformations which form a group (see a good book in modern Algebra). This observation enables substantial simplifications of the earlier treatment of conics and their transforms (see [**?**] and [**?**]). The *inverse*, expressing x_1 and x_2 in terms of x and y, is a Mobius transformation of the form

$$x_1 = \frac{a_{11}x + a_{12}y + a_{13}}{a_{31}x + a_{32}y + a_{33}} \ , \ x_2 = \frac{a_{21}x + a_{22}y + a_{23}}{a_{31}x + a_{32}y + a_{33}} \ , \tag{5.10}$$

[1]Also called *linear rational* transformations.

The conclusion is that

$$\textit{conics in the } xy-plane \;\leftrightarrow\; \textit{conics in the } x_1x_2-plane$$

Classification of the Conic Transforms

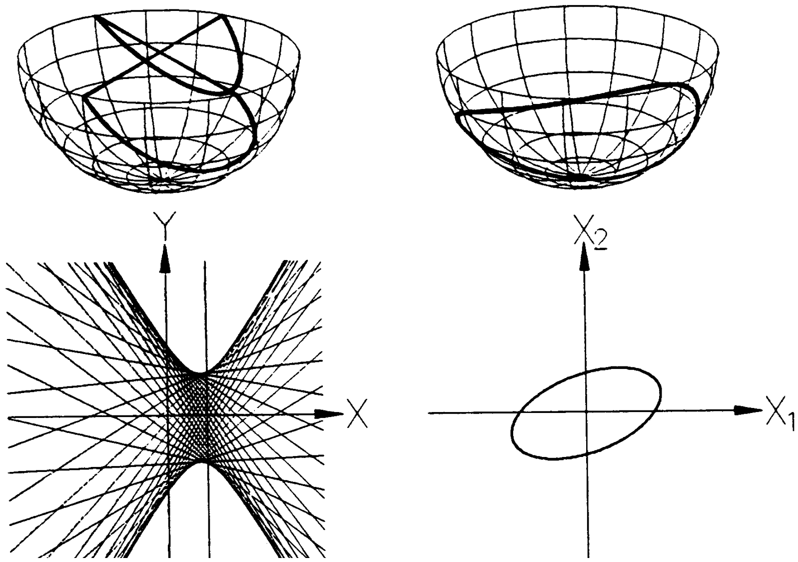

Figure 5.4: Ellipses always map into hyperbolas. Each assymptote is the image of a point where the tangent has slope 1.

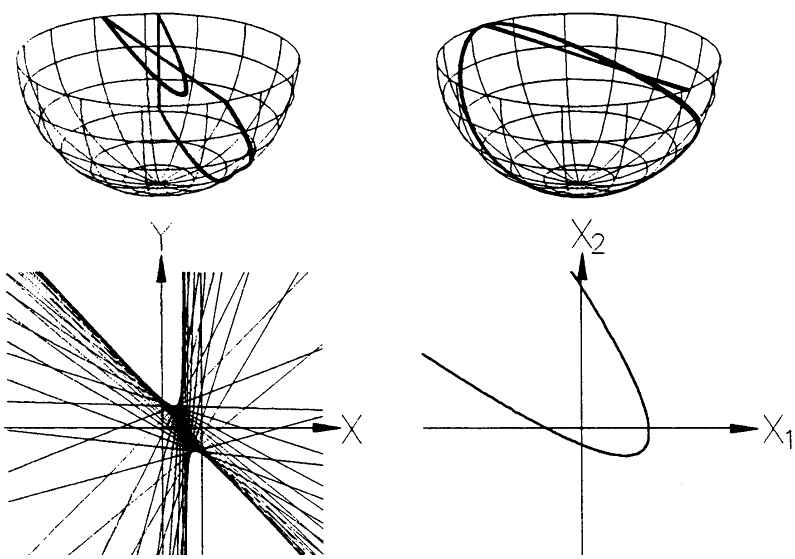

Figure 5.5: A parabola whose ideal point **not** in a direction with slope 1 always transforms to a hyperbola with a vertical assymptote. The other assymptote is the image of the point where the parabola has tangent with slope 1.

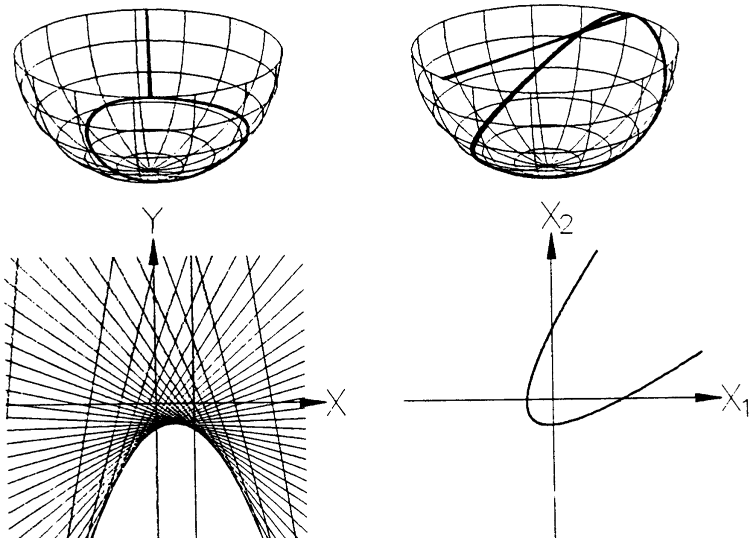

Figure 5.6: A parabola whose ideal point has direction with slope 1 transforms to a parabola - self-dual.

Transforms of Algebraic Curves

Conic transforms are studied for two reasons. For one, it is the ease of use of Mobius transformations which is completely general for *Quadrics*, the surfaces prescribed by quadratic equations, in *any dimension*. For another they are a model for the far more general curves, regions and their ramifications to be seen shortly.

A few words are in order on the transforms of algebraic curves, those described by polynomial equations, in general. An algebraic curve c has many invariants which are properties independent of the particular coordinate system used. Examples are the num-

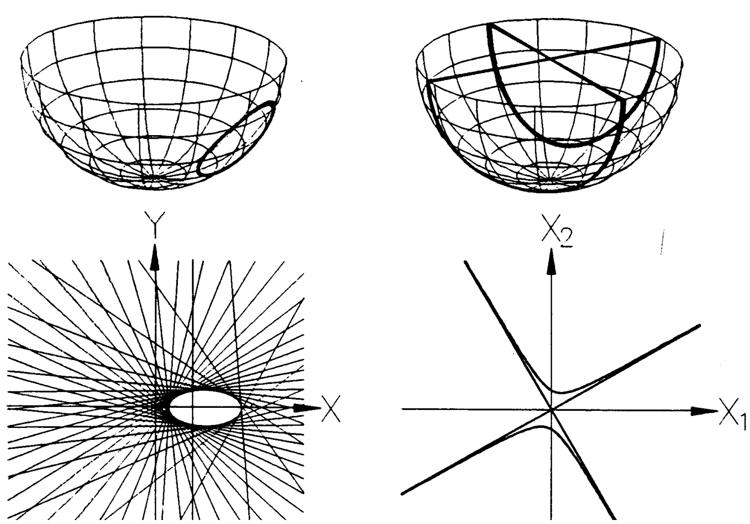

Figure 5.7: Hyperbola to ellipse – dual of case shown in Fig. **??**

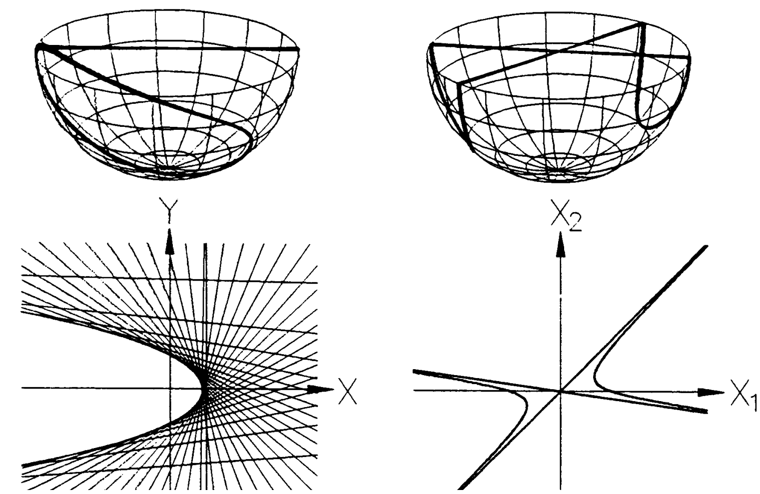

Figure 5.8: Hyperbola to parabola. This occurs when one of the assymptotes has slope 1 – dual of case shown in Fig. **??**

.

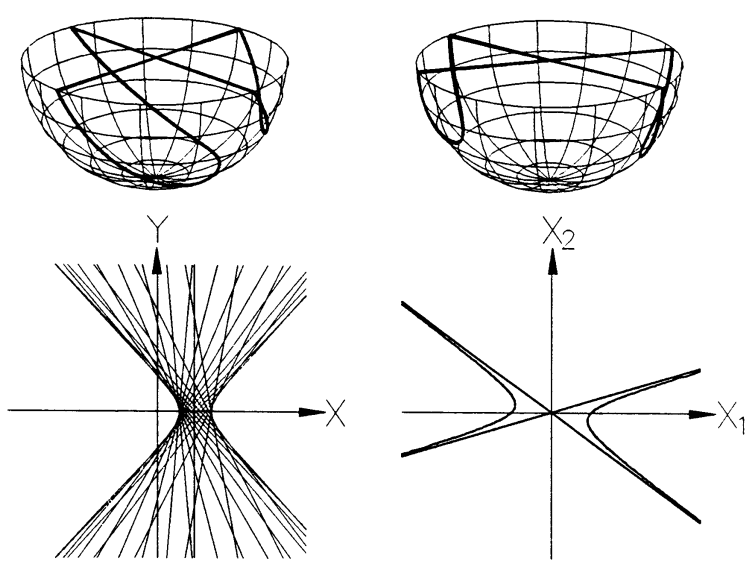

Figure 5.9: Hyperbola to hyperpola – self-dual case.

ber of components in its graph, *degree* n, number of *double-points* d (points where the curve crosses itself once), *cusps* s, *inflection points* ip and *bitangents* b (i.e. tangents at *two* points). The results here apply to any curve c and its *dual* curve c^* for **any** point $\leftrightarrow$ line duality. The same symbols with he $*$ superscript denote the dual's invariants. Algebraic curves and their duals have been studied extensively starting in 1830 by the mathematician and physicist Julius Plücker who also made other important contributions to the field.

Of interest here are the relations between a curve's invariants and those of its dual. As indicated in the equalities tabulated below, in addition to the $ip \leftrightarrow cusp$ duality, see already in Fig. **??**, there is a *bitangent* $\leftrightarrow$ *double* $-$ *point* duality. This is reasonable for the two tangents at a double-point map into the two points on a bitangent which is the double-point's image and in fact it is true for general and not just algebraic curves. The

Point(s) on curve $c \rightarrow$	**map into points of the curve** $\bar{c} \Rightarrow$	**relation**
The 2 points of c on a bitangent	map into a double-point of $\bar{c}$	$b = d^*$.
A double-point of c	maps into two points on a bitangent of $\bar{c}$	$d = b^*$.
An inflection-point of c	maps into a cusp of $\bar{c}$	$ip = s^*$.
A cusp of c	maps into an inflection-point of $\bar{c}$	$s = ip^*$.

Table 5.1: Equalities between invariants of algebraic curves and their duals.

dual of c is an algebraic curve whose degree n^* depends n and the invariants d, s as given by the *Plücker class formula* :

$$n^* = n(n-1) - 2d - 3s \ . \tag{5.11}$$

For $n = 2$ the *Plücker* class formula yields $n^* = 2$ and $s^* = 0$ confirming the conclusions in section **??**.

The polynomial describing the dual c^* can be found for *any point* $\leftrightarrow$ *line* duality by two different methods ([**?**] p. 74). However, with $n^* = O(n^2)$ and the complexity increasing rapidly with the number of non-zero coefficients of the polynomial specifying c the process is very tedious. All this applies to $\bar{c}$, which is the image under the particular $\|$-coords duality, when c is an algebraic curve c whose properties are immediately available

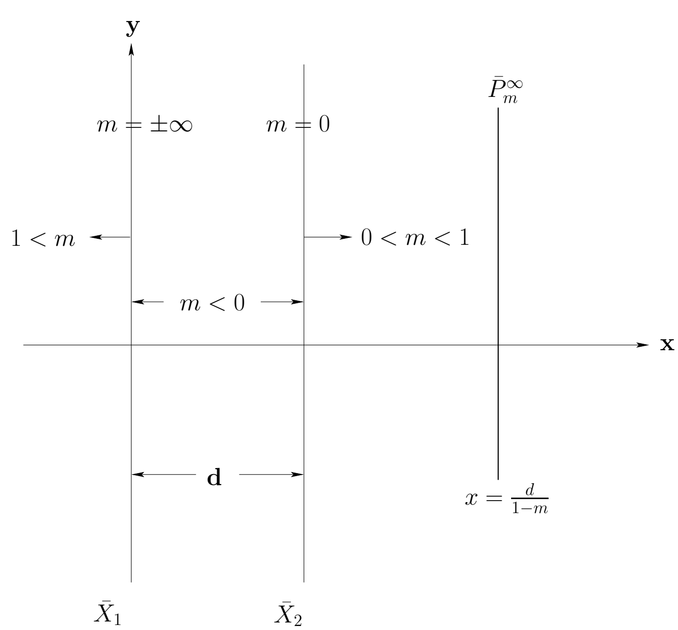

Figure 5.10: Horizontal position of $\bar{\ell}$ depends only on the slope m of ℓ.

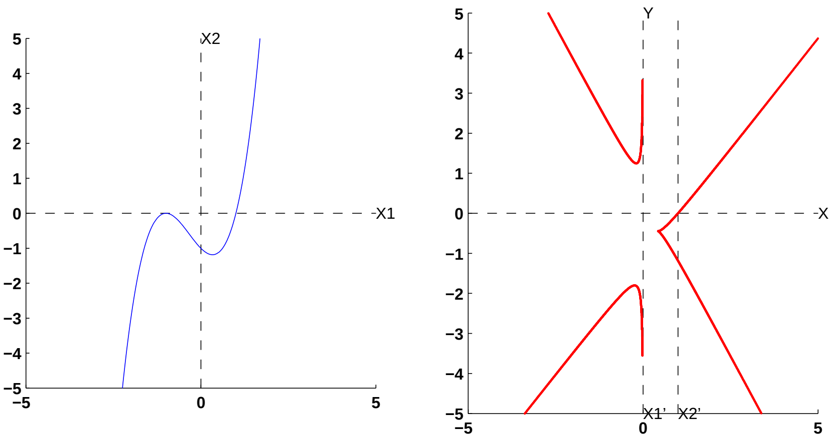

Figure 5.11: The image of algebraic curve $c : x_2 = x_1^3 + x_1^2 - x_1 - 1$ (left) degree 6.

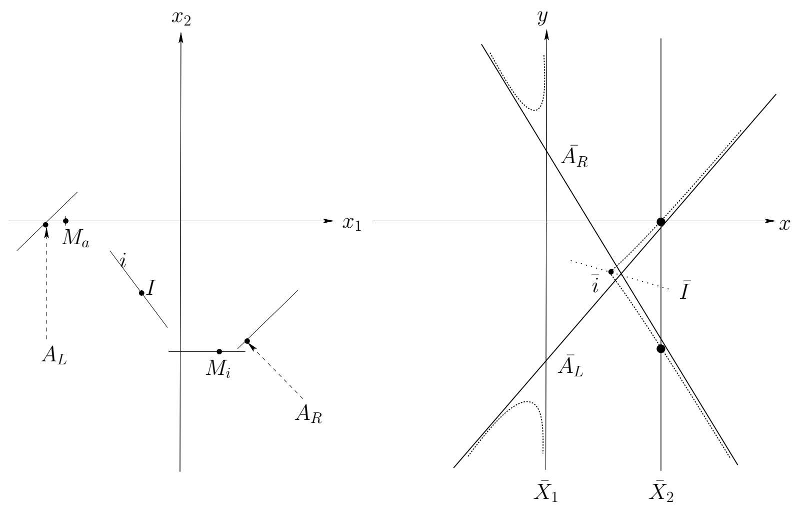

Figure 5.12: Analysis of the image curve.

The portions of the original curve c above are specified in terms of the slope (left) at the cubic curves' important points.

from *Plücker*'s results. Together with the qualitative considerations discussed and a good curve-plotter a complete grasp of $\bar{c}$ and its properties can be obtained. This avoids the laborious process of obtaining the polynomial for $\bar{c}$ *and its subsequent computation for plotting.* Unless the curve is given explicitly, and its transform is easily obtained via eq. (**??**), there is no sensible reason to work with the image of algebraic curves in $\|$-coords. The price in finding the polynomial equation of raised degree and then computing the curve is too steep with no benefit. The same curve can be computed numerically and directly from eq. **??**. Alternatively one can work with approximations as is done routinely in Geometric Modeling and other applications.

Curve Plotting

*T*he image of a piecewise smooth curve can be computed and plotted via eq. (**??**). Qualitatively we can learn quite a bit from some elementary considerations of the duality

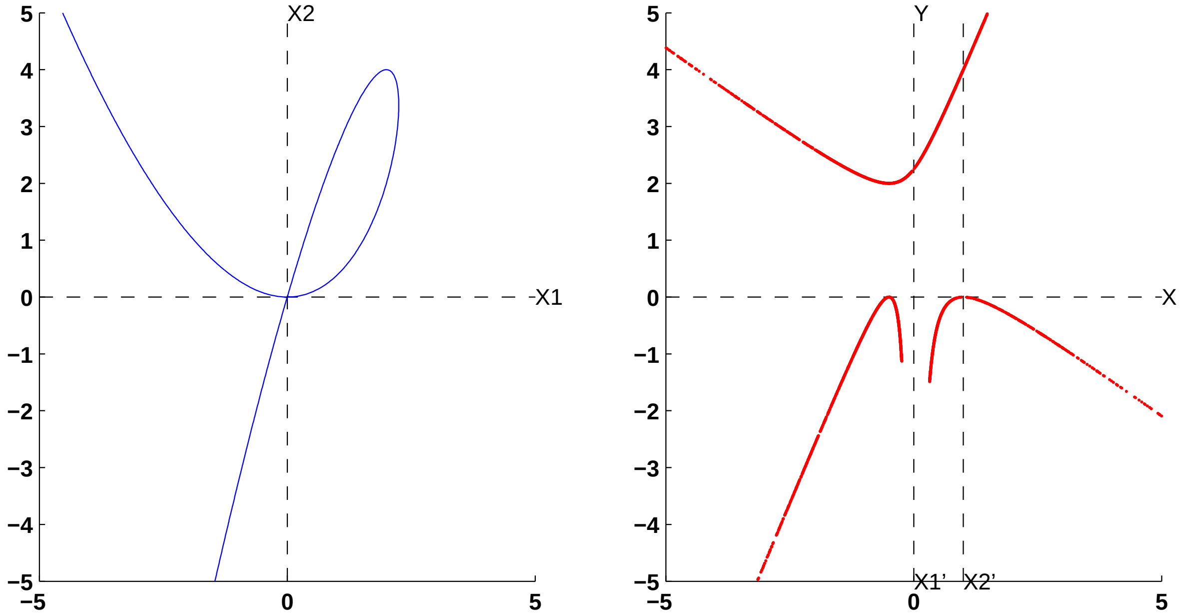

Figure 5.13: The image of the curve $c : F(x_1, x_2) = x_1^3 + x_1^2 - 3x_1x_2 = 0$ has degree 4. Here the crossing-point at the origin is transformed into a bitangent of the image curve an example of the *crossing-point* $\leftrightarrow$ *bitangent* duality.

by reviewing Fig. **??**, which we saw earlier, helping us sketch the curve's image. The accompanying curves and their images, chosen to hone our experenience, are drawn using a "curve-plotter" based on MATLAB[2].

For the curve c on the left of Fig. **??**, $n = 3, d = 0, s = 0$, hence for the image curve (right) is $n^* = 6$. The analysis is facilitated by Fig. **??**. The curve c has slope $m = 1$ at the points A_L and A_R causing the image curve $\bar{c}$ to split, the points of tangency there are mapped to ideal points. The portion c_I of c between A_L and A_R has the the right branch of $\bar{c}$ as its the image. The inflection point I is mapped into the cusp $\bar{i}$ of $\bar{c}$ in between the two axes since its slope m_i is negative. On c_I the curve's slope m are $m_i \leq m < 1$ and for this reason $\bar{c}_I$ opens to the right intersecting the $\bar{X}_2$ at two points; the images of the tangents at the extrema where $m = 0$ the higher for the higher intercept (i.e. b) in this case the maximum M_a of c. The left portion of c_I maps into the upper portion of the of $\bar{c}_I$ and approaching $\bar{A}_L$ assymptotically. Similarly the right portion of c_I being *cu* maps into the lower portion which is *cd* approaching $\bar{A}_R$ assympotically. The left portion of $\bar{c}$ approaches the $\bar{X}_1$-axis assymptotically as $|x_1| \to \infty$ and the curve's slope $m \to \infty$. Note that the symmetry of c with respect to the tangent i at I is transformed to symmetry with respect to the line $\bar{I}$ through the cusp $\bar{i}$ the point image of the tangent i

In the next example shown in Fig. **??** the image curve has degree $n^* = 4$ since $n = 3, d = 1, s = 0$. Both points of c where $m = 1$ are to the right of the double-crossing point with the part c_R to the right of these points is mapped into the upper portion of c. The remaining part c_L of c containing the double-point is mapped into two branches each

[2]This beautiful curve-plotter was written by Tal Tzur and Gilat Schwartz for their course project in 2004.

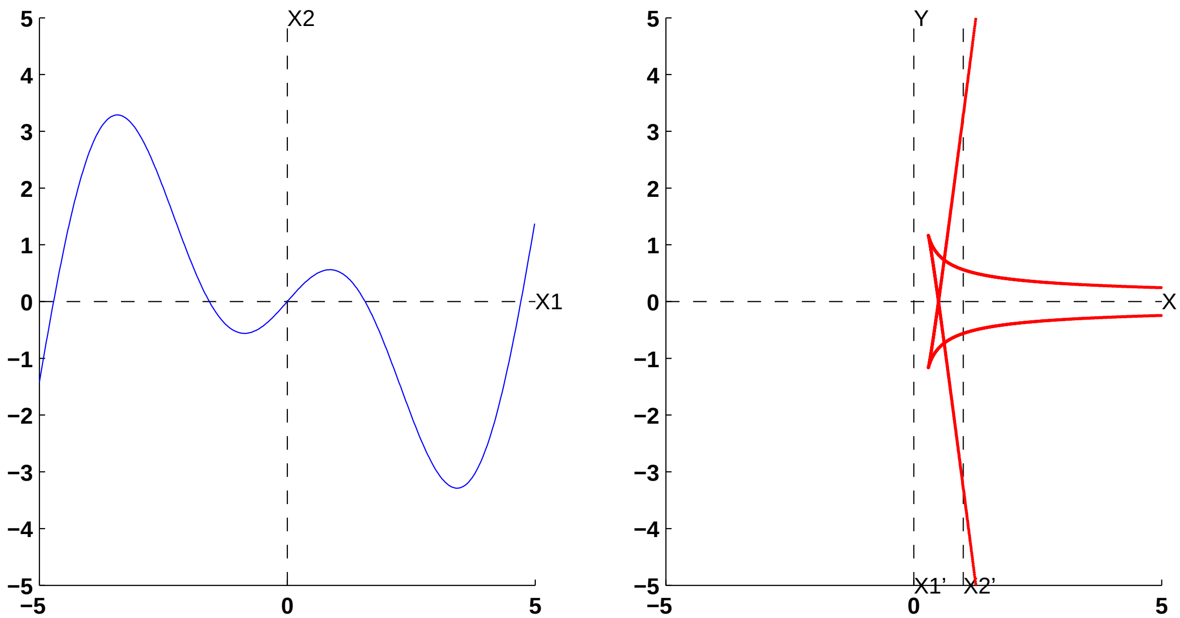

Figure 5.14: The image of the oscillatory curve $x_2 = x_1 cos(x_1)$.

It is a non-oscillating curve symmetrical with respect to the x-axis.

approaching assympotically the negative $\bar{X}_1$-axis. The two tangents at the double-point map into two points; the one on the $\bar{X}_2$ is the image of the horizontal tangent. These two points *have the same tangent* the x-axis. A tangent at two points of a curve is called *bitangent*. It is interesting to trace the image of oscillatory curves. They have mirror as seen in the image of the curve $c : x_2 = x_1 cos(x_1)$ in Fig. **??**.

Convex Sets and their Relatives

Consider a double-cone, as shown in Fig. **??**, whose base is a bounded convex set rather than a circle. The three type of sections shown are generalizations of the conics and are conveniently called *gconics*[3]. They are either a :

bounded convex set is abbreviated by *bc*, or an

unbounded convex set is denoted by *uc* containing a non-empty set of ideal points whose slope m is in an interval $m \in [m_1 \ , \ m_2]$, or a

generalized hyperbola denoted by *gh* consisting of two full(not segments) lines ℓ_u , ℓ_ℓ, called assymptotes two infinite chains, convex-upward chain c_u above both assymptotes, and another convex-downward chain c_ℓ below both assymptotes.

[3]The corresponding regions have been previously referred to as *estars, pstars* and *hstars* [**?**], [**?**].

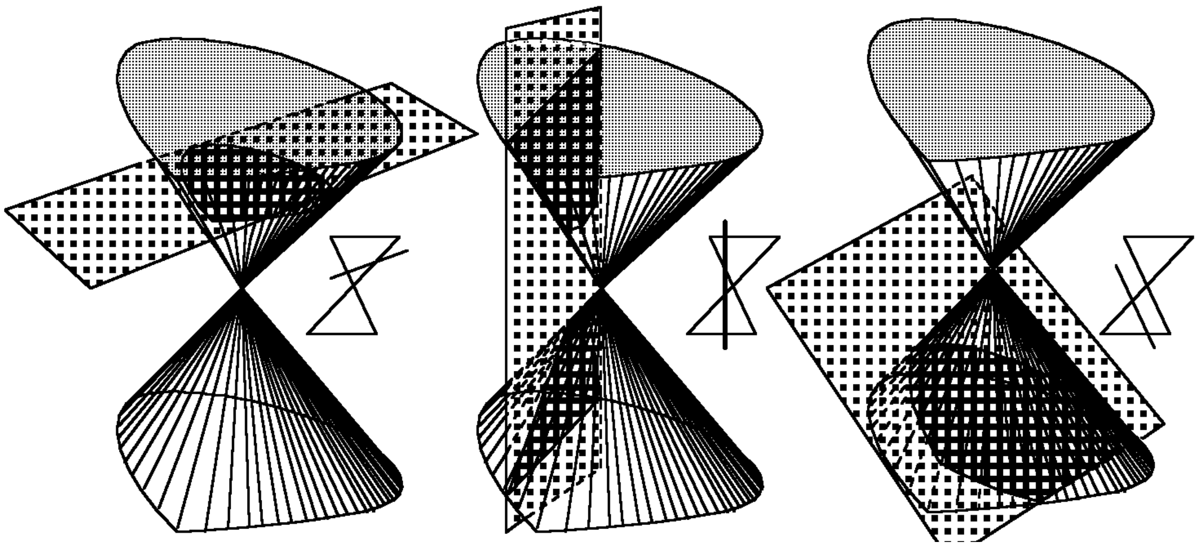

Figure 5.15: Gconics - three types of sections: (left) bounded convex set *bc*, (right) unbounded convex set *uc* and (middle) hyperbola-like *gh* regions.

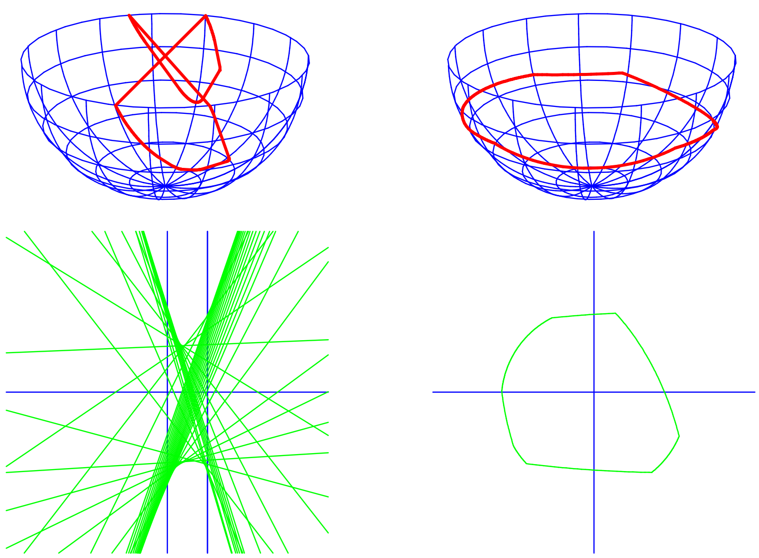

Figure 5.16: A bounded convex set *bc* always transforms to a *gh* (generalized hyperbola) – this is the generalization of the case shown in Fig. **??** .

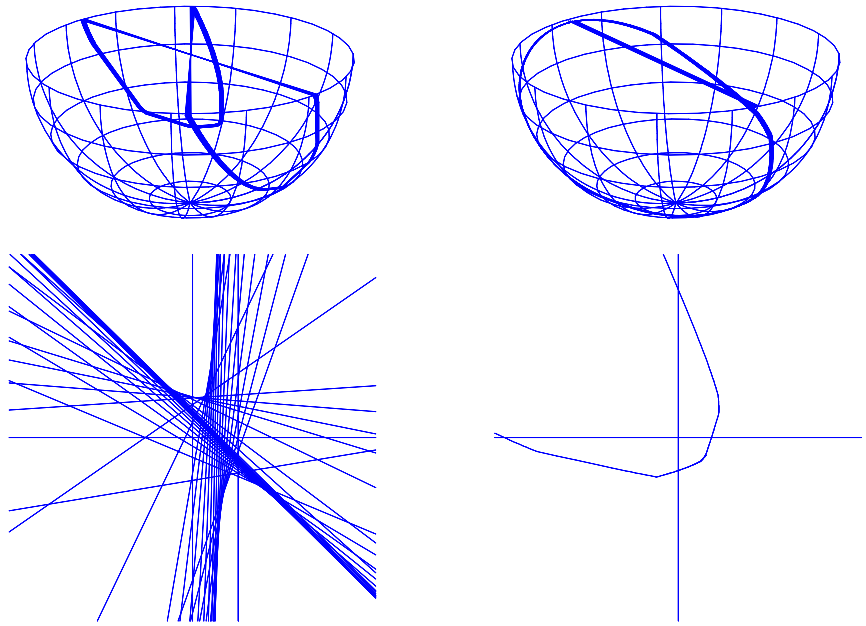

Figure 5.17: An unbounded convex set uc whose ideal points do not have slope 1 transforms to a gh (generalized hyperbola). This is the generalization of the case shown in Fig. **??**.

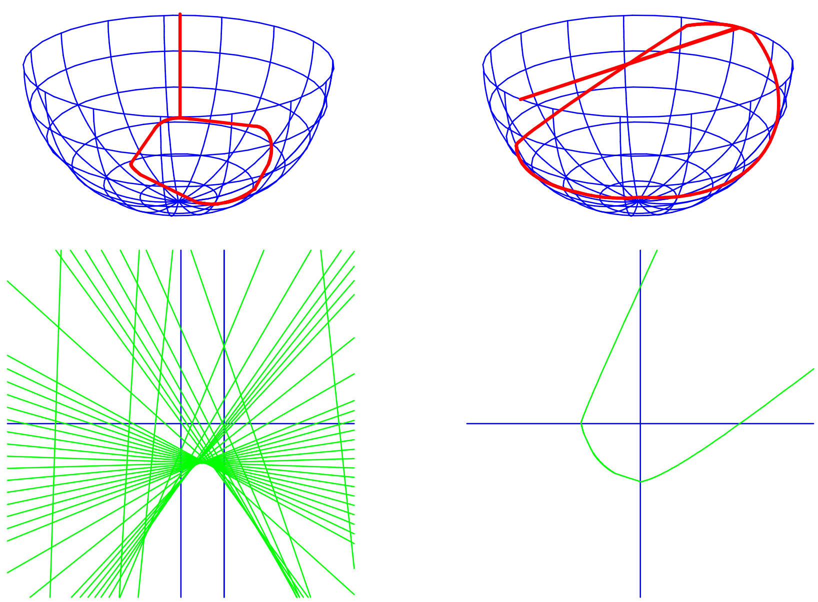

Figure 5.18: Unbounded convex set uc having ideal point with slope 1 transforms to a uc – self-dual case. This is the generalization of the case shown in Fig. **??**.

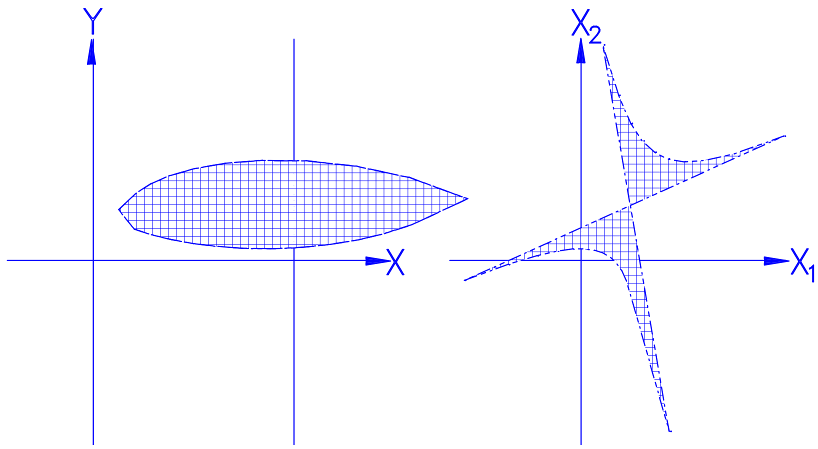

Figure 5.19: A *gh* whose supporting lines have slope $m \in [m_1, m_2]$ where the $m_1 < 1 < m_2$ are the assymptotes' slopes transforms to a bounded convex *bc* set. This is the generalization of the conic case shown in Fig. **??**.

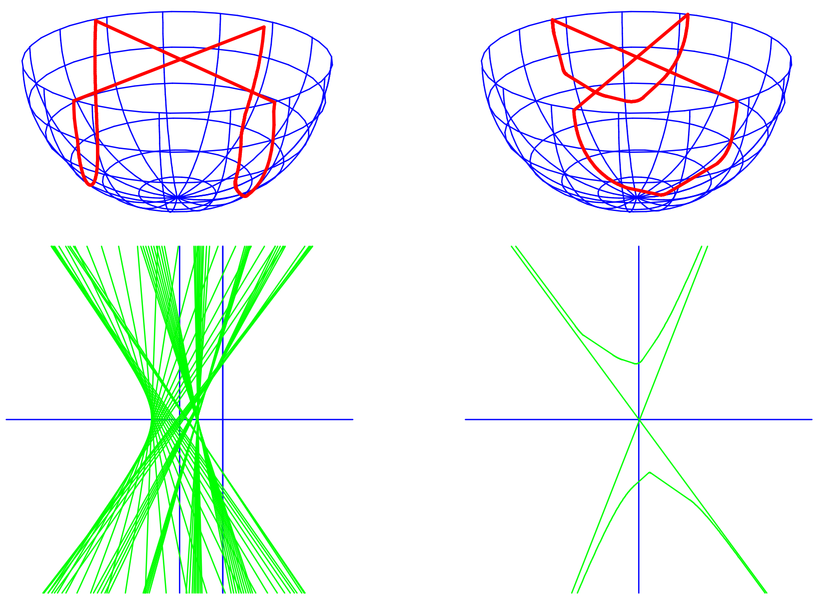

Figure 5.20: A *gh* with $1 \notin [m_1 \ , \ m_2]$, where the m_i are the assymptotes' slopes, transforms to a *gh* – Self-dual case. This is the generalization of the case shown in Fig. **??**.

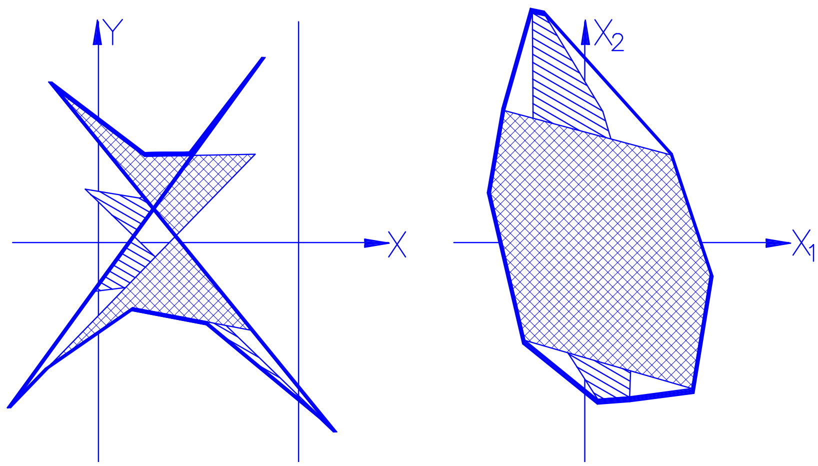

Figure 5.21: The Convex Union (also called “Convex Merge”) of *bc*s corresponds to the Outer Union of their images (*gh*s).

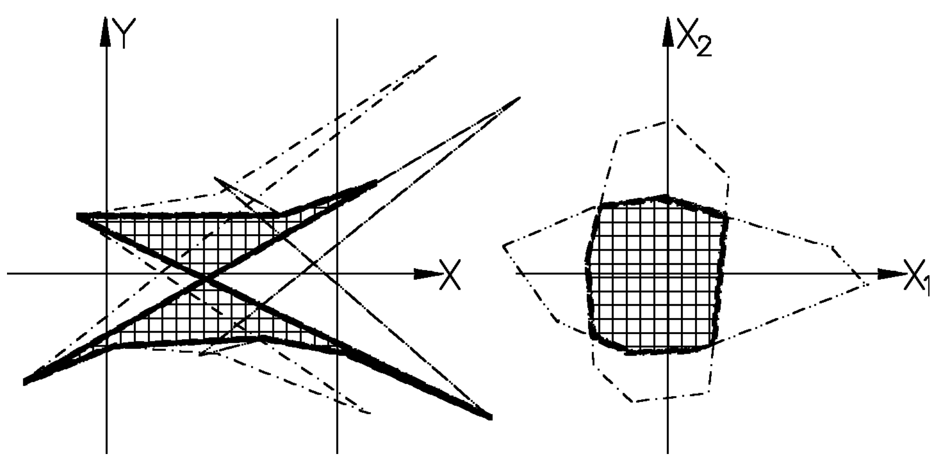

Figure 5.22: Inner intersection and intersections are dual.

Chapter 6

Proximity of Lines, Planes & Flats

$\mathcal{I}$n order to apply the results of the representation of flats by indexed points, their behavior in the presence of errors needs to be understood. While there are many sources of errors

Figure 6.1: Pair of point clusters representing close planes. Note the hexagonal patterns.

in the applications, from our viewpoint, it suffices to consider the accumulated errors in terms of the resulting variations $c_i \in [c_i^-, c_i^+]$ in the coefficients c_i of the plane's equations. This in turn generates a whole *family* $\mathcal{F}$ of "close" flats. Even in R^3 the direct visualization of such a family of planes is difficult. The challenge is not only the visualization but also the construction of tools for appraising the proximity, referred to as "error tolerancing", of the flats in terms of the errors's ranges $|c_i^- - c_i^+|$.

Let us repeat the earlier experiment more systematically and examine the family of "close" planes

$$\{\pi : c_1x_1 + c_2x_2 + c_3x_3 = c_0 \ , \ c_i \in [c_i^-, c_i^+] \ , \ c_i^- < c_i^+\} \ .$$

Computing the two point representation in $\|$-coords of some of these planes we see in Fig. **??** the corresponding pair of point clusters. Closeness is apparent and more significantly the distribution of the points is not "chaotic". The the outline of two polygonal patterns can be seen.

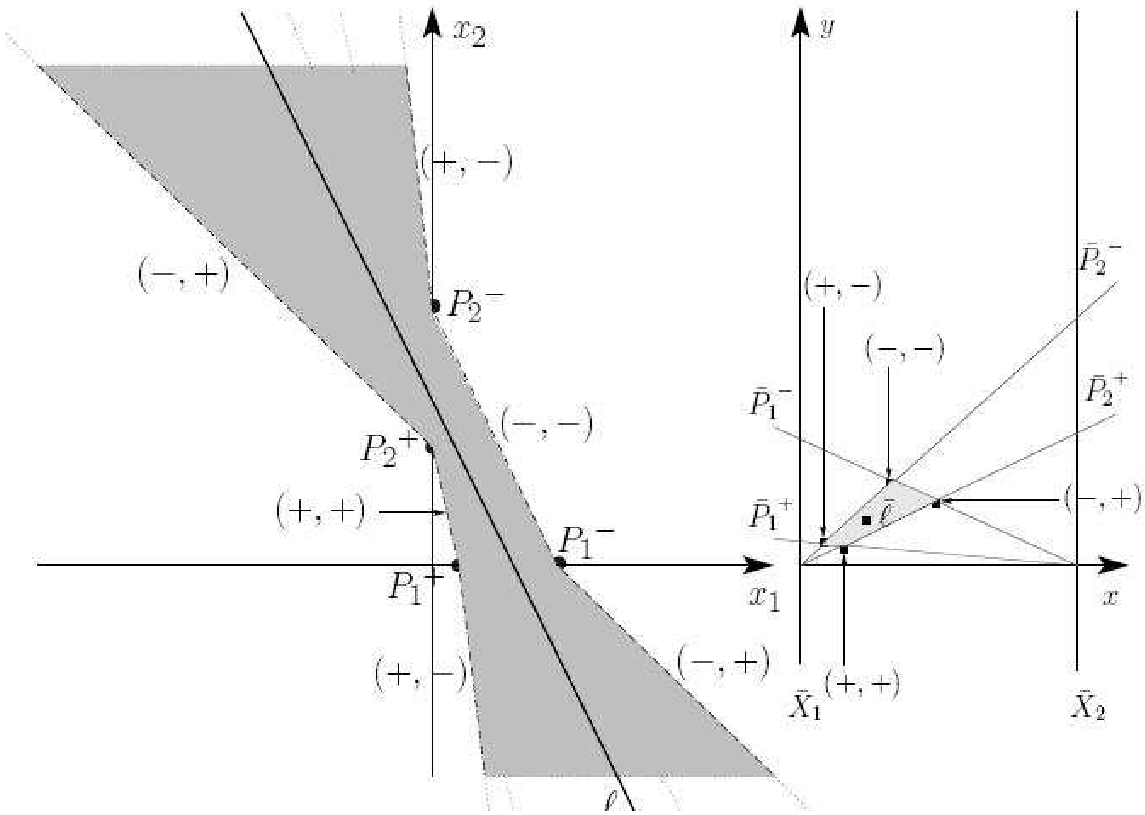

Figure 6.2: Line neighborhood.

On the left is a region covered by lines "close" to ℓ and on the right are the points in $\|$-coords representing the lines in this region. This a *gh* (a "generalized hyperbola") on the left which is is mapped into a *bc* – here a bounded convex quadrilateral(right).

Proximity of Lines and Line Neighborhoods

Is it reasonable to consider lines in $\mathbb{R}^N$ being "close" if the coefficients of their equations are close such as the collection of lines in $\mathbb{R}^2$

$$\mathcal{F} = \{\ell \mid \ell \ : \ c_1x_1 + c_2x_2 = 1 \ , \ c_1, c_2 \in \mathbb{R}\}.$$

The value of the constant c_0 on the right-hand-side is taken as 1 and is allowed to vary later. Of interest is the collection of subsets $\mathcal{N}_\ell = \{NL|NL \subset \mathcal{F}\}$ where

$$NL = \{\ell \mid \ell \ : \ c_1x_1 + c_2x_2 = 1 \ , \quad c_i \in [c_i^-, c_i^+] \quad i = 1, 2 \ \}. \tag{6.1}$$

It is convenient to denote the end-points of the interval $[c_i^-, c_i^+]$ by $sign_i$ the sign of the superscript of $c_i^\pm$; that is $sign_i = -$ and $sign_i = +$ stand for the lower and upper bounds respectively of c_i. The extreme lines obtained by the 4 different combinations of $(sign_1, sign_2)$ are :

$$\left.\begin{array}{l} (-,-) : c_1^-x_1 + c_2^-x_2 = 1 \\ (-,+) : c_1^-x_1 + c_2^+x_2 = 1 \\ (+,-) : c_1^+x_1 + c_2^-x_2 = 1 \\ (+,+) : c_1^+x_1 + c_2^+x_2 = 1 \end{array}\right\} \tag{6.2}$$

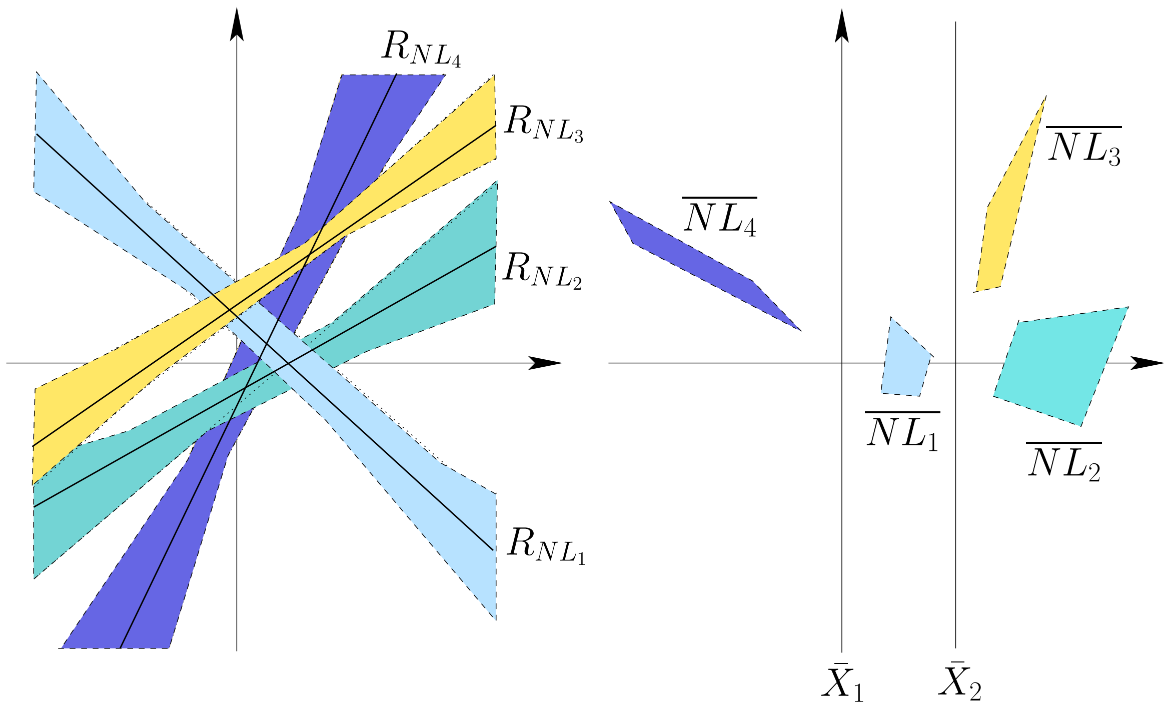

Figure 6.3: Several line neighborhoods.

The regions R_{NL_i}, $i = 1, 2, 3, 4$ covered by 4 families of lines in orthogonal and their images $\overline{NL_i}$ in || coordinates.

These lines bound the region $R_{NL} \subset \mathbb{R}^2$ covered by all the lines of NL; a "template" referred to earlier. An example is shown on the left part of Fig. **??** where the extreme lines in eq. (**??**) are constructed from the points:

$$P_1^+ = \left(\frac{1}{c_1^+}, 0\right) \quad , \quad P_1^- = \left(\frac{1}{c_1^-}, 0\right) \quad , \quad P_2^+ = \left(0, \frac{1}{c_2^+}\right) \quad , \quad P_2^- = \left(0, \frac{1}{c_2^-}\right) .$$

The region R_{NL} resembles a hyperbola and is in fact a generalized hyperbola a *gh* in the terminology of section on curves. All lines in NL are enclosed between two opposite convex unbounded regions with two "assymptotes", the lines $(+,-)$, $(-,+)$, joining them at two ideal points.

$$NL_j = \{\ell \mid \ell \ : \ c_{1,j}x_1 + c_{2,j}x_2 = 1 \ , \quad c_{i,j} \in [c_{i,j}^-, c_{i,j}^+] \quad i = 1,2 \ \ j = 1,2\}, \tag{6.3}$$

and the intersection operation $N = N_1 \cap N_2$ is defined by

$$NL = \{\ell \mid \ell \ : \ c_1x_1 + c_2x_2 = 1 \ , \quad c_i \in [c_i^-, c_i^+] = [c_{i,1}^-, c_{i,1}^+] \cap [c_{i,2}^-, c_{i,2}^+] \quad i = 1,2 \ \}. \tag{6.4}$$

Before getting to that we enlarge the class of lines in N replacing the 1 by c_0 and allowing it to vary within an interval

$$NL = \{\ell \mid \ell \ : \ c_1x_1 + c_2x_2 = c_0 \ , \quad c_i \in [c_i^-, c_i^+] \quad i = 0,1,2 \ \}. \tag{6.5}$$

Each such line ℓ is represented by the point

$$\bar{\ell} = \left(\frac{c_2}{c_1 + c_2}\ ,\ \frac{c_0}{c_1 + c_2}\right) \tag{6.6}$$

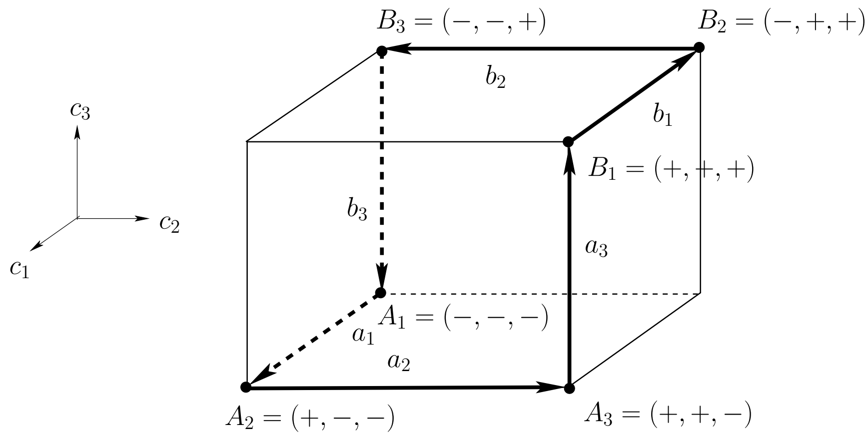

Figure 6.4: 3D-Box B in the space of coefficients.

The vertices and edges 3 each A_k, B_k, a_k, b_k along the path $\mathcal{P}$ are shown. The notation $\pm$ indicates the sign of $c_k^{\pm}$ at the kth component.

Theorem: For $c_0 \in [c_0^-, c_0^+]$ the region Ω is a $2(N+1)$-agon which may have its leftmost or rightmost (or both) edges are vertical and which is

1. ***bc*** if $\pi_c \cap B = \emptyset$,
2. ***uc*** if $\pi_c \cap B = \{A_1\}$ or $\pi_c \cap B = \{B_1\}$,
3. ***gh*** if π_c intersects B at more than one edge, and has a vertical assympote if in addition π_c contains a vertex of B.

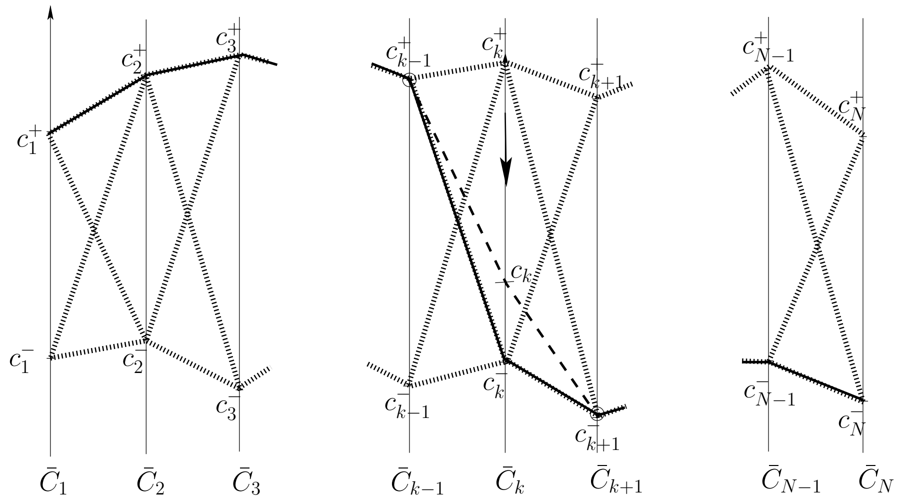

Figure 6.5: Image $\bar{B}$ of domain B.

This is an N-dimensional box in the coefficient space $c_1 \times c_2 \times \ldots \times c_N$. The dotted lines are the polygonal lines representing the box's vertices. The solid line shows vertex $\bar{A}_k$ and the dashed portion (together with the remaining solid line) shows one of the points on the edge $\bar{a}_k$ the arrow on the $\bar{C}_k$ axis is the direction of traversal from $c_k^+ \to c_k^-$. Each full traversal of $c_k \in [c_k^-, c_k^+]$ corresponds to an edge a_k, one of the N edges on the vertex A_k. The full path $\mathcal{P}$ can be traced in this manner.

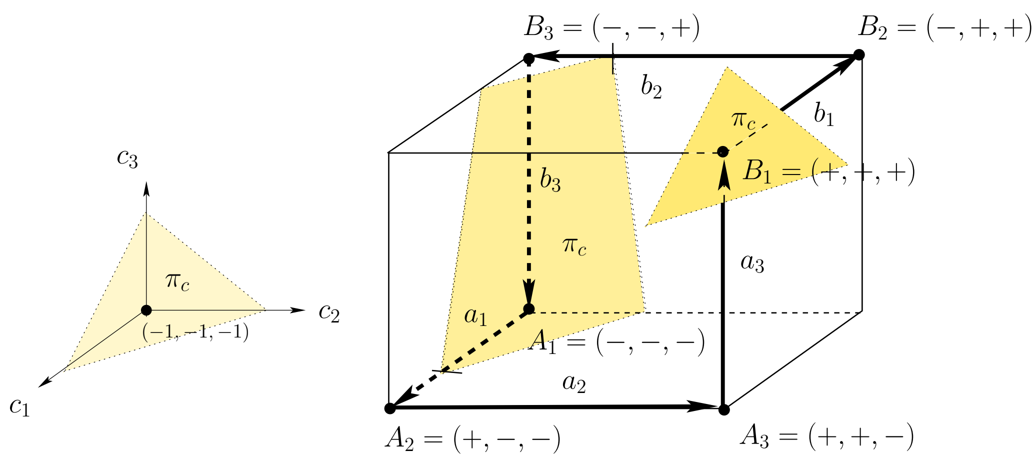

Figure 6.6: The box B in the 3-D space of coefficients c_1, c_2, c_3.

Its positions with respect to the plane $\pi_c : c_1 + c_2 + c_3 = 0$. Namely $\pi_c \cap B = \emptyset$, or if $\pi_c \cap B \neq \emptyset$ π_c is a supporting plane at either vertex A_1 or B_1 or π_c intersects two edges of the path $\mathcal{P}$.

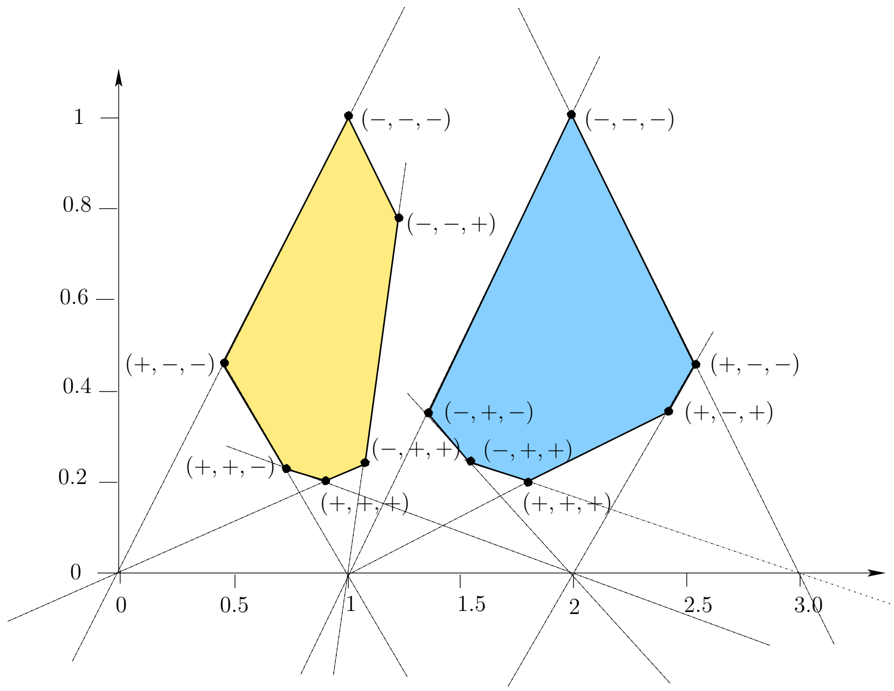

Figure 6.7: The hexagonal regions $\Omega = \overline{NH}_{0'}$ (left) and $\overline{NH}_{1'}$ (right).

Here the family of planes is specified by $c_1 \in [1/3, 1.5], c_2 \in [1/3, 2.5], c_3 \in [1/3, 1]$. Compare this picture with Fig. **??** at the beginning of the section.

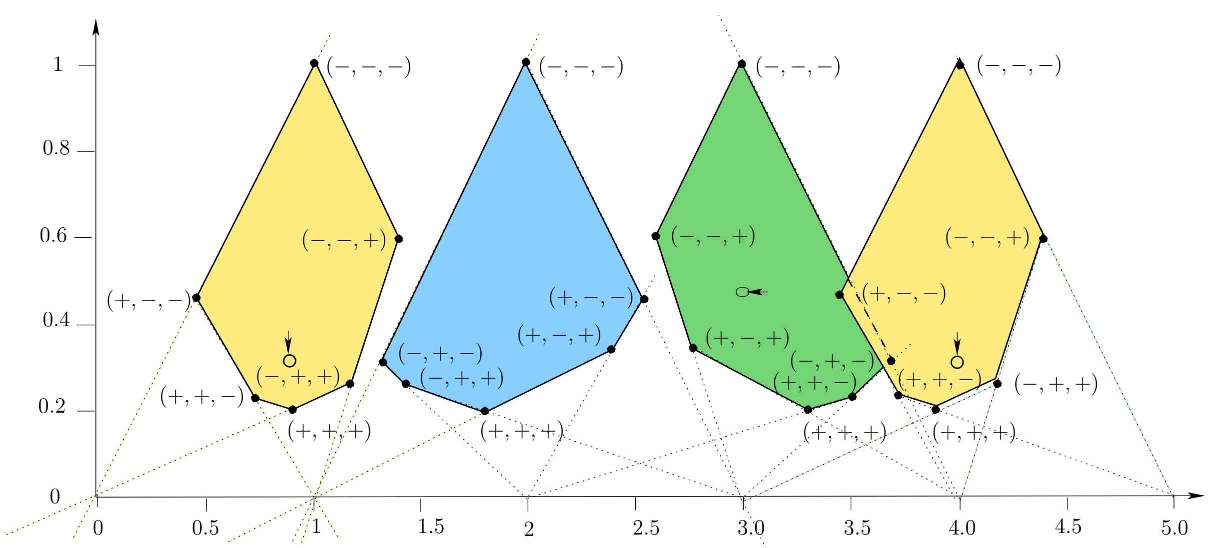

Figure 6.8: The four hexagonal regions.

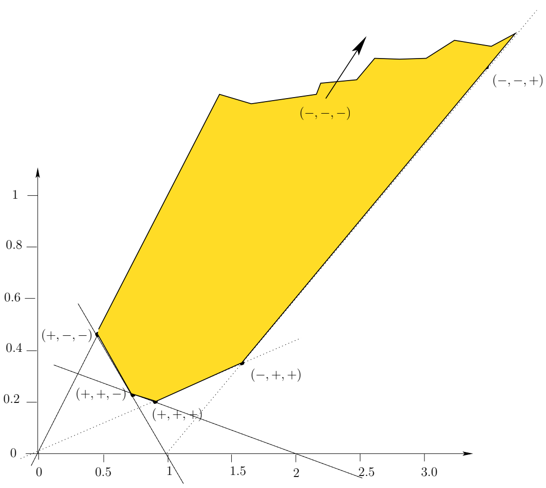

Figure 6.9: A *uc* in 3D for $c_1 \in [-2/3, 1.50], c_2 \in [1/3, 2.50], c_2 \in [1/3, 1.0]$.

Compare with the coefficient ranges of the hexagon(s) in Fig. **??** and note that they differ only for c_1^-. Here the sum $c_1^- + c_2^- + c_3^- = 0$.

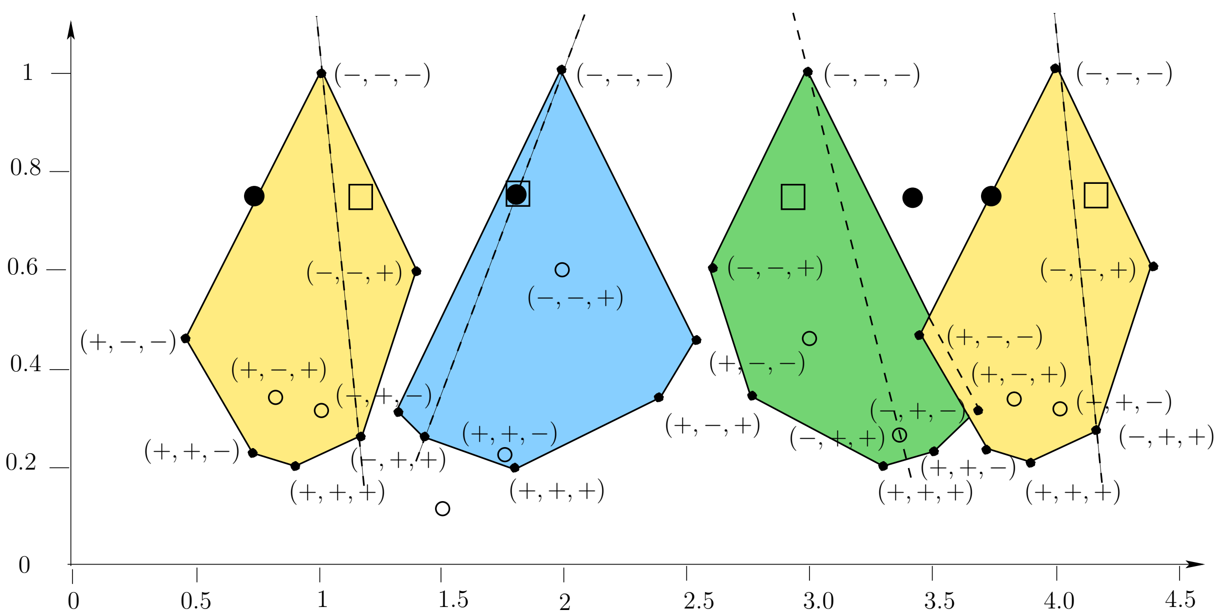

Figure 6.10: The 4 hexagons previously seen in Fig. **??**.

For family of planes Π with $c_1 \in [1/3, 1.5], c_2 \in [1/3, 2.5], c_3 \in [1/3, 1]$ now showing the images of *all* vertices of $\partial\mathbf{B}$ two being interior points. Though the first two points with the same y, marked by $\bullet$, are in $\overline{NH}_1$ and $\overline{NH}_2$ respectively they do **not** represent a plane in Π since $\bar{\pi}_{2'} \notin \overline{NH}_3$.

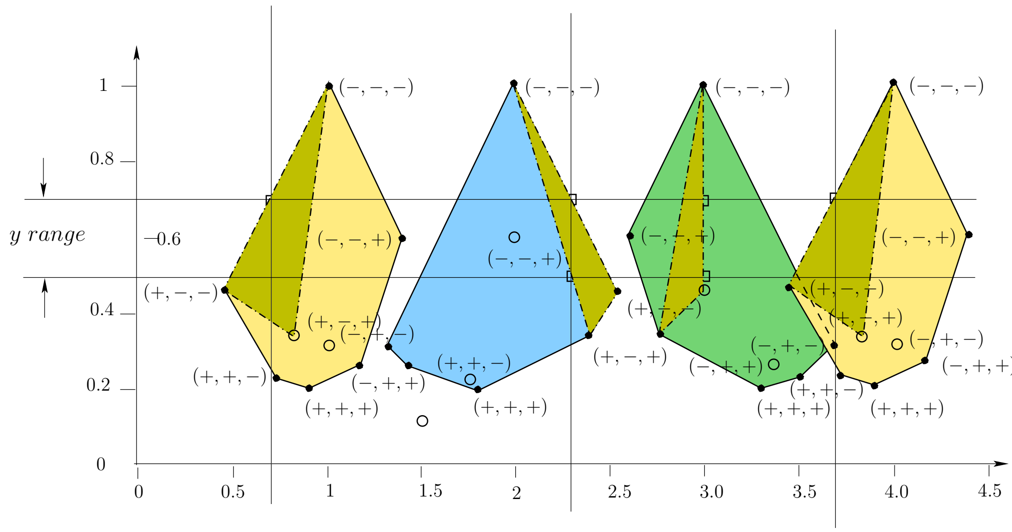

Figure 6.11: Finding interior points

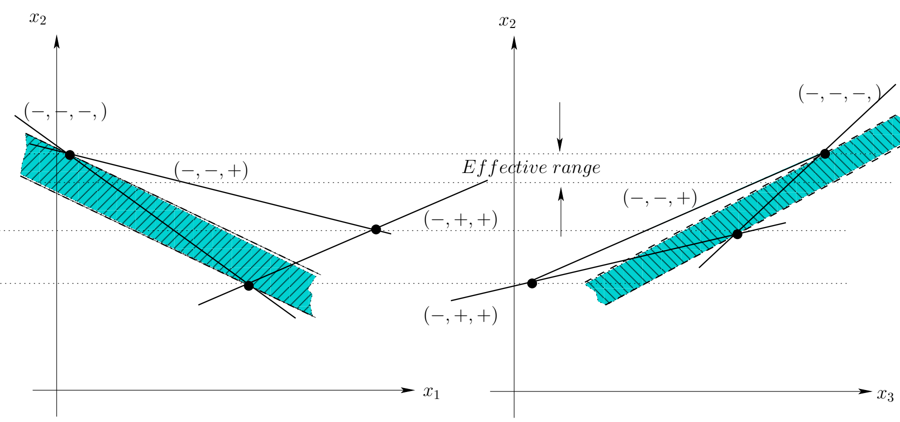

Figure 6.12: Triangulation in orthogonal coords.

Two sections of the family of planes Π perpendicular to the x_3 and x_1 axes. Focus on the point P intersection of the lines $(-,-,-)$, $(-,-,+)$ shown on the the x_1x_2 and x_2x_3 planes. Choose the x coordinates of of $\bar{\pi}_{0'}, \bar{\pi}_1$ to fix a $\bar{\pi} \in \Pi$ and on P. The slopes on the x_1x_2 and x_2x_3 planes are determined from the x-coords of $\bar{\pi}_{0'}, \bar{\pi}_1$ respectively. Generate this the family of the planes parallel to π and in Π by allowing x_2 to vary until it hits the constraint – here the lowest point. The range of x_2 differs in the 2 sections and the effective range is the *minimum*. This corresponds to the triangulation procedure shown above in $\|$-coords.

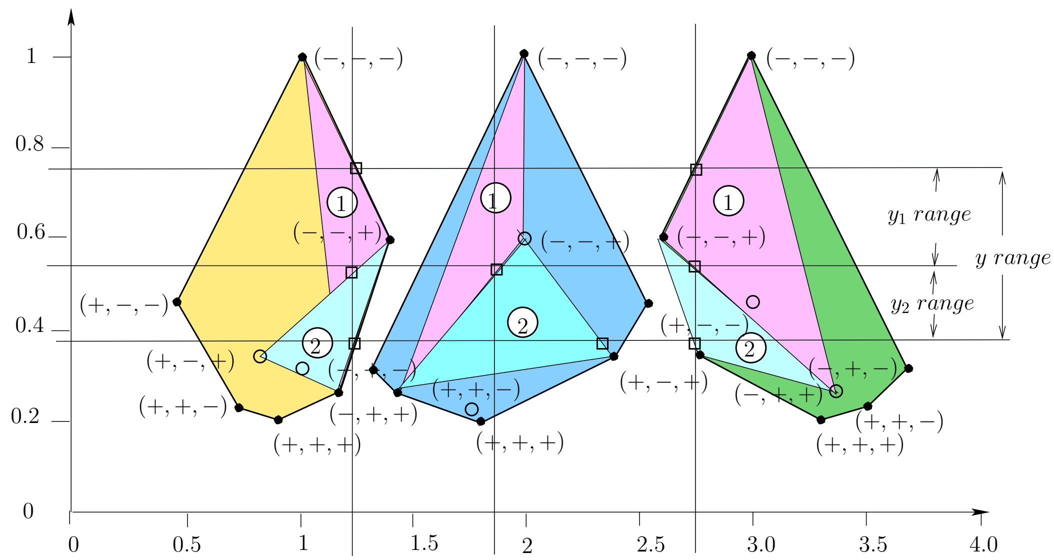

Figure 6.13: Continuing the interior point construction from triange 1 to triangle 2.

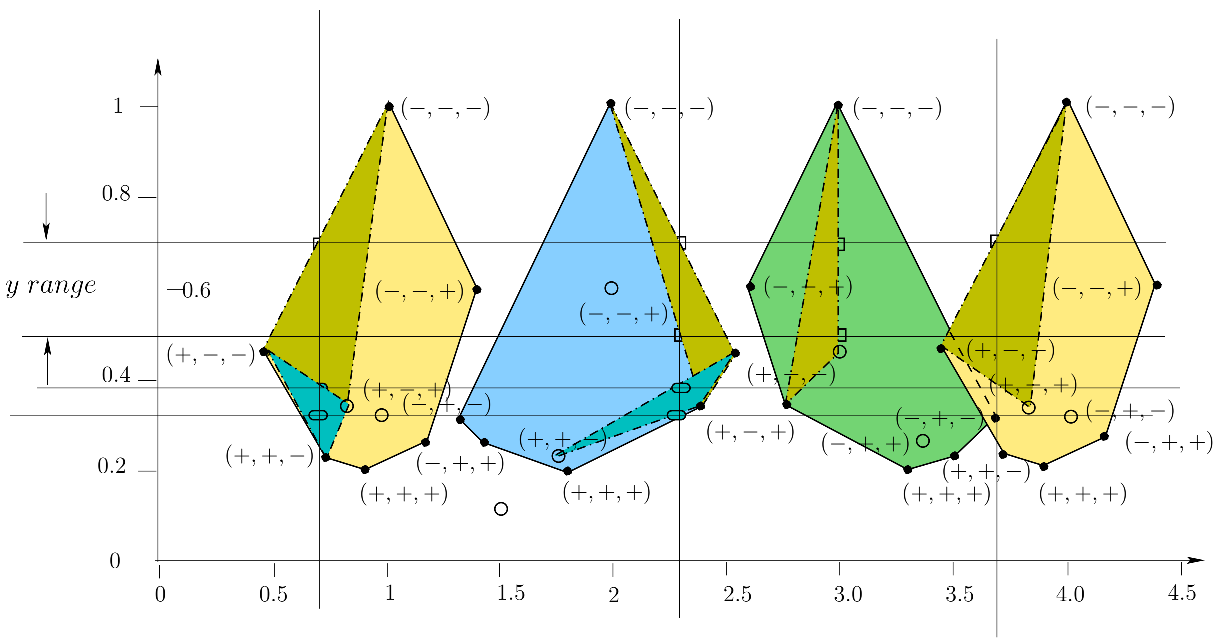

Figure 6.14: Continuation along the vertical by extending the triangulation.

Here it is not possible due to gap between the two triangles in $\overline{NH}_{2'}$.

Chapter 7

Hypersurfaces in $\mathbb{R}^N$

Preliminaries

We revisit Fig. 1 showing the hypercube representation and serves as an excellent paradigm for what is to follow. In (a) a square is seen in Cartesian and ∥-coords. Note the role of duality where a vertex, say A, is mapped into a line, $\bar{A}$ and conversely an edge, say AB, is mapped into a point $\overline{AB}$. Proceeding, in (b) the image of the 3-D cube is *twice* the pattern of the square. From this image the edges can be identified by two points and faces by two vertical lines and (an associated point for origin). In fact, this is a good example where the general representation of lines and [**?**] is needed since here

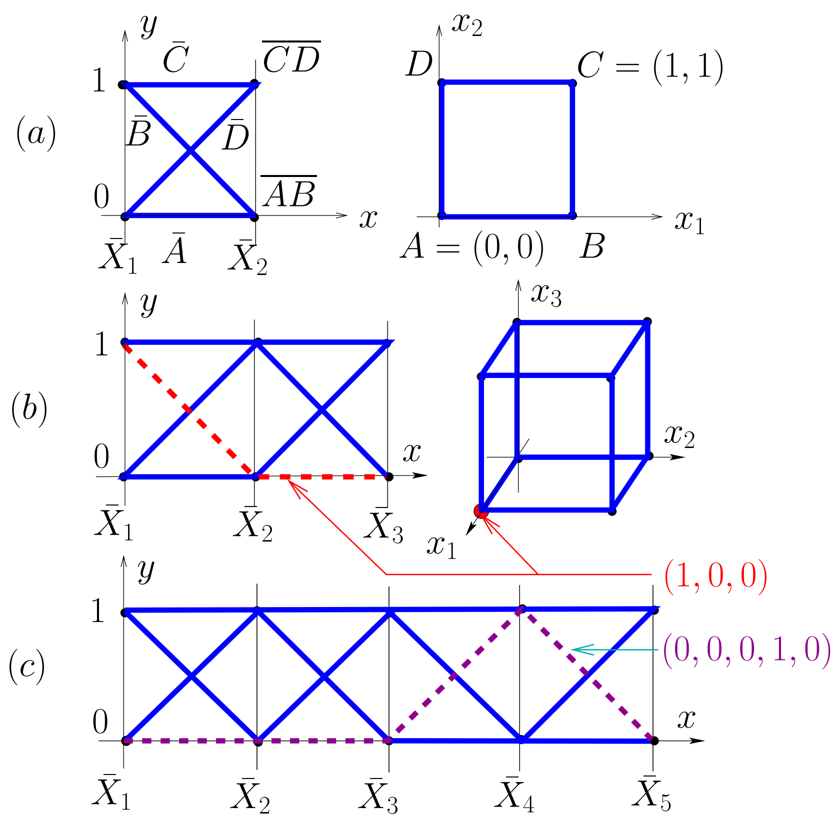

Figure 7.1: (a) Square (b) Cube in $\mathbb{R}^3$ (c) Hypercube in $\mathbb{R}^5$ – all edges have unit length

for some of the edges two of the 3 variables are constant (in effect this simplifies things). The representation of the cube's faces stems directly from vertical line representation of hyperplanes.

The pattern's repetition pleasingly reveals the cube's symmetry and relation to the square. Whereas we do not know how to show a hypercube in cartesian coordinates it is no problem doing so in $\|$-coords. This is shown in (c) where the representation of a hypercube in $\mathbb{R}^5$ consists of 4 times the square's pattern. Again all vertices, edges and faces can be determined from the picture. Interior points are represented by polygonal lines *within* the pattern, and if they share a portion with the boundary they represent surface points. This suggests how the representation of higher dimensional of a surface may be obtained from its 3-D representation. All this generalizes nicely for the representation of polytopes in $\mathbb{R}^N$ [**?**]. A rotated or translated hypercube can still easily represented and recognized.

To lay the groundword recall the recursive notation for the axes spacing (considered as an N-tuple) developed in Chapter on planes. For the initial N axes system $\bar{X}_1, \bar{X}_2, \ldots, \bar{X}_N$ we write

$$\mathbf{d_N^0} = (\overbrace{0, 1, 2, \ldots, i-1}^{i}, \ldots, N-1) .$$

This states that the first axis $\bar{X}_1$ is placed at $x = 0$, $\bar{X}_2$ is placed at $x = 2$ ... until $\bar{X}_N$ which is at $x = N-1$. After translating the $\bar{X}_1$ axis one unit to the right of $\bar{X}_N$, renaming it $\bar{X}_{1'}$, the axes spacing N-tuple is

$$\mathbf{d_N^1} = \mathbf{d_N^0} + (N, 0, \ldots, 0) = (\overbrace{N, 1, 2, \ldots, i-1}^{i}, \ldots, N-1) .$$

And after i such successive unit translations with the $\bar{X}_i$ axis in position $\bar{X}_{i'}$ the axes spacing for $i = 0, \ldots, N$, $k = 1, \ldots, N$ is given by

$$\mathbf{d_N^i} = \mathbf{d_N^0} + (\overbrace{N, \ldots, N}^{i}, 0, \ldots, 0) = (\overbrace{N, N+1, \ldots, N+i-1}^{i}, i, ..., N-1) = (d_{ik}) . \quad (7.1)$$

To clarify the indices, i is the number of axis translations and k is the position (component) within the vector $\mathbf{d_N^i}$. Using the step function

$$S_i(k) = \begin{cases} 1 & i \geq k \\ 0 & i < k \end{cases} , \quad (7.2)$$

the axes-spacing after the ith translation can be conveniently written as

$$\mathbf{d_N^i} = (d_{ik}) = (k - 1 + NS_i(k)) . \quad (7.3)$$

When the dimensionality is clear from the context the subscript N can be omitted. For a flat π^p expressed in terms of the $\mathbf{d_N^i}$ spacing, the points $\bar{\pi}^p_{1',\ldots,i',i+1,\ldots,N}$ of its representation are denoted compactly by $\bar{\pi}^p_{i'}$. Consistent with this notation $\pi^p = \pi^p_{0'}$ for π^p described in terms of the axis spacing $\mathbf{d_N^0}$. So the common spacings are $\mathbf{d_3^0} = (0, 1, 2)$, $\mathbf{d_3^1} = (3, 1, 2)$ and so on.

It is useful to recast the representation of planes in vector form. For

$$\pi : c_1x_1 + c_2x_2 + c_3x_3 = c_0 , \quad (7.4)$$

the coefficient vector $\mathbf{c} = (c_1, c_2, c_3)$ and $\mathbf{u} = (1, 1, 1)$, the representing points of π given in inner-product (denoted by "$\cdot$") form are:

$$\bar{\pi} = (\mathbf{c} \cdot \mathbf{d^i_3} \ , \ c_0 \ , \ \mathbf{c} \cdot \mathbf{u}) = (\mathbf{c} \cdot \mathbf{d^i_3} \ , \ c_0 \ , \ c_1 + c_2 + c_3 \ ) \ . \tag{7.5}$$

The first coordinates of $\bar{\pi}$, with the axes spacing given by eq. (1.3), are:

$$\left\{ \begin{array}{lcl} \mathbf{c} \cdot \mathbf{d^0} = \mathbf{c} \cdot (0, 1, 2) & = & c_2 + 2c_3 \\ \mathbf{c} \cdot \mathbf{d^1} = \mathbf{c} \cdot (3, 1, 2) & = & 3c_1 + c_2 + 2c_3 \\ \mathbf{c} \cdot \mathbf{d^2} = \mathbf{c} \cdot (3, 4, 2) & = & 3c_1 + 4c_2 + 2c_3 \\ \mathbf{c} \cdot \mathbf{d^3} = \mathbf{c} \cdot (3, 4, 5) & = & 3c_1 + 4c_2 + 5c_3 \end{array} \right. \tag{7.6}$$

For $x_i = \mathbf{c} \cdot \mathbf{d^i}/S$ with $S = \sum_{i=0}^{N-1} c_i$, The relations

$$x_2 = 6 - [x_0 + x_1] \quad , \quad x_3 = 3 + x_0 \ ,$$

and in general for $\mathbb{R}^N$ with $x_i = \mathbf{c} \cdot \mathbf{d^i_N}/S$ and $S = \sum_{i=1}^{N} c_i$

$$x_{(N-1)} = N(N-1) - \sum_{i=0}^{N-2} x_i \quad , \quad x_N = N + x_0 \ ,$$

provide the connection between the $N - 1$ independent representing points and the remaining two.

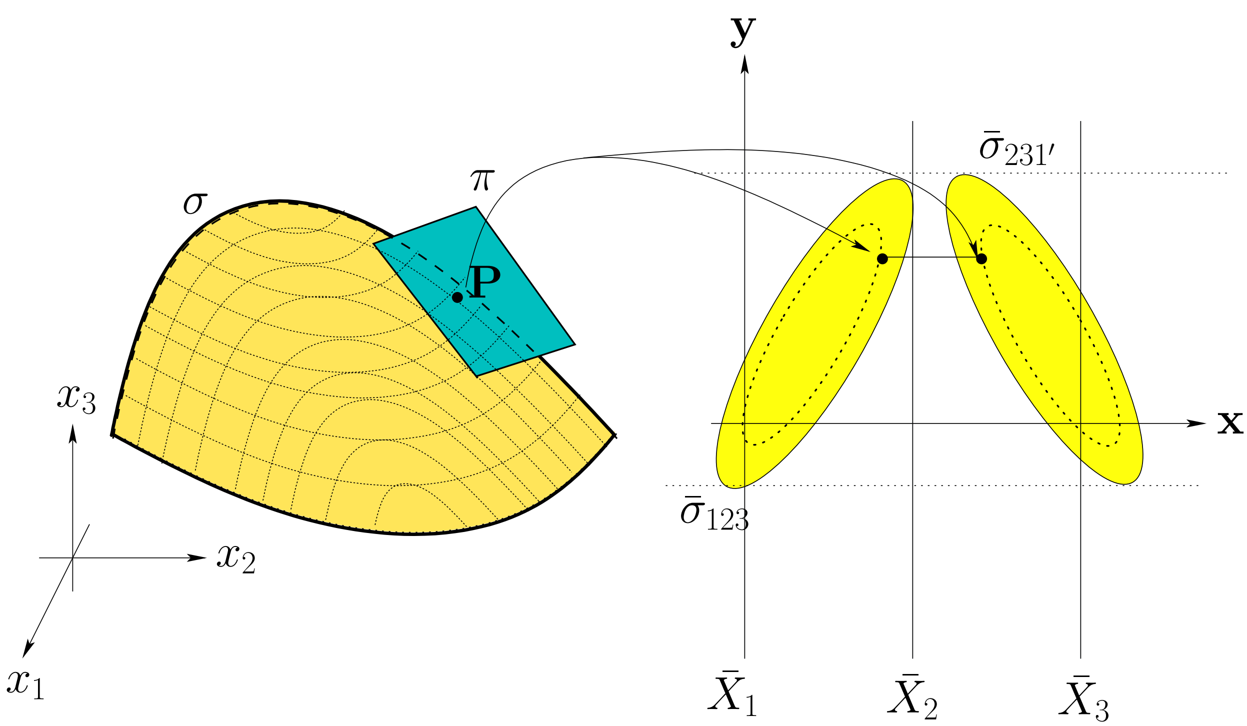

Figure 7.2: A surface $\sigma \in \mathcal{E}$ is represented by two linked planar regions $\bar{\sigma}_{123}$, $\bar{\sigma}_{231'}$. They consist of the pairs of points representing all its tangent planes.

Formulation

$\mathcal{W}$e now pursue the representation of smooth surfaces in $\mathbb{R}^N$ and in particular the family $\mathcal{E}$ of surfaces[1] which are the envelopes of their tangent planes. The discussion is confined to $\mathbb{R}^3$ when the higher-dimensional generalizations are clear. Occasionally, as for curves we use terminology and results which can be found from the references in Differential Geometry. Also recommended is the beautiful and comprehensive website on surfaces [**?**]. The basic idea for the representation of a surface $\sigma \in \mathcal{E}$ is illustrated in Fig. 1.2. The tangent plane π at each point $P \in \sigma$ is mapped to the two planar points $\bar{\pi}_{123}$, $\bar{\pi}_{231'}$. Collecting the points by their indices for all the tangent planes yields two planar regions $\bar{\sigma}_{123}(x, y)$, $\bar{\sigma}_{1'23}(x, y)$ one each for the index triples. The regions must be *linked* by a *matching algorithm* which selects the pairs of points (one from each region) representing valid tangent planes of σ. The two linked regions form the representation $\bar{\sigma}$ of the surface. An example of the linking was already seen in the previous between the polygonal regions representing families of *proximate* planes. The intent is to *reconstruct* the surface from its representation. The manner and extent to which this is possible, i.e. when the $\|$-coords mapping is invertible, are among the issues studied in this chapter.

Formally, a surface $\sigma \in \mathcal{E}$ given by

$$\sigma \ : \ F(\mathbf{x}) = 0 \ , \ \mathbf{x} = (x_1, x_2, x_3) \tag{7.7}$$

is represented in $\|$-coords by

$$\sigma \mapsto \bar{\sigma} = (\bar{\sigma}_{123}(x, y) \ , \ \bar{\sigma}_{1'23}(x, y)) \subset \mathbb{P}^2 \times \mathbb{P}^2 \tag{7.8}$$

where use of the projective plane, $\mathbb{P}^2$ allows for the presence of ideal points. In the notation the *link* between the two regions is indicated by placing them within the (,) which are omitted when the discussion pertains to just the region(s). The functions used are assumed to be continuous in all their variables together with such of its derivatives as are involved in the discussion.

The gradient vector of F, $\nabla F = (\frac{\partial F}{\partial x_1}, \frac{\partial F}{\partial x_2}, \frac{\partial F}{\partial x_3}) \mid_P$, at the point P is normal to the surface σ at $P \Rightarrow$ the tangent plane π of σ at the point $P_0(\mathbf{x^0})$, $(\mathbf{x^0}) = (x_1^0 \ , x_2^0 \ , x_3^0)$ is given by

$$\pi : \nabla F \cdot (\mathbf{x} - \mathbf{x^0}) = \sum_{i=1}^{3} (x_i - x_i^0) \frac{\partial F}{\partial x_i}(x_1^0, x_2^0, x_3^0) = 0 \ . \tag{7.9}$$

Therefore the representing points of π are

$$\bar{\pi}_{i'}(s, t) = (\nabla F \cdot \mathbf{d^i} \ , \ \nabla F \cdot (\mathbf{x^0}) \ , \ \nabla F \cdot \mathbf{u}) \ , \quad i = 0, 1. \tag{7.10}$$

For our purposes it is often preferable to describe a surface in terms of 2 parameters as

$$\sigma \ : \ F(s, t) = F(\mathbf{x}) = 0 \ , \quad \mathbf{x} = \mathbf{x}(\mathbf{s}, \mathbf{t}) \ , \ s \in I_s \ , \ t \in I_t \ , \tag{7.11}$$

where I_s , I_t are intervals of $\mathbb{R}$. The equivalent description for hypersurfaces in $\mathbb{R}^N$ requires $N - 1$ parameters. This form is due to the great mathematician Gauss. Proceeding,

$$\mathbf{x} \in \sigma \mapsto \pi \mapsto (\bar{\pi}_{0'}, \bar{\pi}_{1'}) = (\bar{\pi}_{123} \ , \ \bar{\pi}_{1'23}) = ((x, y), (x', y)) \ , \tag{7.12}$$

[1]Not to be confused with the family of super-planes also denoted by $\mathcal{E}$

with a slight change in notation, $x = x_{0'}$ and $x' = x_{1'}$ for the x-coordinates of $\bar{\pi}_{1'23}$, $\bar{\pi}_{1'23}$ respectively. The y is the same for both points. In terms of the gradient's components, $F_i = \partial F/\partial x_i$

$$\begin{cases} x = \frac{F_2+2F_3}{F_1+F_2+F_3} , \\ \\ y = \frac{x_1F_1+x_2F_2+x_3F_3}{F_1+F_2+F_3} , \\ \\ x' = \frac{3F_1+F_2+2F_3}{F_1+F_2+F_3} . \end{cases} \tag{7.13}$$

These transformations are the direct extension of the 2-D point $\leftrightarrow$ point curve transformations. A word of caution, when the inter-axes distance $d \neq 1$, the right-hand-sides of x and x' above need to be multiplied by d and $2d$ respectively.

The generalization to the hyper-surfaces $\mathcal{E}$ of $\mathbb{R}^N$ is direct. The image of the tangent hyperplane at a point $P \in \sigma \in \mathcal{E}$ consists of $N-1$ points determined from eq. (1.10) by using the appropriate axes spacing $\mathbf{d}^{\mathbf{i}}_{\mathbf{N}}$, $i = 0, \ldots, N-2$ the x-coordinate being the $x_{i'}$ as given above. The resulting transformation, the N-D extension of eq. (1.13) with N terms in the numerator and denominator, determines the point $N-1$-tuples mapping the surface $\sigma \in \mathcal{E}$ into $\bar{\sigma}$ consisting of $(N-1)$ planar regions. Next the construction of the regions is undertaken and subsequently the *link* or *matching algorithm* between them.

Boundary Contours

The development is presented for $\mathbb{R}^3$ where the generalization to $\mathbb{R}^N$, via the vector notation, is straight-forward. The construction of the regions $\bar{\sigma}$ and in particular their boundary $\partial\bar{\sigma}$ is greatly facilated by an observation which is a substantial breakthrough

Figure 7.3: Intersection of a surface σ with the two superplanes $\pi^s_{0'}$, $\pi^s_{1'}$.
The points of the boundary $\partial\bar{\sigma}$ are the images of the tangent planes at the points of the two curves $\sigma \cap \pi^s_{0'}$ and $\sigma \cap \pi^s_{1'}$. The surface above is a hyperboloid of one sheet.

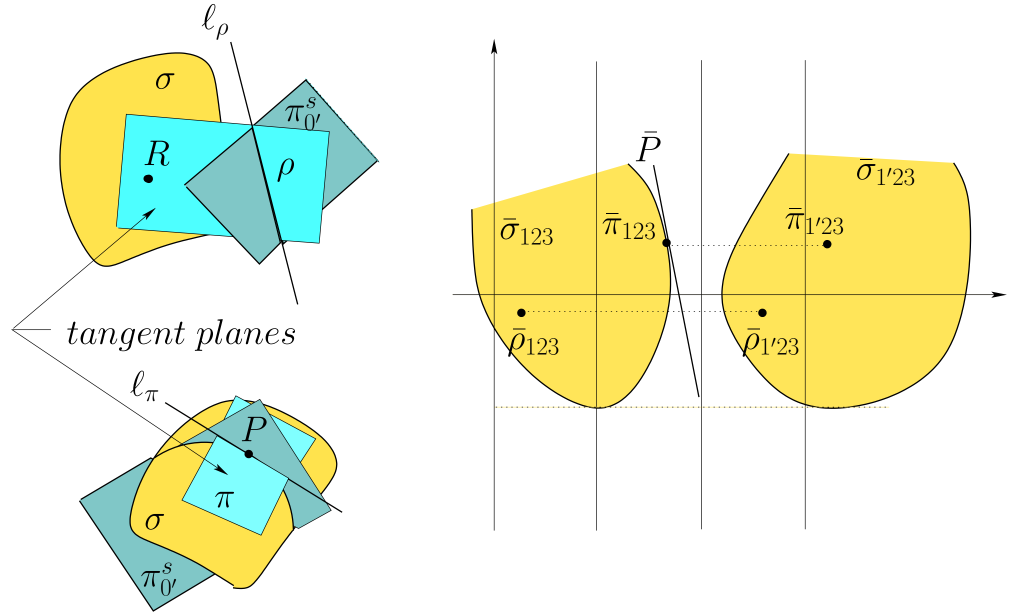

Figure 7.4: Formation of boundary contours

from the earlier approaches. In the ensuing, the surface σ in question is translated and rotated so that its intersection with the first two hyperplanes are curves as for example in Fig. 1.3. There may be lots of such positions and orientations, referred to as *a standard position*, and for our purposes anyone will do. Once the representation of σ in a standard position is found, its representation in the original position and orientation may be found via the *translation* $\leftrightarrow$ *rotation* duality discussed later on.

The following lemma is not true for all surfaces $\sigma \in \mathcal{E}$ as we will discover towards the end of the chapter but it applies to a large subclass which we call $\mathcal{EG}$. Roughly speaking if $\sigma \in \mathcal{EG}$ for every tangent $\bar{P}$ at a point $\bar{\pi}_{i'}$ of $\partial\bar{\sigma}_{i'}$ there exist a neighborhood of $\bar{\pi}_{i'}$ where all points of $\bar{\sigma}_{i'}$ are on the same side of $\bar{P}$. Henceforth, otherwise stated henceforth, when the boundaries of the representing regions of a surface σ are found using the lemma it is assumed that $\sigma \subset \mathcal{EG}$.

Lemma 7.0.1 *(Boundary of $\bar{\sigma}$) For σ a surface in $\mathbb{R}^3$, $\partial\bar{\sigma}_{123}$ is the image of $\sigma \cap \pi^s_{0'}$. That is $\partial\bar{\sigma}_{123} = \overline{\sigma \cap \pi^s_{0'}}$ and similarly $\partial\bar{\sigma}_{1'23} = \overline{\sigma \cap \pi^s_{1'}}$.*

This basic result tremendously simplifies matters. The boundary $\partial\bar{\sigma}$ is simply the image of two *curves*: the intersections of σ with the first two superplanes $\pi^s_{0'}, \pi^s_{1'}$. Note further that for a plane π tangent at a point $P \in \sigma$, $\bar{\pi}_{123} \in \partial\bar{\sigma}_{123}$ and $\bar{\pi}_{1'23} \in \partial\bar{\sigma}_{1'23} \Leftrightarrow P \in \sigma \cap \pi^s_{0'} \cap \pi^s_{1'}$. Finding the boundary of surface representations is one of the major reasons for studying the transform of curves to $\|$-coords in Chapter **??**.

Lemma 7.0.2 *(Boundary of $\bar{\sigma}$ in $\mathbb{R}^N$) For a $\sigma \subset \mathbb{R}^N$, $\partial\bar{\sigma}$ is composed of $N-1$ curves which are the images of the intersections of σ with the first $N-1$ superplanes.*

Corollary 7.0.3 *(Ideal points) An ideal point on the boundary $\partial\bar{\sigma}$ is the image of a tangent plane, at a point of σ, parallel to $\mathbf{u}$.*

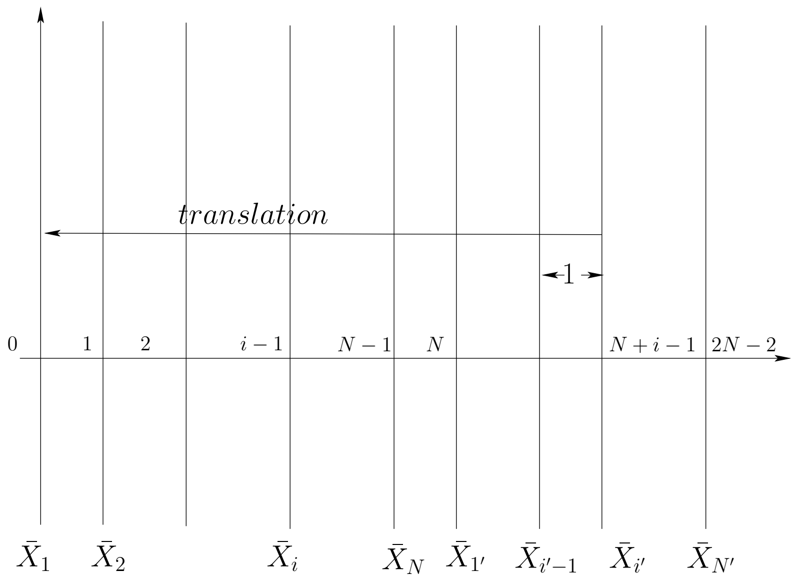

Figure 7.5: Notation and distances for the shift by i units in $\mathbb{R}^N$.

Due to the distance of the $\bar{X}_{1'}$ from the y axis the horizontal translation by $N-i+1$ is needed to obtain the correct x coordinate.

Next, the regions of $\bar{\sigma}$ must be *linked* with a *matching algorithm*, as for the proximate flats regions in Chapter **??**, which selects the valid $N-1$ points representing a tangent plane of σ. This is dealt with incrementaly for surface types of increasing complexity.

Developable Surfaces

*T*he sphere can not be cut and then flattened undistorted. Motivated by map-making, surfaces were sought whose shape is "close" to spherical and can be unrolled into a plane without streching or contracting. Euler first considered this problem and subsequently starting in 1771 Monge made major contributions on the subject of *developable* surfaces. Monge pointed out potential applications especially to architecture paving the way to the modern contoured architectural marvels. Gauss and others followed with the development of the differential geometry of more genenal surfaces. Developable surfaces ("developables" for short), are the class $\mathcal{D} \subset \mathcal{E}$ which are the envelope of a one parameter family of planes, and serve as an excellent starting point for our study of surface representation. Finding their image, matching and reconstruction algorithms is straight-forward and the results offer crucial guides on coping with the more general representation problems.

Formally, let the family of tangent planes describing a developable σ be specified by

$$\pi(t) : \mathbf{c}(t) \cdot \mathbf{x} = c_0(t) \ , \quad t \in I_t \subset \mathbb{R} \tag{7.14}$$

where I_t is an interval of $\mathbb{R}$. The conditions of eq. (1.15) are added, as proved below, to guarantee that the corresponding developable is well defined. In other words it not a single plane, a family of parallel planes or a pencil of planes intersecting on a line.

Theorem 7.0.4 *(***C.K.Hung** *– Developable Surfaces) – Let a surface $\sigma \in \mathcal{D}$ with tangent planes given by eq. (1.14), and a neighborhood $U \subset I_t \subset \mathbb{R}$ where the two conditions :*

$$\frac{dx(t)}{dt} = \frac{\partial}{\partial t}\left(\frac{\mathbf{c}(t)\cdot \mathbf{d}^{\mathbf{i}}}{\mathbf{c}(t)\cdot \mathbf{u}}\right) = 0 \ , \quad \frac{dy(t)}{dt} = \frac{\partial}{\partial t}\left(\frac{c_0(t)}{\mathbf{c}(t)\cdot \mathbf{u}}\right) = 0 \ , \tag{7.15}$$

are not simultaneously satisfied for $\forall t \in U$. Then the set of points $\{\bar{\pi}(t)_{i'} \ |t \in U\}$ representing the tangent planes eq. (1.14) are curves.

Lemma 7.0.5 *(Unique Representation of Developables –) Let σ be a smooth developable with no va tangents represented by two smooth curves $\bar{\sigma}_{123}$, $\bar{\sigma}_{1'23}$ and π (referred to as the* start *plane) any* unambiguous *tangent plane of π. Then the representing curves $\bar{\sigma}_{123}$ $\bar{\sigma}_{231'}$* **together with** *the two points $\bar{\pi}_{123} \in \bar{\sigma}_{123}$, $\bar{\pi}_{231'} \in \bar{\sigma}_{231'}$ uniquely represent σ.*

Specific Developables

Corollary 7.0.6 *(***C.K.Hung***– Cylinders) Elliptic cylinders in $\mathbb{R}^3$ are represented by a pair of hyperbolas.*

A surface's description in vector form is convenient and also clarifies its structure. It was proposed by the mathematical physicist W.J. Gibbs who was also an early advocate for *visualization* in science. His first two papers in 1873 were : "Graphical Methods in the Thermodynamics of Fluids" and "A Method of Geometrical Representation of the Thermodynamics Properties of Substances by Means of Surfaces".

A *general cylinder* is specified by the equation

$$\mathbf{x}(s, v) = \mathbf{c}(s) + v\mathbf{r} \tag{7.16}$$

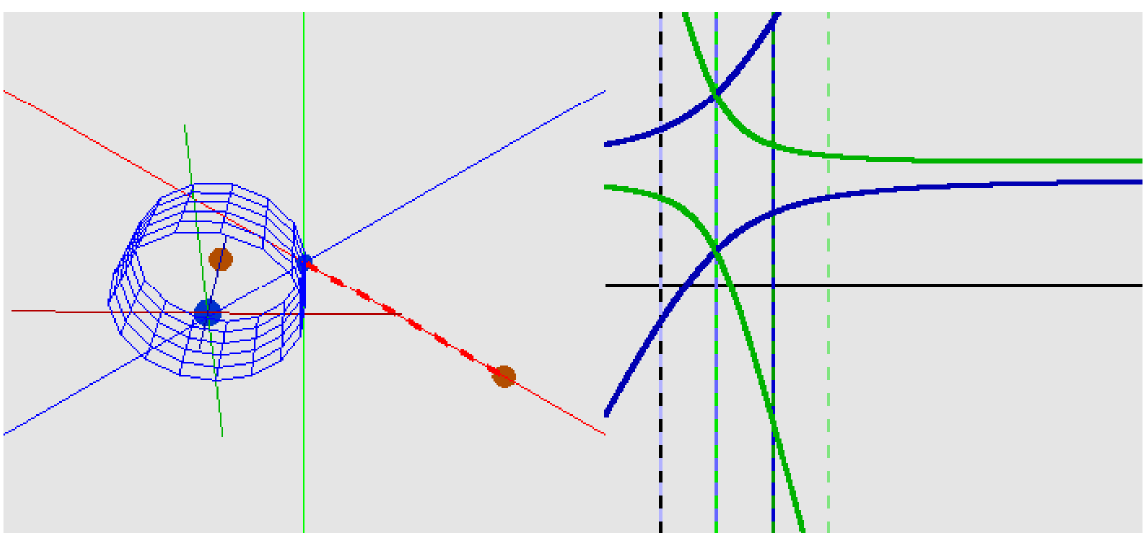

Figure 7.6: A pair of hyperbolas representing the cylinder shown on the left.

The • are the "handles" for changing orientation in the software used and have no significance here.

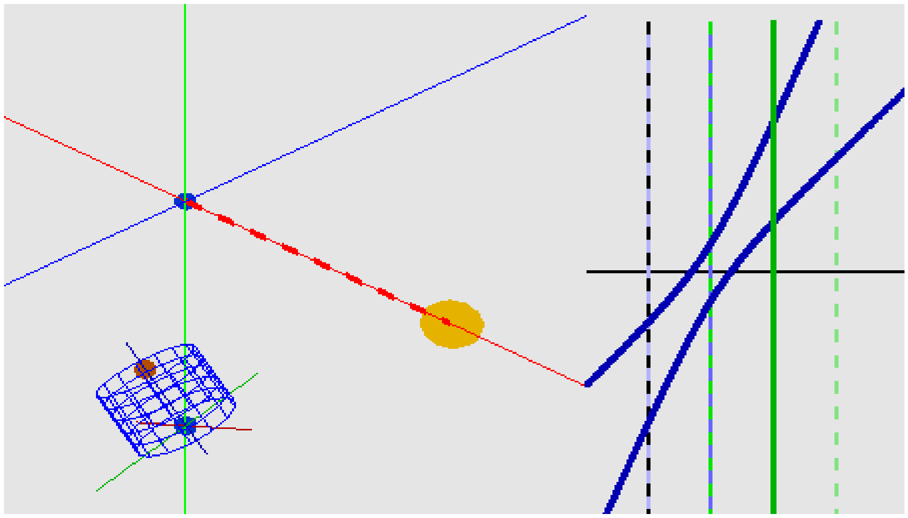

Figure 7.7: Two hyperbolas, one coincident with the $\bar{X}_3$ axis, representing the cylinder.

where $\mathbf{c}(s)$ is a space curve given in terms of its arclength s, v is the second parameter and $\mathbf{r}$ a constant vector. Its rulings are given by $v\mathbf{r}$ with specific values of s and are therefore parallel. From now on unless, otherwise specified, cylinder refers to general cylinders. In Fig. 1.8 a cylinder is shown having cusps along one of its rulings. Its two representing curves each with an inflection point, remind us of the known *developable* $\leftrightarrow$ *curve* duality. There is a further pleasing duality here, the representing curves seen in Fig. 1.9 indicate

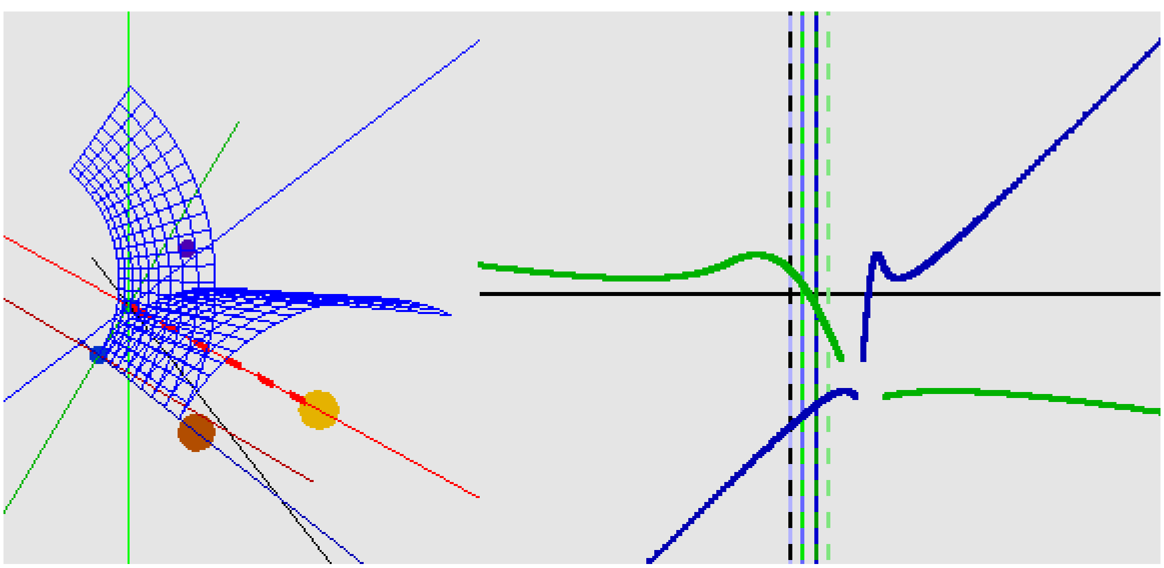

Figure 7.8: A general cylinder illustrating the *developable* $\leftrightarrow$ *curve* duality.

The ruling formed by cusps is transformed to an *inflection* point in each of the representing curves.

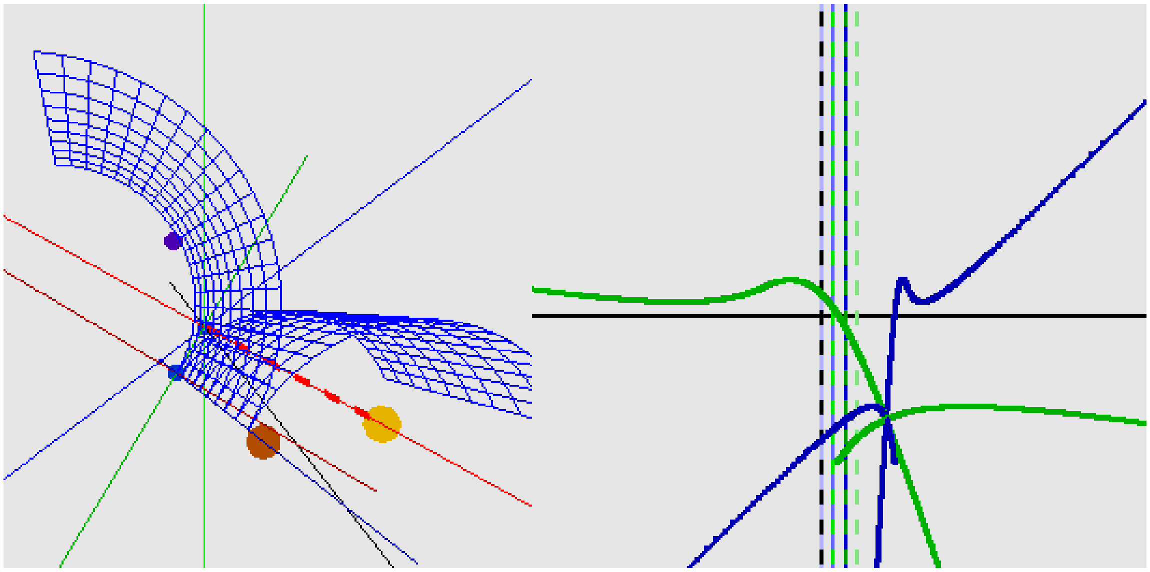

Figure 7.9: The two leaves of the surface in the previous figure are extended. Here there is a *bitangent* plane, tangent to two rulings, represented by a *crossing point* together with the inflection points in each of the representing curves. Such a hypersurface in $\mathbb{R}^N$ is represented by $N-1$ such curves; the inflection points at the same y and all crossing at the same point.

that a plane tangent to *two* rulings (i.e. bitangent) exists and is represented by crossing points one on each curve akin to the *bitangent* $\leftrightarrow$ *crossing point* for curves.

Corollary 7.0.7 *(Cones –* **C.K.Hung***) Circular Cones in* $\mathbb{R}^3$ *are represented by a pair of conic curves.*

Circular cones being quadrics are represented by a pair of conic curves whose type is determined, via Corollary 1.0.3, by the number of tangent planes the cone has parallel to the line u in the direction of the unit vector $\mathbf{u} = 1/\sqrt{3}(\hat{\mathbf{e}}_1 + \hat{\mathbf{e}}_2 + \hat{\mathbf{e}}_3)$. Unlike cylinders all three types of conics can be representing curves as stated in table 1.1. The angle θ between the cone's ruling and the axis of symmetry s is constant. So for $\mathbf{u}$ to be parallel to π_t one of the cone's tangent planes, there must exist a plane π containing $\mathbf{u}$ such that the angle $\pi \cap s = \theta$. Consider two tangent planes π_{t_1}, π_{t_2} intersecting at the line ℓ. If u is parallel to ℓ then it is also parallel to the two tangent planes and it is clear that u can not be parallel to more than two tangent planes.

Number of tangent planes parallel to $\mathbf{u}$	Represented by a pair of
0	ellipses
1	parabolas
2	hyperbolas

Table 7.1: Cones are represented by conic curves

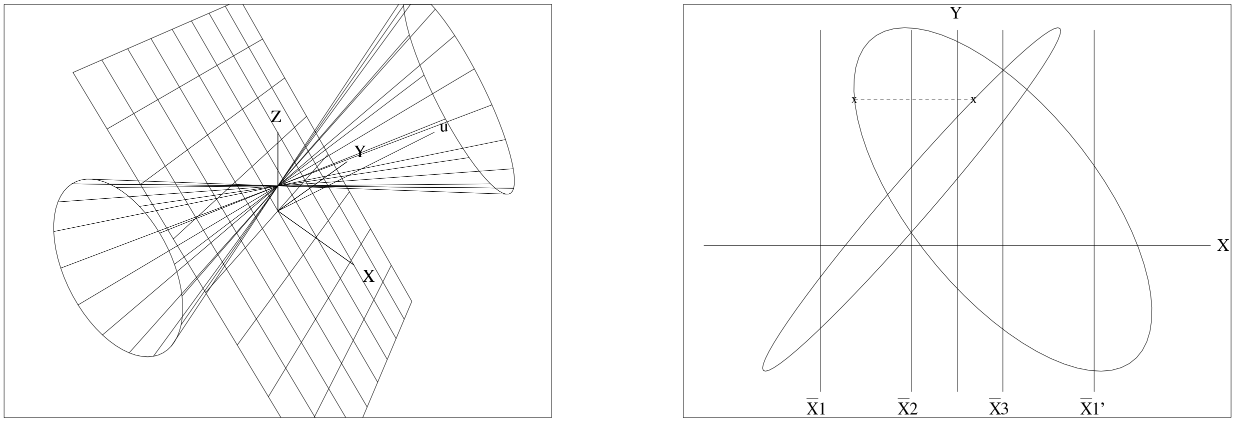

Figure 7.10: A circular (double) cone without tangent planes parallel to the line u. Cone is represented by two ellipses. Two points, one on each ellipse, represent one of the tangent planes.

A general cone can be described by

$$\mathbf{x}(s, v) = \mathbf{a} + v\mathbf{t}(s) \tag{7.17}$$

where $\mathbf{t}(s)$ is a unit vector field described on a curve, such a circle for circular cones, all rulings passing through the vertex at $\mathbf{a}$ and a point of the curve $\mathbf{t}(s)$ ([**?**] pp.90-1).

General developable surfaces

A developable surface is described by

$$\mathbf{x}(s, v) = \mathbf{y}(s) + v\mathbf{g}(s), \quad |\mathbf{g}(s)| = 1, \quad (\mathbf{y}' + v\mathbf{g}')\times\mathbf{g} = 0\ . \tag{7.18}$$

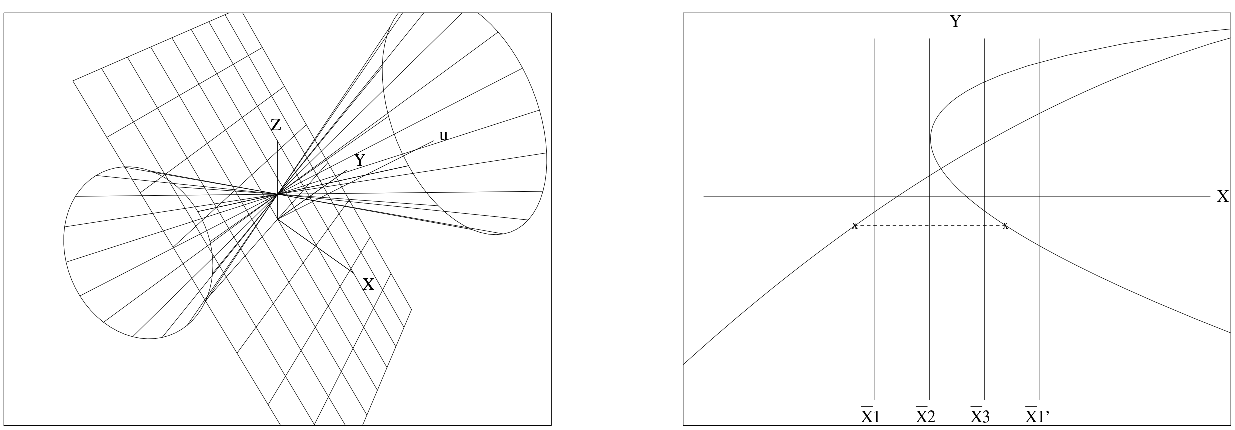

Figure 7.11: A circular (double) cone with one tangent plane parallel to the line u. Cone is represented by two parabolas. Two points, one on each parabola, represent one of the tangent planes.

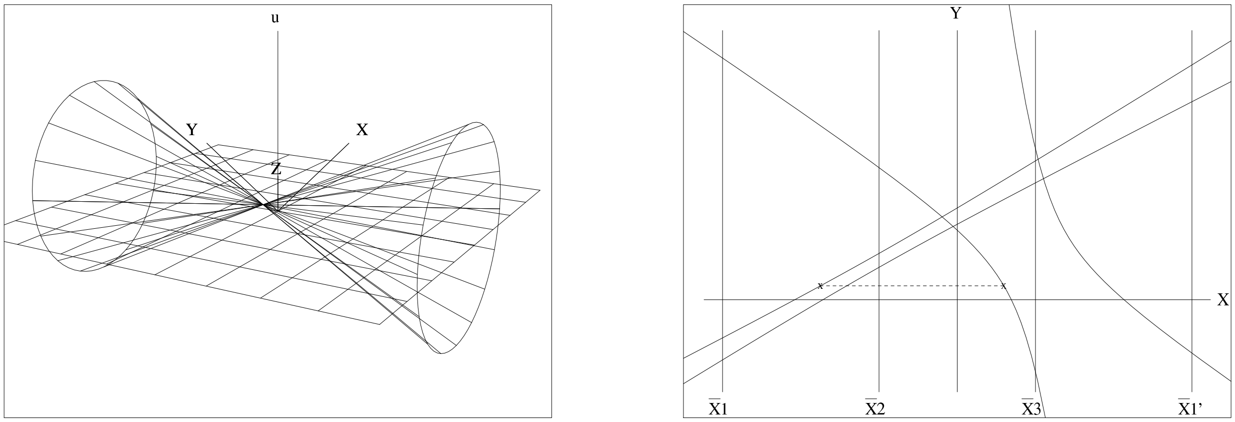

Figure 7.12: A circular cone with two tangent planes parallel to the line u.

Cone is represented by two hyperbolas. The two points, one on each hyperbola, represent one of the tangent planes.

The equation specifies the more general *ruled* surfaces; and it is the additional condition on y', v, g, g' that specializes it to the developables. An example of an intricate developable is the helicoid

$$x_1 = a\,cos\,s - av\,sins\ ,\ x_2 = a\,sin\,s + av\,coss,\ ,\ x_3 = b(s + v)\ . \tag{7.19}$$

The representing curves at two orientations, shown in Figs. 1.13, **??**, are instances of interactive exploration reminding us of interactivity's importance in visualization. The class of developables consists of planes, cylinders, cones, *tangent surfaces of a curve* or a combination thereof. Quite a few, e.g. *helicoid, polar, tangential, and rectifying developables*

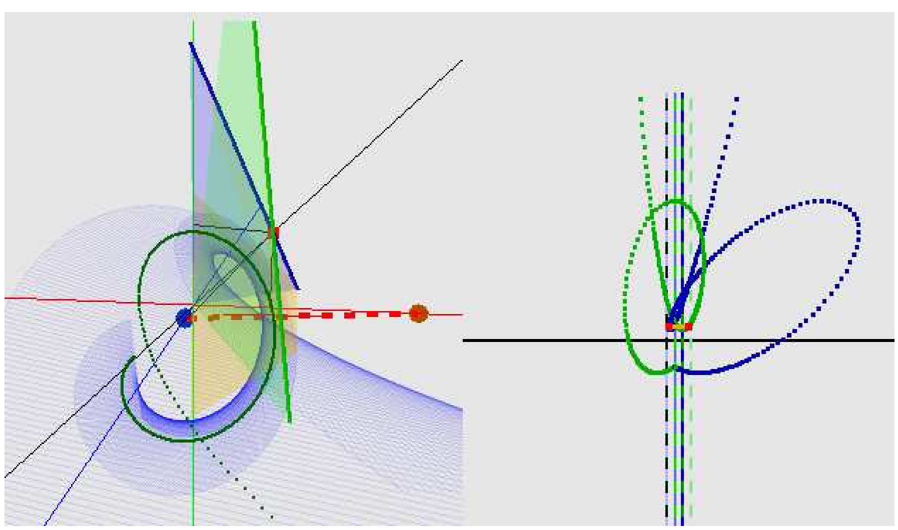

Figure 7.13: Developable helicoid and its two representing curves.

The two points on the right (one on each curve) represent the tangent plane shown on the left determined by the two line intersections with the first $\pi^s_{0'}$ and second $\pi^s_{1'}$ super-planes.

which are examples of tangent surfaces of a curve ([**?**] pp. 66-72), are difficult to visually recognize as developables. Yet in $\|$-coords they are immediately recognizable, being represented by curves, and some properties are apparent from the duality *developables* $\leftrightarrow$ *space curves* i.e. *cusp* $\leftrightarrow$ *inflection-point* Fig. 1.8, *bitangent plane* $\leftrightarrow$ *crossing-point* Fig. 1.9. It is significant that for developables in the above examples the two representing curves are similar. These curves are images of the surfaces' section with the first two super-planes so they are projectively equivalent (i.e. one can be obtained from the other by a projective transformation) for the cylinders and cones. For the helicoid, whose rulings are a pencil of lines on its axis, the reason is not so obvious. Still for other developables this may not be true.

In our surroundings there are lots of objects that look "nearly" developable and many parts are manufactured by deforming flat sheets. This and the simple $\|$-coordinate representation motivate the study of "approximate developables", as for the proximate planes in chapter **??**, by introducing perturbations in the developables' equation allowing $|(\mathbf{y}' + v\mathbf{g}')\times\mathbf{g}| < c \neq 0$ but small (see also the following section on ruled surfaces), and there may be other useful definitions. The conjecture is that families of "nearly developables" are represented in $\|$-coords by curved "strips" with properties "close" to those discovered by duality (of developables) with representing curves and amenable to an intuitive treatment. New classes of surfaces (patches), with their N-D generalizations, easy to visualize and work with interactively may emerge suitable for applications like Geometric Modeling.

Ruled Surfaces

Developable surfaces are a subset of the more general class of *ruled* surfaces $\mathcal{R}$ which are generated by a one parameter family of lines. A ruled surface, also called a *scroll*, can

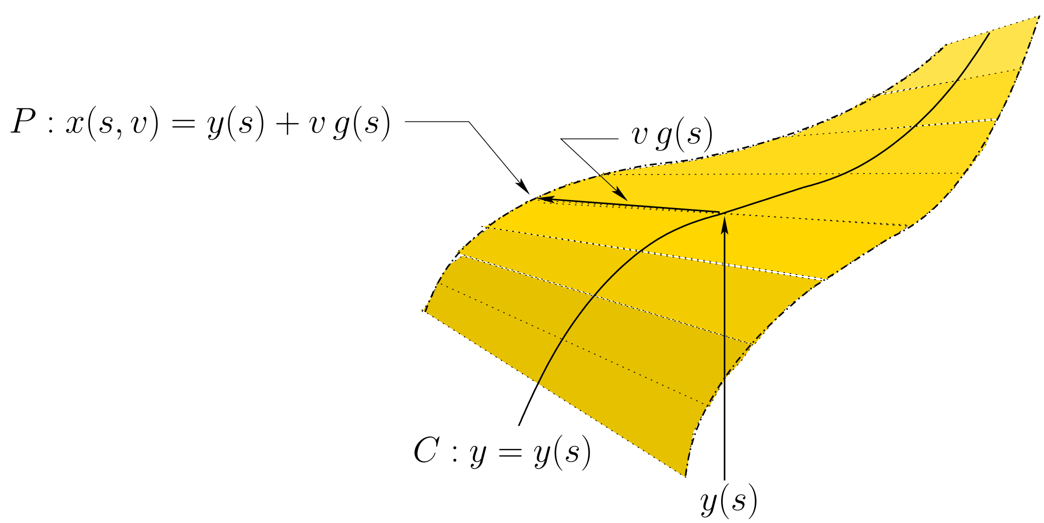

Figure 7.14: Generation of a ruled surface.

Notice the rulings successively "twisting" about the base curve C.

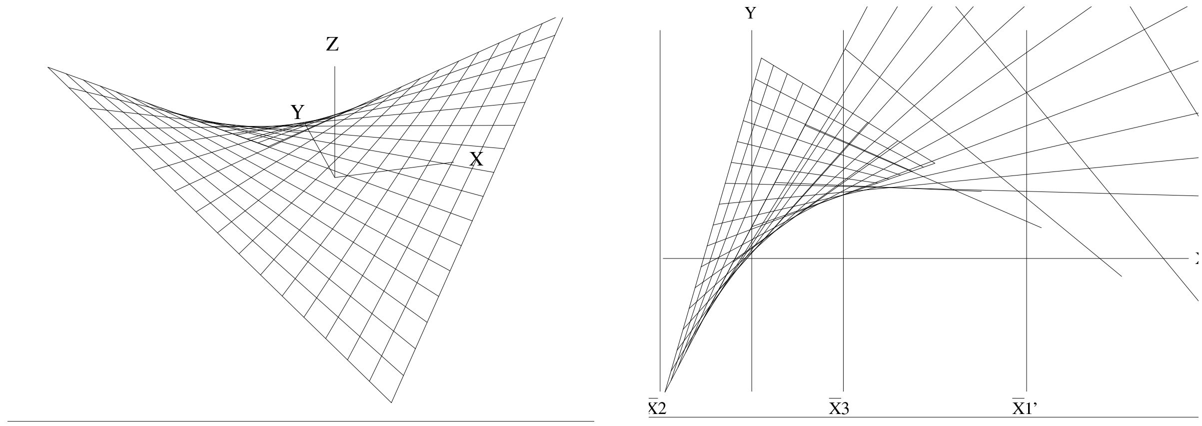

Figure 7.15: The saddle (left) is a doubly-ruled surface.
One of the two regions representing it on the left. Note the conic (parabolic) boundary.

be created by the motion of a line called *generating line, generator, or ruling* as shown in Fig. 1.14. Let $C : \mathbf{y} = \mathbf{y}(s)$ be a curve and $\mathbf{g}(s)$ a unit vector in the direction of a ruling passing through a point $\mathbf{y}(s)$ of C. A point $P : \mathbf{x}(s, v)$ on the surface is then given by

$$\mathbf{x}(s, v) = \mathbf{y}(s) + v\mathbf{g}(s) \quad (\mathbf{y}' + v\mathbf{g}') \times \mathbf{g} \neq 0 \quad \forall\ (s, v)\ . \tag{7.20}$$

The curve $C : \mathbf{y} = \mathbf{y}(s)$ is called the *base curve* or *directix*. The rulings are the curves $s = constant$. When $\mathbf{y}$ is a constant the surface is a cone and when $\mathbf{g}(s)$ is a constant the surface is a cylinder. The difference here is that $\mathbf{y}' + v\mathbf{g}' \times \mathbf{g} \neq \mathbf{0}$ allowing ruled surfaces to "twist" unlike developables. The tangent plane π_P at a point P on a ruled surface ρ contains the whole ruling r_P on P. For another point $Q \in \rho$ the tangent plane π_Q still contains r_p. Whereas all points on a ruling of a developable have the *same* tangent plane, moving along points on a ruling r of a ruled surface causes the corresponding tangent planes to *rotate* about r this being the essential difference and the basis for the $\|$-coords representation of ruled surfaces.

There is a wonderful collection of ruled and many other kinds of surfaces in [**?**]. Ruled surfaces used as architectural elements are not only beautiful but also have great structural strength. A surface can be *doubly-ruled* in the sense that any one of its points is on *two* lines completely contained in the surface (i.e. it can be generated by either one of two sets of moving lines). An elegant result ([**?**] p. 42) is that in $\mathbb{R}^3$ the *only* doubly ruled surfaces are quadrics: the hyperboloid of one sheet and saddle (hyperbolic hyperboloid).

The representing curve $\bar{\sigma}_{0'}$ of a developable σ can be obtained as the *envelope* of the family of lines $\bar{R}_{0'}$ on the points $\bar{r}_{12}, \bar{r}_{13}, \bar{r}_{23}$ for each ruling r of σ. Similary $\bar{\sigma}_{1'}$ is the envelope of the lines $\bar{R}_{1'}$ on $\bar{r}_{1'2}, \bar{r}_{1'3}, \bar{r}_{23}$. A matched pair of points $\bar{\pi}_{0'} \in \bar{\sigma}_{0'}$, $\bar{\pi}_{1'} \in \bar{\sigma}_{1'}$ represents the *single* plane containing $r \subset \sigma$ and tangent to everyone of its points. By contrast, a plane tangent to a ruled surface ρ at a point contains a full ruling r but as the point of tangency is translated continuously along r the tangent plane continuously rotates about r. In $\|$-coords the points $\bar{\pi}_{0'}, \bar{\pi}_1$ continuously *translate* in tandem (with the same y coordinate) along the corresponding lines $\bar{R}_{0'}, \bar{R}_{1'}$ representing the rotating tangent planes along r. An example is the *saddle* Fig. 1.15 (left) and it is represented by two regions whose boundaries are conic curves.

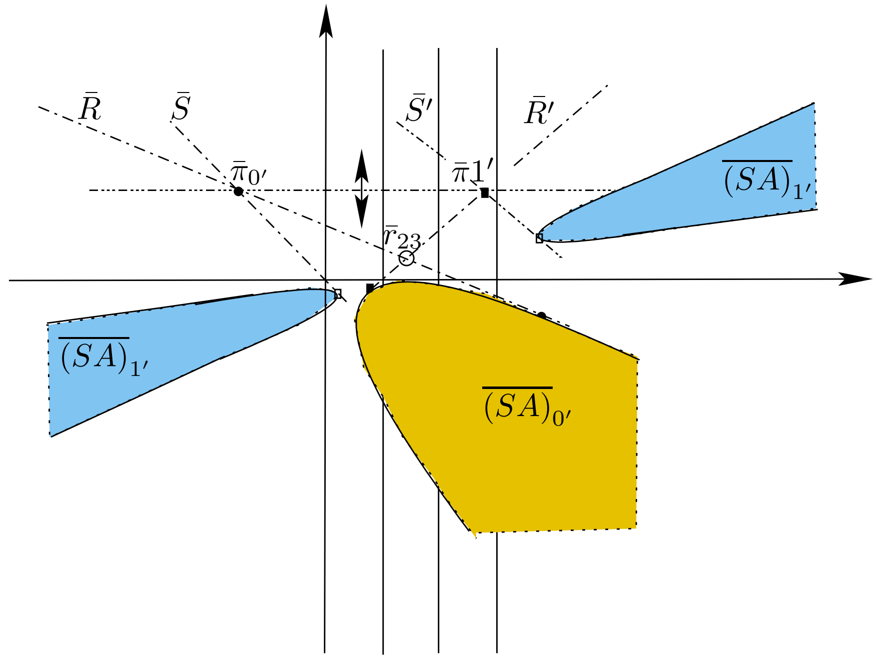

Figure 7.16: The saddle's representation is the compliment of the shaded regions.

The saddle SA is represented by the complements of the two shaded regions ($\overline{(SA)}_{0'}$ and $\overline{(SA)}_{1'}$) having parabolic and hyperbolic boundaries respectively. The points $\bar{\pi}_{0'}, \bar{\pi}_{1'}$ representing a tangent plane and the ruling $r \subset \pi$ are constructed with the matching algorithm. A different ruling on π can be constructed suggesting that SA is doubly-ruled.

Theorem 7.0.8 *Representation of Ruled Surfaces – A. A ruled surface ρ is represented by the regions $\bar{\rho}_{j'}$, $j = 0, 1$ containing the families of lines $\mathcal{R}_j = \{\bar{R}_j\}$ whose envelopes*

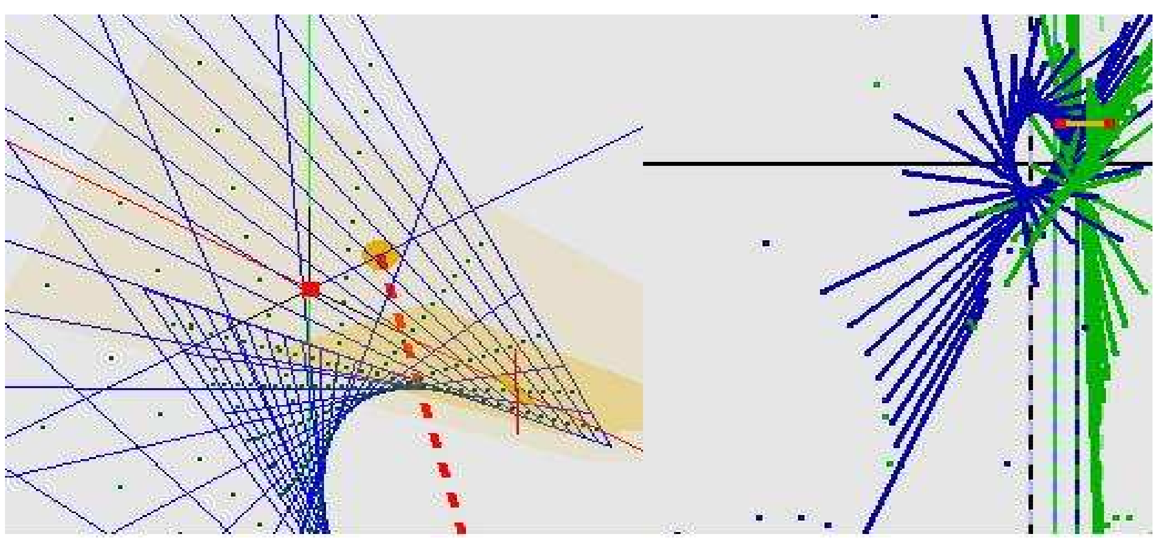

Figure 7.17: Conics representing the saddle.

Representation of the saddle showing an elliptical boundary and the tips of the two hyperbolic branches. For ruled surfaces, the regions are covered by the line tangents to the two boundaries. The two linked points represent a tangent plane.

are the boundaries $\partial\bar{\rho}_{j'}$ specified by Lemma 1.0.1.

To emphasize, a developable is represented by two curves which are the envelopes of the families of lines $\mathcal{R}_{j'}$ (formed from the representation of its rulings as described above). A ruled surface ρ is represented by two regions $\bar{\rho}_{j'}$, $j = 0, 1$ whose boundaries $\partial\bar{\rho}_{j'}$ are also the envelopes of the lines $\mathcal{R}_{j'}$ (obtained in the same way from the representation of its rulings), **together** with the lines $\mathcal{R}_{j'}$. Equivalently, it is helpful to consider $\partial\bar{\rho}_{j'}$ as a *line-curve* and $\bar{\rho}_{j'}$ the region covered by its tangents. The region's structure enables the construction of the matching algorithm for choosing pairs of points, representing the surface's tangent planes. By the way, the boundary curves deriving from the rulings of a developable *differ* from those obtained from the rulings of a ruled surface. These points are clarified with the examples.

To keep the discussion intuitive and reasonably precise without getting bogged down in technical details, we state without proof that the regions encountered have boundaries consisting of a finite number of simple (i.e. non self-crossing) curves, each of which can be partitioned into a finite number of convex (upward or downward) curves. The *Jordan Theorem* states that a simple closed curve separates the plane $\mathbb{R}^2$ into two regions: the interior and exterior. For our needs, we generalize this result to $\mathbb{P}^2$ by allowing a finite number of ideal points on the boundary which we consider "projectively" as a simple closed curve. Of course, the presence of ideal points needs to be treated judiciously. Relative to a region Ω a point is *exterior* if there is a tangent from it to the boundary. Otherwise it is *interior*. For a $\partial\Omega$ simple and closed there is a tangent in each direction except those of the ideal points it contains. Hence, other than these all other ideal points are exterior to Ω. Two points are on opposite sides of $\partial\Omega$, one interior and the other exterior, if the line on the points crosses the boundary an *odd* number of times. To avoid complicating this rule, the line is not allowed to cross at points where two portions (one convex upward and

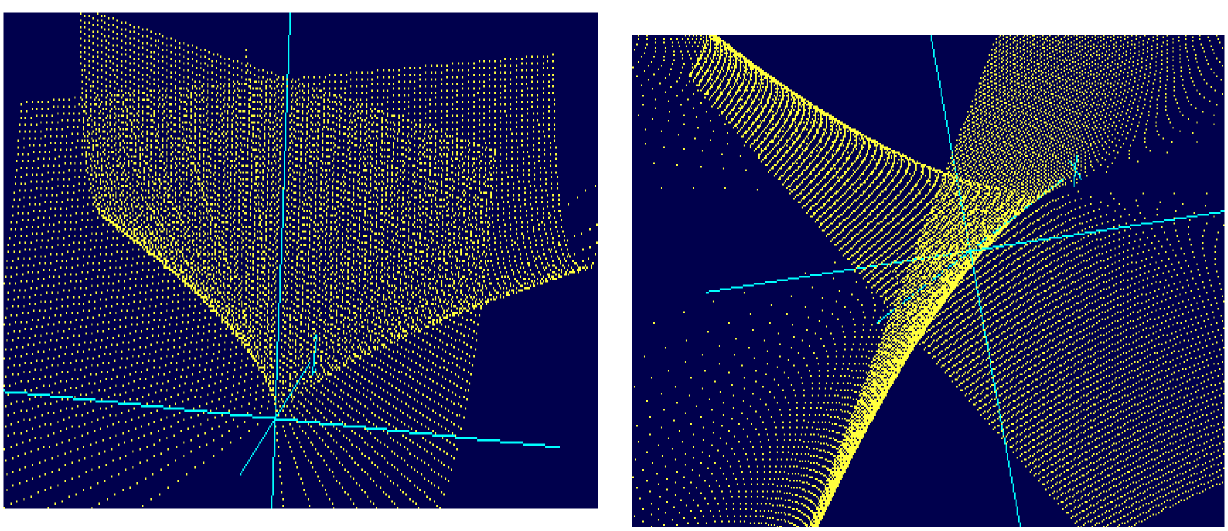

Figure 7.18: Conoids.

The rulings of Whitney's umbrella (left) and Plüker's-conoid (right) are perpendicular to a line which here is coincident with the vertical axis. They are both *conoids*.

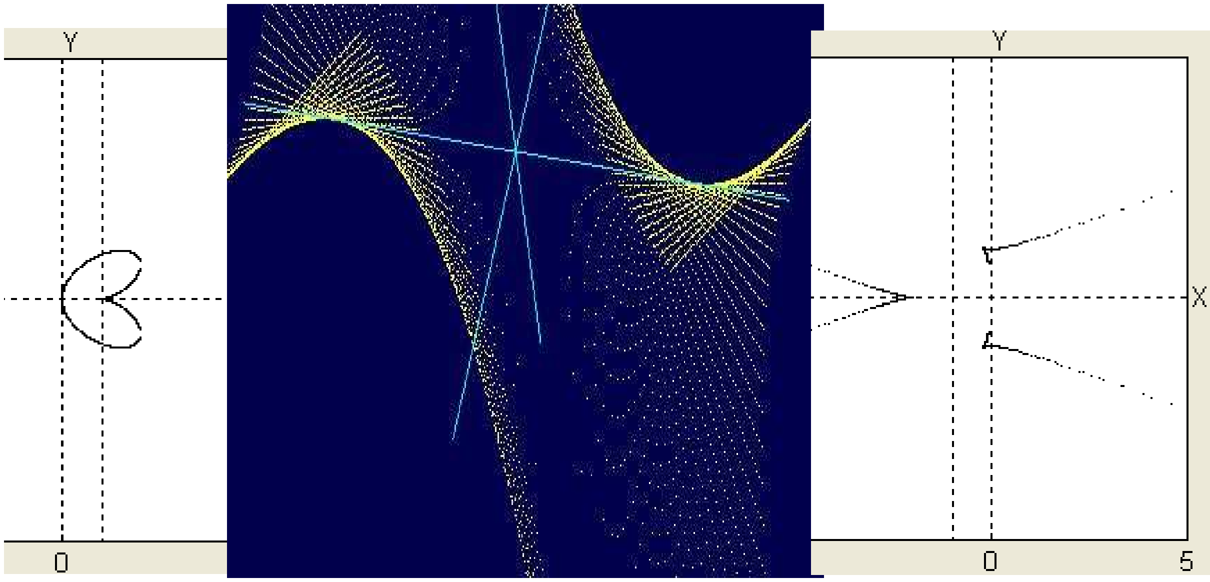

Figure 7.19: (Center) The parabolic conoid PC is a ruled algebraic surface of degree 3. The first representing region $\overline{(PC)}_{0'}$ a cardioid is on the left and the second $\overline{(PC)}_{1'}$ on the right. The cusps are the images of inflection points.

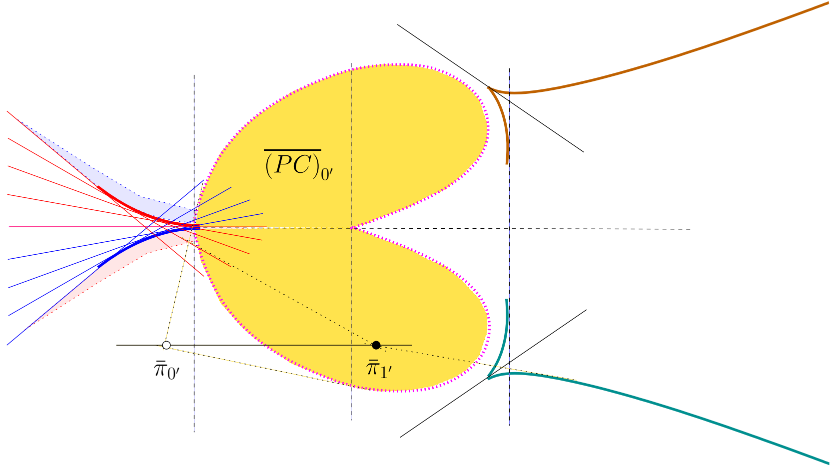

Figure 7.20: Representation of the parabolic conoid and one of its tangent planes.

the other downward) of $\partial\Omega$ are joined. For $\partial\Omega$ a convex curve (not closed) it is helpful to consider it as a line-curve to recognize that its exterior is still the region covered by its tangents. It is clear from theorem 1.0.8 that for each point $\bar{\pi}_{j'} \in \partial\bar{\rho}_{j'}$, the region $\bar{\rho}_{j'}$ must contain at least a segment of the tangent at $\bar{\pi}_{j'}$ and hence all its points are on $\partial\bar{\rho}_{j'}$ or its exterior.

Conoids are ruled surfaces whose rulings are parallel to a plane and are perpendicular to an *axis* normal to the plane like those shown[2] in Fig. 1.18. Spiral staircases are shaped after the *right conoids*. Another specimen is the *parabolic conoid* seen in Fig. 1.19 (center) which, like the saddle, has a parabolic directix.

[2]The figures were obtained using the beautiful software written by M. Spivak for her course project.

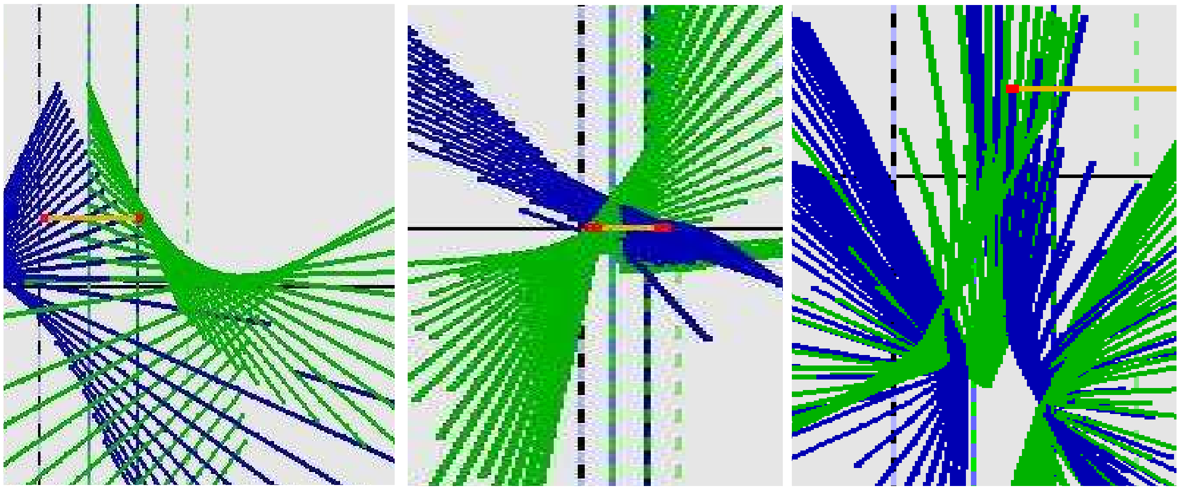

Figure 7.21: Representations (left and center) of a *parabolic conoid* for two orientations. Representation of the *ruled cubic* on the right.The straight lines reveal that the surfaces are ruled and partially outline the regions' boundaries. A tangent plane is represented by the two linked points.

A famous ruled surface is the *Möbius strip* described by:

$$\mathbf{x} = \mathbf{y}(\theta) + v\mathbf{g}(\theta)\ ,\ -\tfrac{1}{2} < v < \tfrac{1}{2}\ ,\ 0 \leq \theta \leq 2\pi\ , \tag{7.21}$$
$$\mathbf{y}(\theta) = (cos\,\theta)\hat{\mathbf{e}}_{\mathbf{1}} + (sin\,\theta)\hat{\mathbf{e}}_{\mathbf{2}}\ ,$$
$$\mathbf{g}(\theta) = (sin\,\tfrac{1}{2}\,\theta\,cos\,\theta)\hat{\mathbf{e}}_{\mathbf{1}} + (sin\,\tfrac{1}{2}\,\theta\,sin\,\theta)\hat{\mathbf{e}}_{\mathbf{2}} + (cos\,\tfrac{1}{2}\,\theta)\hat{\mathbf{e}}_{\mathbf{3}}\ ,$$

It is *non-orientable* in the sense that tracing the normal vector at a moving point along a loop, specified by its directrix the circle $\mathbf{y}(\theta) = cos\,\theta\hat{\mathbf{e}}_{\mathbf{1}} + sin\,\theta\hat{\mathbf{e}}_{\mathbf{2}}$ ([**?**] p. 170), the normal flips by 180^0 from its original direction when the traversal is completed. In other words, this surface has only one side. The strip's structure is elucidated in Fig. 1.22 (right) showing the a ruling moving along the directrix twisting at an angle $\theta/2$ from the vertical, where θ is the angle swept along the directrix, intersecting the central axis in 3 positions inverting its orientation by 180^0 by the time it completes the circuit to create the twisted wonder we see in Fig. 1.22 (left).

How does this surface appear in $\|$-coords? Dazzling patterns represent it at various orientations Fig. 1.23. Of particular interest is the search for a pattern characterizing non-orientability. In Fig. **??** we see a closed circuit on the strip and the corresponding pair of representing curves. This is repeated for a different orientation producing a pair of representing curves easier to study Fig. 1.24 (right). Each intersection point represents a tangent plane π for which $\bar{\pi}_{0'}$ and $\bar{\pi}_{1'}$ coincide, that is π is perpendicular to the x_2x_3 principal plane with its first coefficient $c_1 = 0$. A nice way to understand the twisting is suggested in Fig. 1.24 (left) where the strip is placed on a plane, in this case the x_2x_3, creating three "folds" which do not have be symmetrically positioned as the ones in the picture. At each of the folds the tangent plane is perpendicular with respect to the x_2x_3 plane where, by the "Flip" Corollary in the Chapter on planes, the first coefficient c_1 of the tangent plane's eq. changes sign say $+ \rightarrow - \rightarrow + \rightarrow -$ from the start to the completion of the circuit. The $c_1 = 0$ corresponds to three intersections of the representing curves in

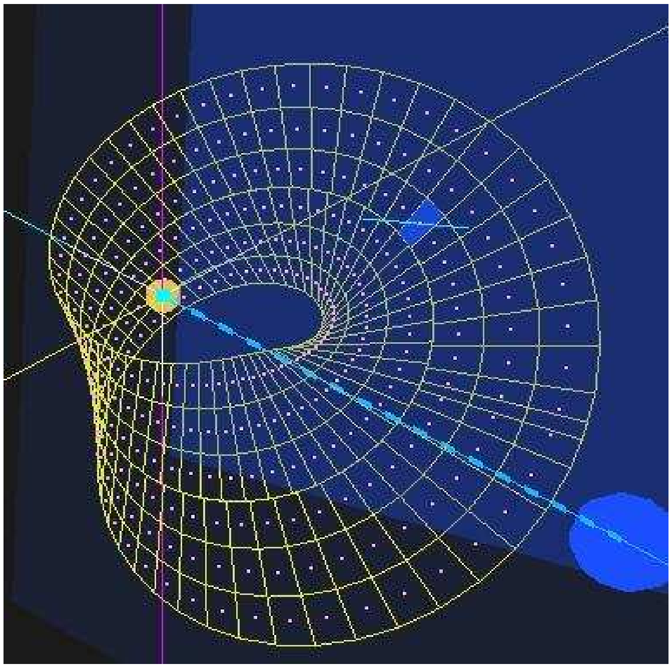

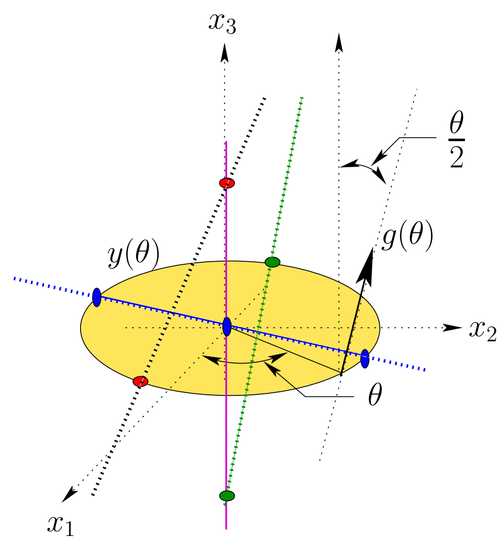

Figure 7.22: *Möbius strip* surface and its structure(left).

A ruling traversing the circular directrix intersects the central axis three times in one complete circuit.

Fig. 1.24 (right). By the same argument the remaining coefficients c_2, c_3 vanish 3 times and change their sign. Hence the tangent plane's normal vector $\mathbf{c} = (c_1, c_2, c_3) \rightarrow -\mathbf{c}$ and flips direction. The three intersections together with the ensuing flip is clearly a necessary

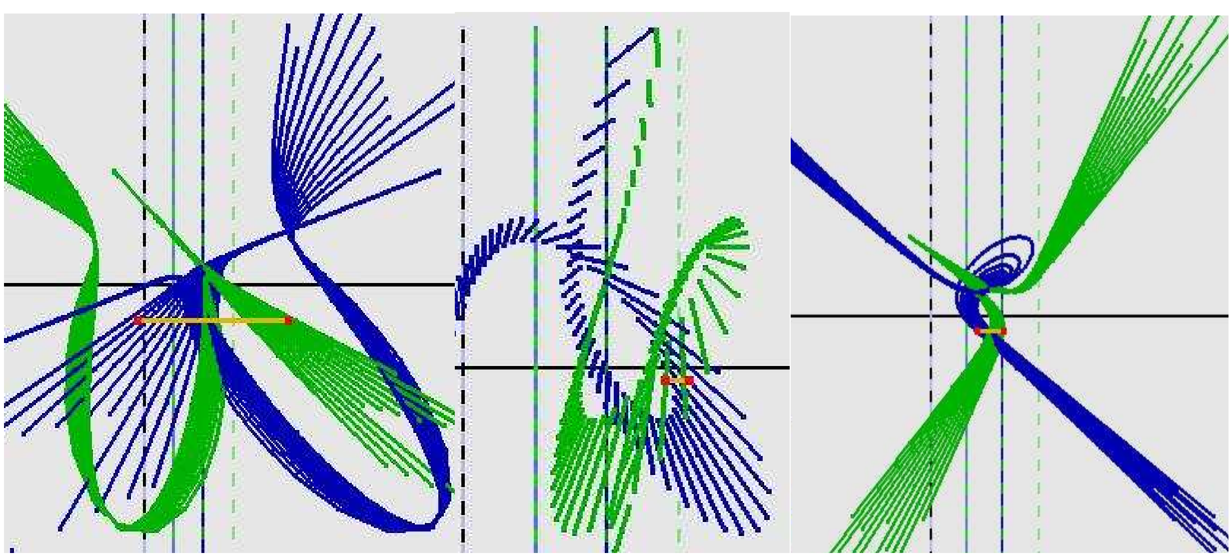

Figure 7.23: Representation of a *Möbius strip*.

On the right, the cusp (which is the dual of an inflection point) of the "bird-like" pattern suggests that the *Möbius strip* is a "3-D inflection point". A tangent plane is represented by the two linked points.

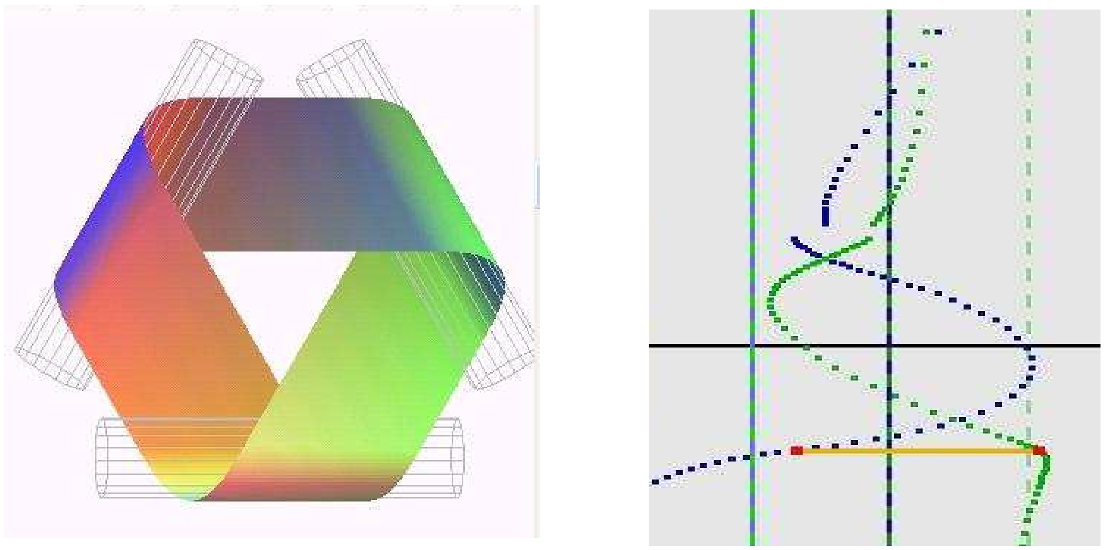

Figure 7.24: Visualizing non-orientability.

(left) *Möbius strip* (thanks and acknowlegment to [**?**]) placed on one of the principal planes say x_2x_3. Note the 3 folds resulting in 3 tangents planes perpendicular to the x_2x_3 plane. (right) Traversal of a closed circuit on the *Möbius strip* represented in $\|$-coords by two curves. There are 3 crossing points each corresponding to a tangent plane perpendicular to the x_2x_3 plane.

and sufficient condition for non-orientability. For a closed circuit on a doubly-twisted Möbius strip, the representing curves the $\bar{\pi}_{0'}$ and $\bar{\pi}_{1'}$ coincide at six intersection points corresponding to six folds and so on.

It appears then that a pattern characteristic of non-orientability has been found whose verification relies on interactively tracing a closed circuit on the representing curves. The picture, of course, is not proof but provide insights that may lead to a proof – this is an objective of visualization.

This points the way for researching non-orientability in $\mathbb{R}^4$ and higher dimensions as well as knot theory. Here is another thought: twisting a curve about its tangent at a point creates an inflection point. So is the cusp seen in Fig. 1.23 (right), which is the dual of an inflection point, together with the surrounding pattern in the second curve an inkling of an non-orientable twist; like a "3-D inflection point" produced by twisting and then joining a curved strip? Though imprecise this depiction, in the spirit of visualization, is intuitive stimulating ideas. Does the bird-like pattern represent the Möbius strip's non-orientability. These observations and questions will hopely stimulate further research on the representation of non-orientability and ruled surfaces. We close this section with a conclusion partially anticipating a forthcoming result on convex surfaces.

Theorem 7.0.9 (Representation of developable, ruled and convex surfaces in $\mathbb{R}^N$**)** *A surface* $\sigma \subset \mathbb{R}^N$ *and represented by* $N-1$ *regions* $\bar{\sigma} \subset \mathbb{P}^2$ *is*

1. **ruled but not developable** $\Leftrightarrow$ *all points of* $\bar{\sigma}$ *are* **exterior** *with respect to the boundary of at least one of its* $N-1$ *regions,*

2. **developable** $\Leftrightarrow$ $\bar{\sigma}$ *consists of* $N-1$ *curves, the boundaries of* $\bar{\sigma}$*, all having the same* y*-range,*

3. **convex** $\Rightarrow$ *the boundaries of the* $N-1$ *regions are* **gh** *(generalized hyperbola) and all points of* $\bar{\sigma}$ *are* **interior** *with respect to the boundary of at least one of the regions.*

Prior to treating more general surfaces, an older inexact but very useful surface representation is included illustrated with an application to instrumentation and process control. It is of specialized interest and independent so that it may be skipped without impairing other chapter topics.

More General Surfaces

*T*he formulation in eq. 1.13 applies to any sufficiently smooth surface. We open this last section by examining the representation of the venerable sphere in $\mathbb{R}^3$

$$SP \,:\, x_1^2 + x_2^2 + x_3^2 = r^2 \tag{7.22}$$

Its intersection with the first superplane $\pi^s_{0'}$, a circle $C1$ and its hyperbolic image $\overline{C1}$ are :

$$C1 \,:\, 2x_1^2 - 4x_1x_2 + 5x_1^2 - r^2 = 0 \,,\; \overline{C1} = \partial(\overline{SP})_{0'} \,:\, 3r^2x^2 - 6y^2 - 6r^2x + 5r^2 = 0 \,. \tag{7.23}$$

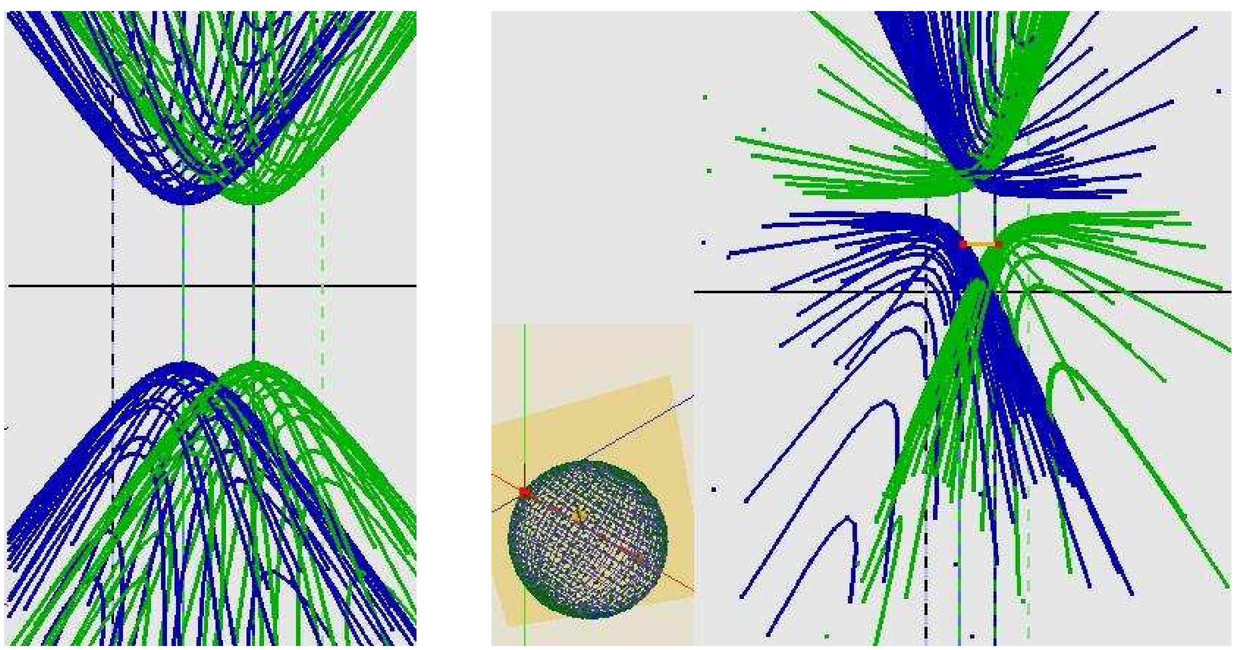

Figure 7.25: Representation of a sphere.

Representation of a sphere centered at the origin (left) and after a translation along the x_1 axis (right) causing the two hyperbolas to rotate in opposite directions. As in previous figures the two linked points represent a tangent plane.

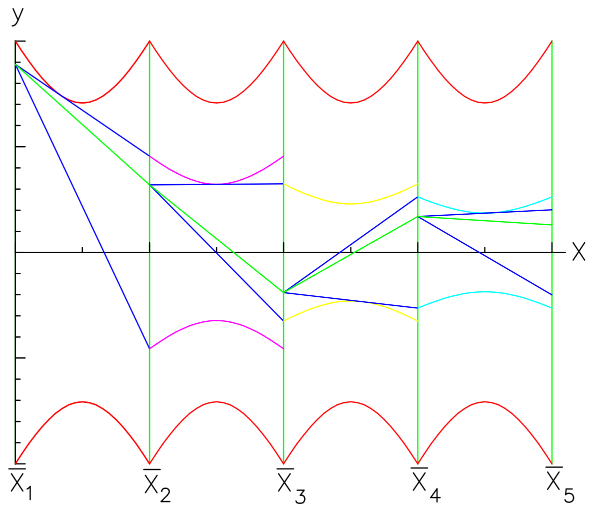

Figure 7.26: Interior point construction of a sphere in $\mathbb{R}^5$.

The hyperbola's vertices (i.e. min & max) are at the points $(1, \pm\sqrt{2/3}r)$. The second boundary $\partial(\overline{SP})_{1'}$ is the same hyperbola translated to the right by one unit as shown on the left of Fig. 1.25. Clearly the representation of a sphere in $\mathbb{R}^N$ consists of $N-1$ such hyperbolas spaced successively one unit apart. Translation of the sphere along the x_1 axis rotates $\partial(\overline{SP})_{0'}$ clockwise and $\partial(\overline{SP})_{1'}$ *counter-clockwise*, Fig. 1.25 (right), an interesting manifestation of the *translation* $\leftrightarrow$ *rotation* duality we encountered on previous occasions. It is useful to compare this representation with the inexact one given in the previous section. Consider the 5-D sphere

$$5SP\,;\; x_1^2 + x_2^2 + x_1^3 + x_4^2 + x_5^2 = r^2 \tag{7.24}$$

whose projection on the principal x_1x_2 plane is the circle $x_1^2 + x_2^2 = r^2$ represented by the hyperbola $2r^2x^2 - y^2 - 2r^2x + r^2 = 0$ going through the points $(\ x = 0\,,\ y = \pm 1\ )$ and $(\ x = 1, y = \pm 1\ )$. The other projections are represented by translations of this hyperbola successively by one unit. All four are superimposed as in Fig. 1.26 showing that the exact representation, also with hyperbolic boundaries, is an "upgrade" though the hyperbolae differ. The picture helps in following the construction of a point interior to $5SP$. Let us start by choosing a value of $x_1 = a_1 \in [-r, r]$ placing this on the $\bar{X}_1$ axis and drawing the tangents from this point $(0, a_1)$ to the upper and lower branches of the first hyperbola. This equivalent to intersecting $5SP$ with the plane $x_1 = a_1$ resulting in the $4-D$ sphere:

$$4SP\ :\ x_2^2 + x_1^3 + x_4^2 + x_5^2 = r^2 - a_1^2\ , \tag{7.25}$$

with radius $\sqrt{r^2 - a_1^2}$ seen in the figure on the $\bar{X}_2$ axis at its intersection with each of the two tangents. Also shown is the hyperbola representing the projection of $4SP$ on the x_2x_3 plane. A choice $x_2 = a_2 \in [\ -\sqrt{r^2 - a_1^2}\ ,\ \sqrt{r^2 - a_1^2}\ ]$ is made reducing the dimension providing a 3-D sphere and so on. As long as the successive choices are in the allowable range (i.e. radius of reduced sphere) the polygonal line joining the a_i does not intersect the intermediate curves as the one shown and it represents an interior point of $5SP$. If the polygonal line is tangent to any of the intermediate curves it represents a point on

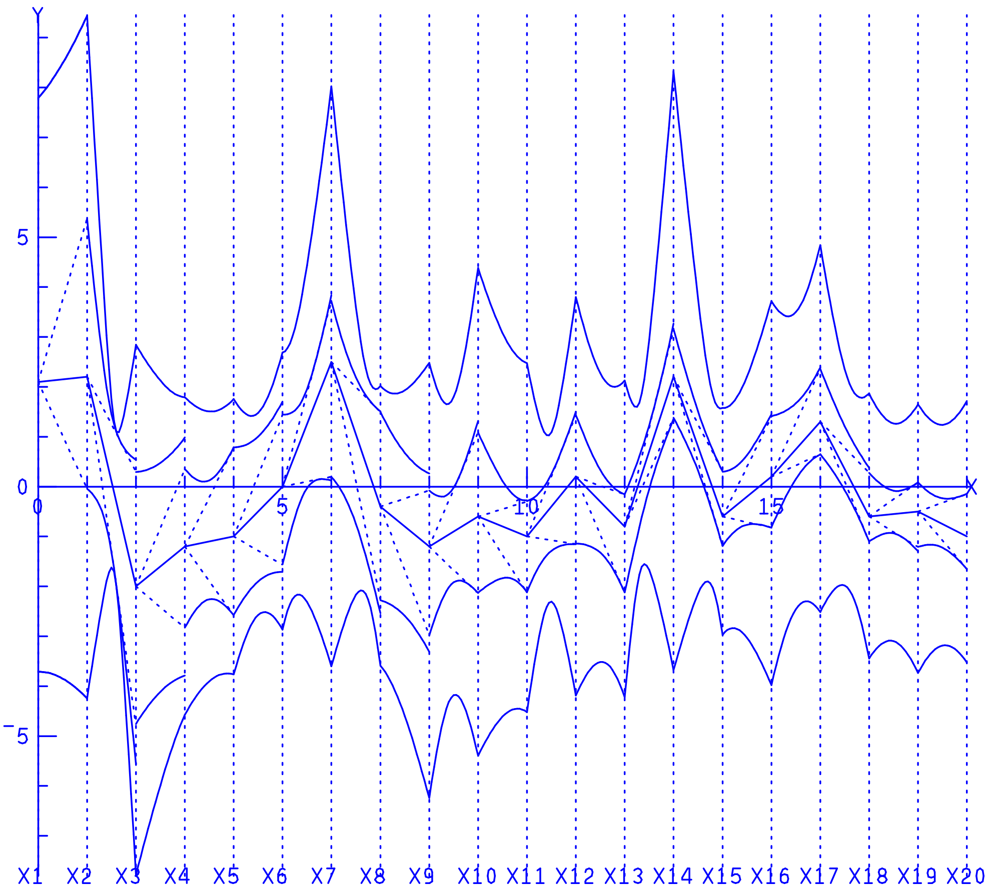

Figure 7.27: Interior point construction for a convex hypersurface in $\mathbb{R}^{20}$.

the surface and if it intersects then it represents an exterior point. It is clear then that all interior and surface points of a sphere $SPN \subset \mathbb{R}^N$ are represented by the polygonal lines in between the hyperbolae representing the projections on the principal planes and therefore slightly overlapping the hyperbolae $\partial(\overline{SP}_{i'})$ intersect at their the $\bar{X}_i$ axes at $y = \pm\sqrt{2/3}r$ their extreme points. This algorithm is useful and more general as shown in Fig. 1.27.

All the points representing tangent planes are in the *interior* of the upper and lower branches. Recall the unit vector $\hat{\mathbf{u}} = 1/\sqrt{3}(\hat{\mathbf{e}}_\mathbf{1} + \hat{\mathbf{e}}_\mathbf{2} + \hat{\mathbf{e}}_\mathbf{3})$ along the line u. Let π_u be the plane through the origin with unit normal $\hat{\mathbf{u}}$. The intersection $\pi_u \cap SP = CU$ is a great circle playing an important role in the representation of SP. All tangent planes of SP along CU have the sum of their coefficients $S = c_1 + c_2 + c_3 = 0$ vanishing, for $\mathbf{N} = (c_1, c_2, c_3)$, $\mathbf{N} \cdot \hat{\mathbf{u}} = 0$ since these planes are all parallel to the line u they are represented by ideal points thus causing the split into two hyperbolic branches. The tangent planes The representing points of the tangent planes above CU are on the branch and those below form the lower branch. Note that at the north and south pole the tangent planes are $\pi_p : x_3 = \pm 1$ with representing points $\bar{\pi}_{0'} = (\ 2, \pm r, 1\ )$ on the $\bar{X}_2$ axis but *not on the boundary* $\overline{SP}_{0'}$ which is formed by the representing points of tangent planes on $\pi^s_{0'} \cap SP$ and does not include the poles. Similarly the $\bar{\pi}_{1'}$ are on the $\bar{X}_{1'}$-axis and the same $y = \pm r$.

Whereas the interior points of the hyperbolic regions properly matched represent the sphere's tangent planes there is another interesting matching which gives a feel about the sphere's interior. Consider the representation of concentric spheres (centered at the origin) with radii r ranging between a minimum r_m and r_M and maximum values. As r increases the hyperbolas' vertices and the rest of the curve rise linearly with r enlarging the region in between the upper and lower branches. Let a pair of points at $y = y_a$ be given on the hyperbolic boundaries representing a tangent plane π_a of one of the spheres. Its radius a is found from the vertices of the hyperbolas, the points are on, which are at $y = \pm\sqrt{2/3}a$. Draw the vertical lines on the pair of given points. Any other pair of points at $y = y_c$ represents a tangent plane π_c parallel to π_a on the sphere with radius $c = y_c/y_a a$.

The intersection of the superplanes with ellipsoids and paraboloids are ellipses ergo their representation by hyperbolic regions Fig. 1.28. For the paraboloid, the intersections may also be parabolas in which case the representing regions would be either hyperbolas each with one vertical assympotes or vertical parabolas – see section on conics in Chapter on curves. In general the intersection of the super-planes with bounded and convex surface σ is a boundex convex set *bc* whose $\|$-coords representation is a generalized hyperbola *gh* and such an example is shown on the left in Fig. 1.29.

Theorem 7.0.10 (Convexity) *A bounded surface $\sigma \subset \mathbb{R}^N$ is convex $\Leftrightarrow$ if for* **any orientation** *it is represented by* **gh** *regions.*

Varying the orientation of σ interactively and viewing that the resulting representations are *gh* regions is an *empirical* indication of σ's plausible convexity. There is a better way. We examine the representation of surfaces having small deviations from convexity. In Fig. 1.29 on the right is a surface σ_b with protuberance a small bump. Its orientation

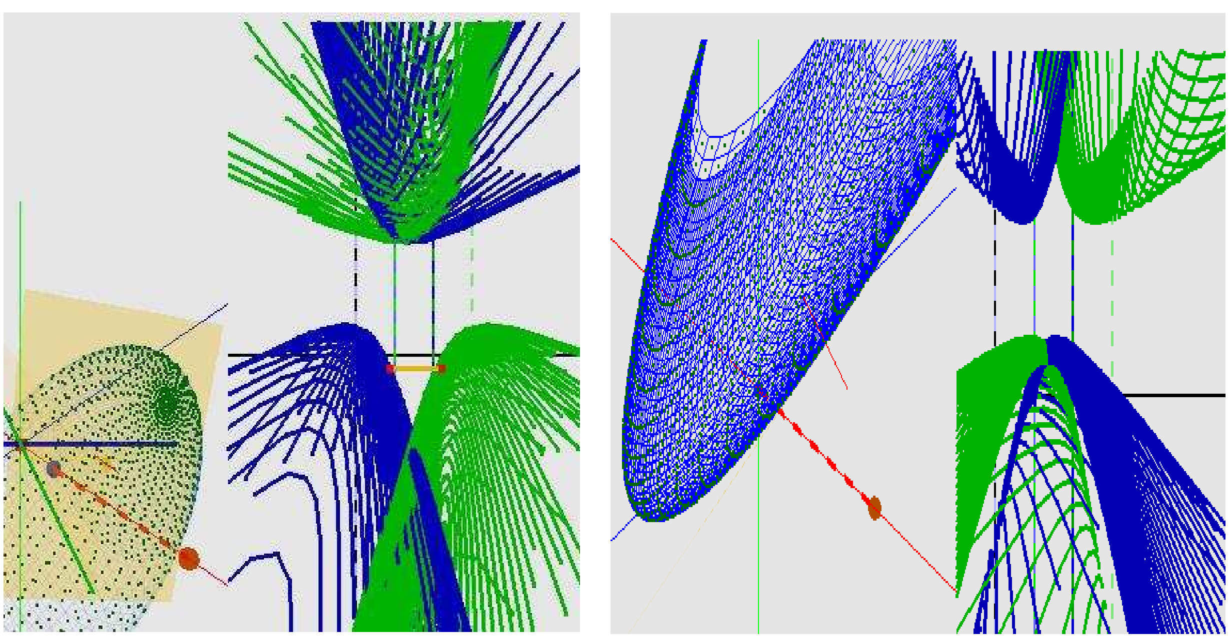

Figure 7.28: Representation of an ellipsoid on the left and a paraboloid on the right.

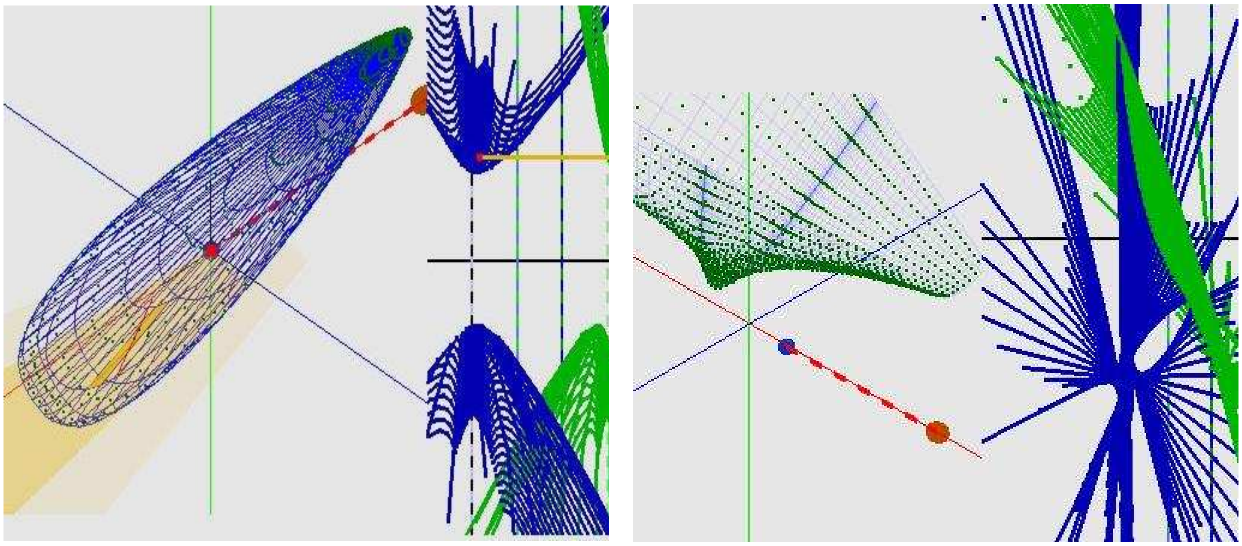

Figure 7.29: Representations: non-quadric convex surface (left) and small bump (right).

was interactively varied in every imaginable way and significantly its represenations like the one shown were invariably markedly different than a *gh*. In certain orientations the intersections of σ_b with the super-planes are *bc* – bounded and convex – yet the representation regions were not *gh*. This is important observation is explored further. No less significant is that the representing regions are not chaotic having very interesting shapes continuously varying with changing orientation Proceeding, a surface σ_d with three small dimples – depression being considered here as a perturbation of convexity "opposite" to that in σ_b – shown in Fig. 1.30 is explored next. Interesting representation patterns are seen with varying orientations one (on the right) contains two hyperbolic regions, and other patterrs *outside* them, evidence of "near-convexity". The three crossings (center)

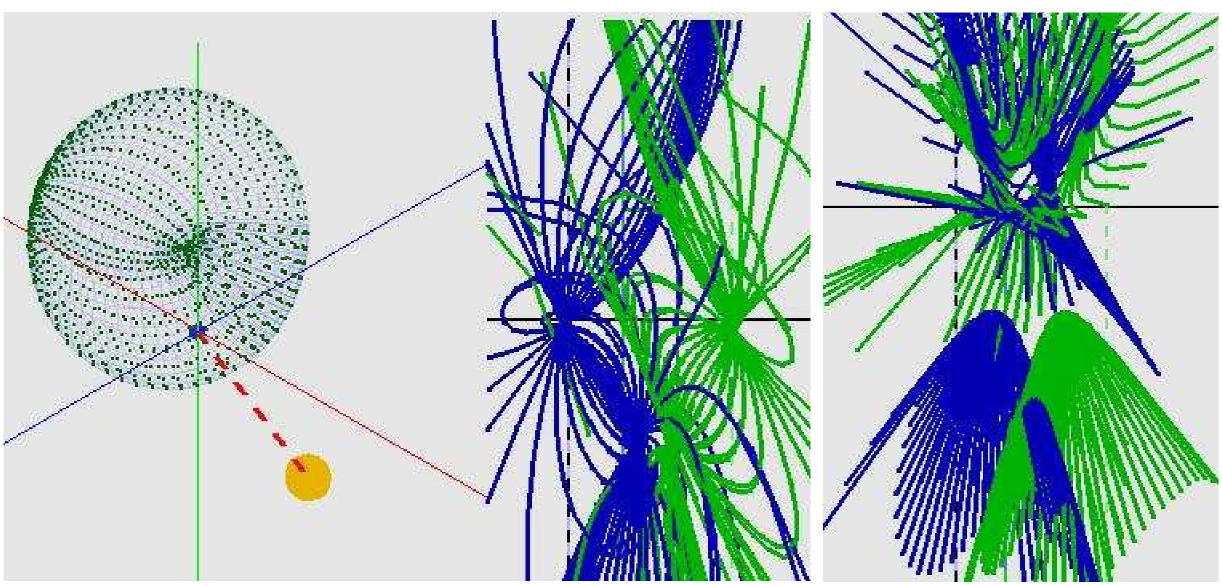

Figure 7.30: Representation of a non-convex surface with 3 dimples.
The depressions correspond to the "swirls" in the representation (center).

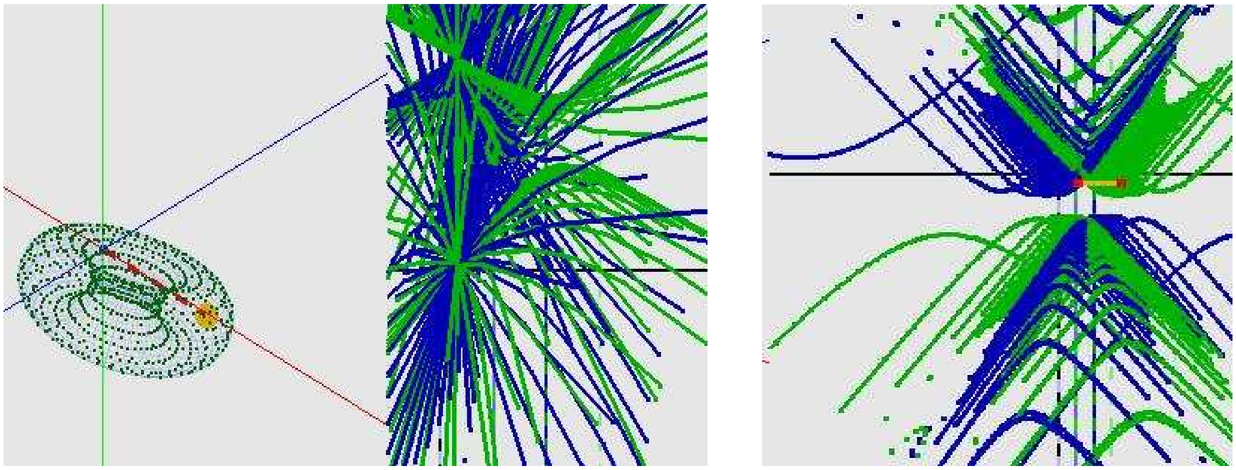

Figure 7.31: Torus has two “multitangent” planes (left) corresponding to the two crossings (center) and hyperbolic slices (right).

correspond possibly to the three dimples. Again it is rather remarkable that for a multitude of orientations none of the representations consists of *just* two hyperbolas as may naively be expected.when the intersection with the super-planes is a bounded convex set *bc*.

Lots of hyperbolas appear in the representation of the torus Fig. 1.31 (right) but unlike those in the representation of convex surfaces. Here the hyperbolas are not contained within a largest outer one but are spread in the horizontal direction. Curves from the two representing regions intersect at two points with the same x coordinate. This is reminiscent of the crossing points corresponding to bitangent planes. We surmise that the

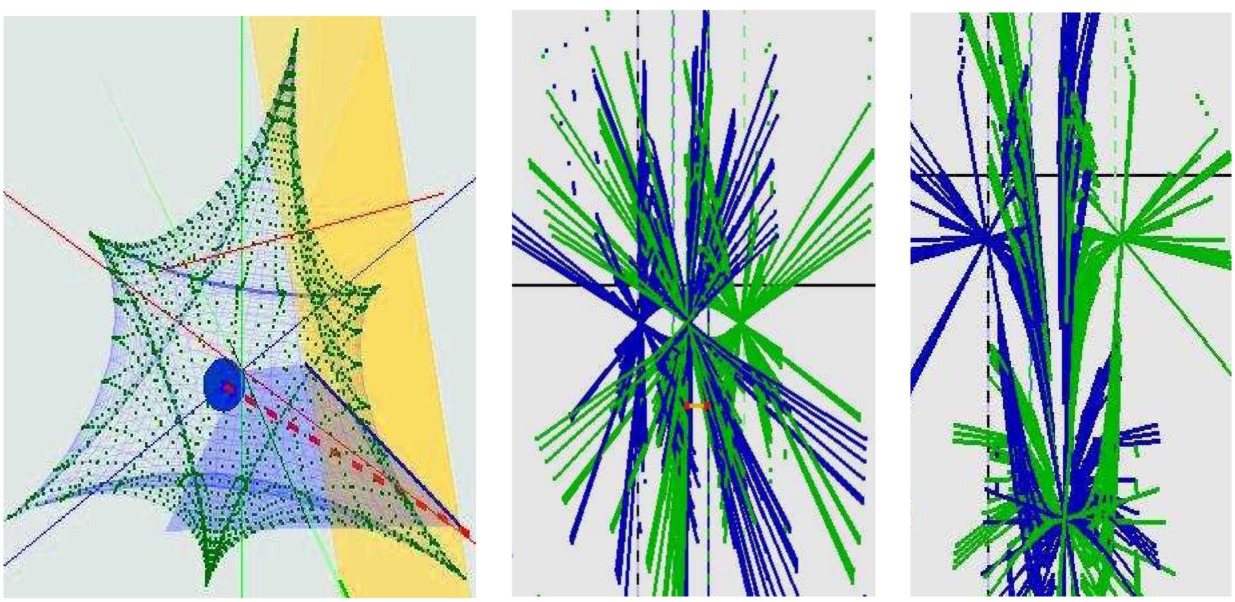

Figure 7.32: Astroidal surface and its representations for two orientations. The 3 crossing-points pattern persists for various orientations.

crossing points represent two *parallel* planes tangent at two circles at the top and bottom of the torus. The representation of the asteroidal surface [?] in Fig. 1.32 has a pattern with 3 crossing points which persists in several orientations. Upon careful scrutiny only at the mid-point do curves from the two regions intersect resembling the crossing points in the torus' representation. Could this point represent a tangent plane approaching one of the surface's vertices and becoming a bitangent plane in the limit? Another association that comes to mind is of an exterior supporting plane touching the surface at exactly three vertices.

The significant finding from these examples is that, the $\|$-coords representation even of complex non-convex surfaces in various orientations is not chaotic but consists of discernible patterns corresponding to their properties. It may also lead new surface classifications. A corollary of this discussion is what happened to the claim the representing boundaries are the images of the surface's intersection with the super-planes?

Let us return to the Lemma 1.0.1 noting that its proof is based on the assumption that the curve is on *one side of its tangent*. Similarly in the theory of envelopes the analysis is based on the family of curves *being on one side of the envelope* leading to necessary and sufficient conditions for the existence and a method for obtaining the envelope. As was seen in the subsequent examples the method works even when there are singularities and when this condition fails. In such cases the envelope has several components each consisting of special points on the family of curves e.g. inflection points, cusps, extrema, crossing points and others. For the problem now at hand, the boundary of a representing region is an envelope of lines "touching" it (but not necessarily tangent to it) and the curves formed by the representing points. We saw that the method of Lemma 1.0.1 applies well to developable, convex and even *ruled non-convex* surfaces the representing regions lie on interior or exterior respectively and *on one side of the boundary.* We found that for non-convex surfaces parts of the representing regions lie on both sides of the boundary, so the condition of Lemma 1.0.1 fails and the boundary is no necessarily only the image of the surfaces intersection with the super-planes. As pointed out below this has important ramifications and is basically good news. The refinement of Lemma 1.0.1 for non-convex surfaces is a difficult research problem, related to that for the envelopes of general families of curves and surfaces. These observations, even if partially true, may lead to a new approach for the construction of (also approximate) convex hulls in $\mathbb{R}^N$ as for $\mathbb{R}^2$ [?].

Conjecture (non-convexity in $\mathbb{R}^N$): A surface $\sigma \subset \mathbb{R}^N$ is *non-convex* if any boundary of the $N-1$ regions in $\bar{\sigma}$ is not *gh* (a generalized hyperbola) or a *uc* (unbounded convex) for *any orientation* of σ.

Though we did not find an example where a representing boundary of a convex surface is a *uc* unbounded convex, it is in principle possible which is why it is added to the conditions. If the conjecture turns out to be true then the convexity of a surface in $\mathbb{R}^N$ is immediately recognizable from its representation at any orientation.

Conjecture (convexity in $\mathbb{R}^N$): A surface $\sigma \subset \mathbb{R}^N$ is *convex* if the boundaries of the $N-1$ regions in $\bar{\sigma}$ are *gh* (a generalized hyperbola) or *uc* all with the same y-range for *any orientation* of σ.

These assertions are supported by the examples of convex surfaces above whose representing boundaries are *gh* including the hypercube in Fig. 1, as well as those of the non-convex surfaces. The representation of the saddle Fig. 1.16 is particularly instructive with the regions having *gh* and *uc* boundaries. Since their y range is not the same the surface they represent is not convex.

Dualities

- *rotation* $\leftrightarrow$ *point translation in* $\mathbb{R}^2$ – *imprecise*
- *cusp in* $\mathbb{R}^2$ $\leftrightarrow$ inflection point (ip) in $\mathbb{R}^2$
- *line of cusps in* $\mathbb{R}^N$ $\leftrightarrow$ $(N-1)$ *ips with same y-coord in* $\mathbb{R}^2$
- *bitangent plane in* $\mathbb{R}^3$ $\leftrightarrow$ *2 coinciding crossing points in* $\mathbb{R}^2$ – *at least for developables*
- *bitangent hyperplane in* $\mathbb{R}^N$ $\leftrightarrow$ $(N-1)$ *coinciding crossing points in* $\mathbb{R}^2$ – *at least for developables*
- *cusp in* $\mathbb{R}^3$ $\leftrightarrow$ *2 "swirls" in* $\mathbb{R}^2$
- *"twist" (tangent plane intersecting surface) in* $\mathbb{R}^3$ $\leftrightarrow$ *2 cusps in* $\mathbb{R}^2$
- *conjecture :* *cusp in* $\mathbb{R}^N$ $\leftrightarrow$ $(N-1)$ *"swirls" in* $\mathbb{R}^2$
- *conjecture :* *"twist" (tangent hyperplane intersecting surface) in* $\mathbb{R}^N$ $\leftrightarrow$ $(N-1)$ *cusps in* $\mathbb{R}^2$